Early interventions in keratoconus

Daniel Mark Gore BSc FRCOphth

A thesis submitted to University College London for the degree of

Doctor of Medicine (Res), 2015

Declaration

I, Daniel Mark Gore, confirm that the work presented in this thesis is my own. Where information has been derived from other sources, I confirm that this has been indicated in the thesis.

Signed…….. Dated……..

Abstract

Keratoconus is a condition in which the corneal shape becomes steeper and more irregular between adolescence and the mid-thirties. It is a common cause of visual impairment with disease progression typically managed with rigid contact lens. Traditionally, no intervention has been available to arrest or slow disease progression. As a result, keratoconus is the commonest indication for corneal transplantation in young people. Over the last decade, outcome data has accumulated for new interventions for keratoconus that have radically altered the treatment options for these patients and promises to avoid the sight loss associated with this condition. These interventions include corneal collagen cross-linking (CXL), intracorneal ring implantation and photorefractive keratectomy (PRK). The laboratory and clinical work presented in this thesis explores these new interventions under two key headings: corneal shape stabilisation and visual rehabilitation.

I have developed two novel ex vivo techniques which provide quantitative means of measuring riboflavin across the whole cornea in both epithelium-off and –on techniques. Using these methods I have concluded that no existing commercial transepithelial CXL protocol matches the riboflavin penetration achieved following epithelial debridement. I present novel iontophoretic protocols that, by increasing riboflavin concentration, soak duration and current dosage, matches epithelium-off absorption.

I additionally report prospective outcomes of an accelerated version of CXL in keratoconus confirming it is a safe and effective iteration of the original 'Dresden' protocol. Finally, I present interim outcomes from a prospective study of simultaneous ocular wavefront-guided PRK and CXL showing significant improvements in corrected distance visual acuity beyond that expected with standard CXL.

Acknowledgments

This research has received a proportion of its funding from the Department of Health's NIHR Biomedical Research Centre for Ophthalmology at Moorfields Eye Hospital and UCL Institute of Ophthalmology. The views expressed are my own and not necessarily those of the Department of Health. I additionally acknowledge financial support from Fight for Sight (1348/9), the Rosetrees Trust (JS16/M282) the Ian Collins Rayner Fellowship (Rayner Intraocular lenses Ltd, United Kingdom and Ireland Society of Cataract and Refractive Surgeons), and the Special Trustees of Moorfields Eye Hospital (ST1415A). I disclose free provision of riboflavin solution from Avedro, Inc., Waltham, MA, USA and Sooft Italia S.p.A. Montegiorgio, Italy.

I also acknowledge my supervisors (Bruce Allan, Stephen Tuft) and collaborators (Chris Dunsby, Paul French, David O'Brart) who have mentored and guided me through this endeavour. I additionally wish to thank Dr Chris Thrasivoulou, imaging team manager at the University College London confocal unit, for microscopy technical support.

Finally this work would not have been possible without the support of my family to whom I am forever grateful.

Dan Gore
June 2015

Table of Contents

Abbreviations

BAC	Benzalkonium chloride
CCT	Central corneal thickness
CDVA	Corrected distance visual acuity (spectacle-corrected vision, not contact lens correct vision)
CI	Confidence interval
CXL	Corneal cross-linking
D	Diopter
DALK	Deep anterior lamellar keratoplasty
DM	Descemet's membrane
ECC	Endothelial cell count
EDTA	Ethylenediaminetetraacetic acid
EKC	Early Keratoconus Clinic
HPLC	High performance liquid chromatography
HPMC	Hydroxypropyl methylcellulose
ICRS	Intrastromal corneal ring segment
ISV	Index of surface variation
LogMAR	Logarithm of the Minimum Angle of Resolution
µm	Micrometer
mA	Milliamp
mm	Millimeter
MRSE	Manifest refractive spherical equivalent
nm	nanometer
OCT	Optical coherence tomography
OCT	Optimal Cutting Temperature compound
PBS	Phosphate buffered saline
pIOL	Phakic intraocular lens
PK	Penetrating keratoplasty
PRK	Photorefractive keratectomy
RCT	Randomised controlled trial
RGP	Rigid gas permeable lens
SD	Standard deviation
SEq	Spherical equivalent
SHG	Second harmonic generation
TPF	Two-photon fluorescence
TransPRK	Transepithelial photorefractive keratectomy
UDVA	Uncorrected distance visual acuity
UV	Ultraviolet
VA	Visual acuity

List of publications, presentation & awards from this work

Publications

Gore DM, French P, O'Brart D, Dunsby C, Allan BD. Transepithelial riboflavin absorption in an ex-vivo rabbit corneal model. Invest Ophthalmol Vis Sci. June 2015 in press
Gore DM, French P, O'Brart D, Dunsby C, Allan BD. Two-photon fluorescence microscopy of corneal riboflavin absorption through an intact epithelium. Invest Ophthalmol Vis Sci. 2015 Feb 19;56(2):1191-2.
Gore DM, Margineanu A, French P, O'Brart D, Dunsby C, Allan BD. Two-photon fluorescence microscopy of corneal riboflavin absorption. Invest Ophthalmol Vis Sci. 2014 Apr 17;55(4):2476-81
Gore DM, Shortt AJ, Allan BD. New clinical pathways for keratoconus. Eye (Lond). 2013 Mar;27(3):329-39

Presentations

Transepithelial riboflavin absorption in an ex-vivo rabbit corneal model. Gore DM, French P, O'Brart D et al. *ARVO* 2015
Femtosecond laser-assisted intrastromal corneal ring segment implantation in keratoconus. Gore DM, Allan BD. *ESCRS* 2014
Rapid corneal collagen cross-linking for progressive corneal ectasia – 12-month results. Gore DM, Nicholae MN, Kopsachilis N. *ESCRS* 2014
Two-photon fluorescence microscopy of corneal riboflavin absorption. Gore DM, Margineanu A, French P et al. *ARVO* 2014
Accelerated corneal collagen cross-linking – 6-month results. Gore DM, Allan BD. *International Congress for Advanced Corneal Cross-Linking* 2013
Rapid corneal cross-linking for progressive ectasia. Gore DM, Kopsachillis N, Allan BD. *RCOphth Congress* 2014
Nurse-led corneal cross-linking. Mason M, Gore DM, Allan BD. *RCOphth Congress* 2014
Two-photon fluorescence microscopy – applications to corneal collagen cross-linking. Gore DM *UKISCRS* 2013

Awards

2015 Bayer Educational Grant Award
2014 The Peel and Rothwell Jackson Postgraduate Travelling Fellowship
2014 Moorfields Alumni Association Bursary
2014 Aylward QIPP Prize Winner, Moorfields Eye Hospital
2014 Moorfields Stars' Chief Executive's Team of the Year Award

Table of figures

List of Tables

1 Introduction

Keratoconus is a condition in which the corneal shape becomes steeper and more irregular between adolescence and the mid-thirties. For the age group 10-44 years, the prevalence of keratoconus in white Europeans has been estimated at 1 in 1750, rising to 1 in 450 in South Asians.(Pearson et al. 2000) Traditionally no intervention has been available to arrest or slow disease progression. As the corneal shape becomes more abnormal, first spectacles, then rigid contact lenses become ineffective. Prior to the availability of newer surgical interventions, including corneal collagen cross-linking (CXL) and intrastromal corneal ring segments, approximately 20% of patients eventually required a corneal transplant to correct vision. As a result, keratoconus is the commonest indication for corneal transplantation in young people. Although corneal transplantation for keratoconus usually achieves good visual outcomes, long-term graft survival in keratoconic eyes is poor. The Australian Graft Registry data identified only 17% of penetrating grafts functioning at 23 years, with survival rates falling further with second and third grafts.(Kelly, Coster, et al. 2011; Kelly, Williams, et al. 2011)

Over the last decade, outcome data has accumulated for new interventions for keratoconus that have radically altered the treatment options for these patients and promise to reduce transplantation rates significantly, arrest disease progression, and save many patients from long-term reliance on rigid contact lens wear.

This thesis presents the findings of laboratory and clinical studies of these new keratoconus interventions under two key aims:

1. To measure riboflavin absorption through an intact epithelium in an animal model.
2. To determine visual and refractive outcomes for accelerated corneal cross-linking, intrastromal corneal ring segments and photorefractive keratectomy in progressive keratoconus.

In the following chapter, using the current evidence base, I review these new treatment options addressing two essential treatment strategies: shape stabilisation and visual rehabilitation.

2 Systematic review

2.1 Methodology

I searched MEDLINE (1950-2015) and the Cochrane Central Register of Controlled Trials using the following search terms: keratoconus; corneal cross-linking; cross-linkage; intracorneal ring segment; topographic photorefractive keratectomy; phakic intraocular lens. For the meta-analysis, two investigators (Alex Shortt & I) independently assessed the search results for randomised controlled trials (RCTs) of corneal cross-linking in keratoconus. The authors of 2 RCTs (O'Brart et al. 2011; Wittig-Silva et al. 2014) were contacted for clarification of trial methodology and provision of additional unpublished data. A risk of bias assessment was performed on studies and only studies with a low risk of selection, performance, detection and attrition bias were included. Data extraction was done independently by DG and AS. Data synthesis was performed using a meta-analysis software package, Review Manager (RevMan, The Nordic Cochrane Centre, The Cochrane Collaboration, Copenhagen, 2008). The effect of the intervention was expressed as odds ratios and confidence intervals were calculated. The Mantel-Haenszel fixed-effect method of meta-analysis was used.

2.2 Conventional keratoconus management

Traditional management focused on maintaining useful vision in either spectacles until irregular astigmatism necessitated rigid contact lens fitting, then corneal transplantation where contact lenses failed (Figure 2.1).

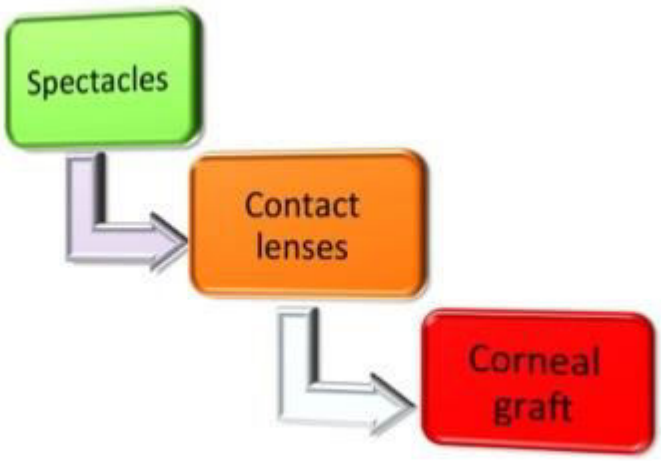

Figure 2.1 Traditional management pathway

2.2.1 Contact lens fitting

Soft lenses and soft toric lenses can provide good visual rehabilitation in early keratoconus; but RGP lenses are generally required to neutralize significant corneal surface irregularity. RGP lenses provide good tear exchange, but lens stability deteriorates as the corneal profile steepens in more advanced keratoconus. Traditional corneal RGP lenses are between 8 and 10 mm in diameter. Newer intralimbal RGP lenses (10.5 - 12 mm diameter) can improve corneal coverage and centration in some patients,(Ozbek & Cohen 2006) but the increased diameter may make application and removal more difficult. 'Piggyback' (soft beneath RGP) lens combinations and hybrid (RGP center and a soft skirt) lenses can improve wearing time in patients with poor RGP lens tolerance. The SynergEyes™ lens is a relatively new hybrid lens with a silicone hydrogel skirt providing greater oxygen permeability than earlier

hydrogel-based models. Hybrid lenses should ideally fit with apical clearance over the central cornea with little or no touch in the RGP portion of the lens.

Where these options fail, RGP scleral (and semi-scleral) lenses, which vault clear of the corneal surface, are a solution applicable to almost any corneal shape.(Pecego et al. 2012) Scleral lenses can rescue vision in patients with late stage disease – particularly where technical obstacles such as a thin peripheral cornea limit options for corneal transplantation.

Despite advances in contact lens fitting for keratoconus, contact lens dependence may be associated with significant impairment of vision-related quality of life that continues to decline over time.(Kymes et al. 2008)

2.2.2 Corneal transplantation

Without treatments to halt disease progression in keratoconus, up to 21% of eyes have required a corneal transplant.(Lass et al. 1990) Using established techniques (Markov modelling), the lifetime cost of conventional keratoconus treatment has been estimated at US$25,168 per patient, with the likelihood of primary and repeat corneal transplantation being the key cost determinants.(Rebenitsch et al. 2011) Given the relatively high prevalence of keratoconus and the frequency with which corneal transplantation is required, this represents a significant health economic burden.

While penetrating keratoplasty (PK) for keratoconus generally achieves good visual outcomes, long-term graft survival in keratoconic eyes declines rapidly

after the second decade. Primary graft survival rates from the Australian Graft Registry are 89% at 10 years, 49% at 20 years and 17% at 23 years.(Kelly, Williams, et al. 2011) These rates fall further with repeat grafts. 10 year survival rates are 53% for second and 33% for third grafts.(Kelly, Coster, et al. 2011) Most grafts for keratoconus are performed in relatively young patients. In an effort to reduce the rate of repeat transplantation and associated complications, many surgeons now use deep anterior lamellar keratoplasty (DALK), with preservation of the host endothelium, as the transplantation procedure of choice in keratoconus. Accelerated long-term endothelial cell loss observed after PK does not occur after DALK.(Reinhart et al. 2011) Extrapolation from observed endothelial cell loss rates predicts a median graft survival of 49 years for DALK versus 17 years for PK.(Borderie et al. 2012) But current DALK techniques are technically challenging. Intraoperative complications and conversion to PK are common. A recent UK transplant registry comparison of results for PK and DALK in keratoconus showed a high early failure rate for DALK.(Jones et al. 2009) This was attributed to the learning curve in the surgical transition from PK to DALK for many surgeons in the period studied (1999-2005). Where transplantation is successful, irregular astigmatism and high postoperative anisometropia commonly prevent successful visual rehabilitation in spectacles without recourse to further surgical intervention.(Kelly, Williams, et al. 2011)

Corneal transplantation is an effective but costly intervention in advanced keratoconus (stage IV modified Krumeich classification,(Colin & Velou 2003) [Table 2.1]), with an estimated incremental cost-utility ratio of between $1,942 and $3,025 per quality-adjusted life-year.(Roe et al. 2008; Koo et al. 2011)

The life impact of repeat intervention, and slow, often incomplete, visual rehabilitation after transplantation should not be underestimated.(Yildiz et al. 2010) Transplantation costs, and evidence for reduced quality of life in contact lens wearers,(Kymes et al. 2008) underline the need for a new, more proactive approach to keratoconus management.

Table 2.1 Modified Krumeich classification of keratoconus

Stage	Characteristics
I	Eccentric corneal steepening Induced myopia and/or astigmatism <5D Corneal radii ≤48D Vogt's striae, no scars
II	Induced myopia and/or astigmatism >5D, <8 D Corneal radii ≤53D No central scars Corneal thickness ≥400µm
III	Induced myopia and/or astigmatism >8D, <10D Corneal radii >53D No central scars Corneal thickness 200 - 400µm
IV	Refraction not measurable Corneal radii >55D Central scars, perforation Corneal thickness <200µm

Originally published by (Colin & Velou 2003)

2.3 Defining disease progression – monitoring keratoconus

Defining disease progression and the threshold for surgical intervention in keratoconus patients under observation remains a challenge. Assuming no diurnal variation in corneal shape, the coefficient of repeatability (CoR) should correspond closely to the limits of agreement for successive measures of corneal tomography indices,(Fraser & Fogarty 1989) defining a threshold beyond which there is a 95% probability that an observed difference reflects disease progression rather than measurement inaccuracy. Keratometry measurement repeatability in keratoconic eyes (stage II, 3mm zone steep K ≤ 53 D) has been shown to be significantly poorer than in normal corneas, with a 1D CoR for steepest keratometry (Kmax) using Fourier-domain anterior-segment OCT (Casia SS-1000 Tomey Corp. Japan) and between 1.5 – 2 D using a Scheimpflug-based imaging device (Pentacam HR, Oculus GmbH, Wetzlar, Germany).(Szalai et al. 2012; Hashemi et al. 2015) This compares with CoR values in normal corneas of less than 0.5 D for both imaging devices.(Szalai et al. 2012) Based on this, a change in Kmax of +1.5 D versus measurement at presentation on Pentacam image comparison maps may be a useful contemporary threshold indication for CXL using a widely available corneal tomography device. A lower threshold (+1 D versus baseline Kmax) is used in contemporary studies (Table 2.2). Changes in other criteria used to define disease progression (Table 2.2) may tip the balance in favour of intervention where the observed increase in Kmax is less than 1.5 D.

The frequency with which patients should be screened and the optimum corneal tomography method also require additional research. More frequent

initial monitoring may be valuable in younger patients at high risk of rapid progression. Where possible, rigid contact lenses should be left out for a minimum of 2 weeks prior to each topography examination to reduce corneal warpage.

Table 2.2 Progression criteria used in published clinical trials

Kmax *≥1D increase*
Kmax – Kmin *≥1D increase*
Kmean *≥0.75D increase*
Pachymetry *≥2% decrease in CCT*
Corneal apex power *>1D increase*
MRSE *>0.5D*

RCTs vary in how progression is defined. I have listed different definitions above, one or more of which has been used in any one trial. D = dioptres; Kmax = steepest keratometry; Kmin = flattest keratometry; Kmean = (Kmax+Kmin)/2; CCT=central corneal thickness; corneal apex power is measured with cone location and magnitude index (CLMI), MRSE = manifest refractive spherical equivalent

2.4 Shape stabilisation

Corneal cross-linking (CXL) is the only treatment proven to halt disease progression in keratoconus.(Wittig-Silva et al. 2014; O'Brart et al. 2011) CXL is performed by irradiating riboflavin-soaked corneal tissue with an ultraviolet A (UVA) light source (370 nm). The riboflavin acts both as a photosensitizer to encourage UVA-induced corneal stiffening (cross-linking), and a shield to reduce UVA levels at the endothelial level below the cytotoxic threshold. The exact mechanisms of CXL-induced corneal shape stabilisation remain unclear. The original CXL protocol (Wollensak, Spoerl, et al. 2003a) described mechanical removal of the corneal epithelium with repeated application of riboflavin 0.1% drops before and during UVA treatment (3 mW/cm2 power for 30 minutes). The optimum corneal riboflavin soak and UVA irradiation required to achieve effective corneal stabilisation is unknown. A number of protocol variations emerging including speeding up the treatment (accelerated CXL) and delivering riboflavin through an intact epithelium (transepithelial CXL), both of which I investigate in this thesis.

2.4.1 Mechanism of cross-linking

Corneal cross-linking is a natural phenomenon that stiffens and strengthens the cornea. This cumulative age-related process is attributable to glycation-end-products inducing cross-link formation within collagen lamellae, which explains why for most patients stability is achieved by their fourth decade, as well as the protective effect against the development of keratoconus in young diabetics.(Naderan et al. 2014) Instead of glycation, the molecular

mechanisms of UVA/riboflavin-induced CXL appear to rely on photoactivated riboflavin forming singlet or triplet states. These react with oxygen to produce 'reactive oxygen species' which photo-oxidate stromal proteins (Type II mechanism).(Kamaev et al. 2012) Once the oxygen supply is depleted within the first few seconds, reactive species of radical ions form which can then form covalent cross-links with numerous molecules within the corneal stroma (type I mechanism). (Wollensak 2006) Ex vivo measured tissue oxygen concentrations suggests that type I photochemical kinetic mechanisms predominate.(Kamaev et al. 2012) While the exact nature and location of these cross-links remains unclear(Meek & Hayes 2013) they are thought to mediate increases in corneal rigidity, elastic modulus and resistance to enzymatic degradation.(Wollensak, Spoerl, et al. 2003b; Spoerl, Wollensak, Dittert, et al. 2004; Spoerl, Wollensak & Seiler 2004; Kohlhaas et al. 2006; Wollensak & Iomdina 2009)

2.4.2 Effect of cross-linking on corneal structure and biomechanics

Compounding the uncertainty regarding the mechanism of CXL is our inadequate understanding of what this treatment does to structures within the cornea (i.e. how it stabilises keratoconus). One theory relates to the concept of lamella slippage. X-ray scattering has previously revealed that keratoconic corneal lamellae lack the orthogonal fibrillar uniformity of normal corneas, particularly at the cone.(Meek et al. 2005) Displacement between (and probably within) these lamellae is postulated to underlie steepening and thinning as tissue is redistributed (as apposed to lost).(Meek et al. 2005; Daxer & Fratzl 1997) The sequitur would be that increased cohesion force

between corneal lamellae mediated by additional collagen cross-links would prevent these sliding movements. Interlamellar cohesion forces have been specifically measured by the Dresden group (Wollensak et al. 2011). In this study, the investigators prepared 400 µm (porcine) corneal strips which were cleaved at 50% depth just at one end of the strip. Once this split had been created, the 200 µm anterior and posterior flaps were clamped into a microcomputer-controlled biomaterial testing machine. This machine measured the cohesive force required to propagate the stromal split as the clamps were moved apart. The investigators compared untreated controls with standard cross-linked tissue and observed no change in interlamellar cohesion force. This finding probably rules out the lamellar slippage theory.(Meek & Hayes 2013)

An alternative mechanism relates to enzymatic degradation resistance. Enzyme digestion studies have demonstrated that CXL increases the stromal resistance to collagenolytic enzymes, (Spoerl, Wollensak & Seiler 2004) as well as increasing the temperature threshold for hydrothermal shrinkage.(Spoerl, Wollensak, Dittert, et al. 2004) This appeared to corroborate transmission electron microscopy findings by the same group of an increase in collagen fibrillar diameter (Wollensak et al. 2004), although this finding has not been replicated since (by x-ray scattering). (Hayes et al. 2013) A consensus, therefore, is lacking as to the direct involvement of collagen fibrils themselves in the cross-linking process.

A lack of validated clinical devices capable of measuring in vivo mechanical properties is a current limitation to further understanding the effects of CXL. Different measures of corneal biomechanical properties may not necessarily correlate between different tests. For example, the original stress/strain tests of excised strips of cornea pulled in a tangential direction do not measure the same property as pneumatically deforming the corneal in the sagittal direction (e.g. Ocular Response Analyzer (ORA); Reichert, Inc, Buffalo, NY). The Corvis ST (Oculus GmbH, Wetzlar, Germany) uses a Scheimpflug camera to record a similar air-puff corneal indent, the characteristics of which are expected to yield more information of biomechanical behaviour than deformation alone. Significant challenges remain, however, in interpreting these images due to the contributions of intraocular pressure and corneo-scleral geometry.(Girard et al. 2015)

More recently, Brillouin microscopy has been used to map corneal biomechanics in three dimensions with a high spatial resolution.(Scarcelli et al. 2012; Scarcelli et al. 2013) This non-contact technique measures light-scattering arising from the interaction of incident light with hypersonic acoustic waves (phonons) generated within the tissue. Brillouin-scattered light is characterized by a frequency shift which is proportional to the longitudinal modulus of elasticity of the tissue.(Scarcelli & Yun 2008) Although not commercially available, this no-touch, non-deformational optical test has great potential as a tool to both monitor the response to CXL, as well as screen keratoconus suspects.

2.4.3 Standard cross-linking

Corneal collagen cross-linking (CXL) using the standard, epithelium-off protocol originally developed at the University of Dresden (Wollensak, Spoerl, et al. 2003a) is effective in arresting disease progression (52% stabilising, 45% regressing) with 3% of eyes progressing despite treatment.(Hersh et al. 2011; O'Brart et al. 2011; Wittig-Silva et al. 2014)(Table 2.3, Table 2.4) Long-term outcomes (mean 52 months follow-up, range 48-60 months) for standard CXL have been reported in the Siena Eye Cross Study, a prospective, non-randomised study of 44 eyes with progressive keratoconus treated with CXL and fellow eye controls.(Caporossi et al. 2010) Control eyes, in which disease progression was less rapid than treated eyes prior to assignment, were observed initially then crossed over to CXL after 2 years. Their data confirmed a halt in ectatic progression in all treated eyes, with a mean reduction in Kmax of 2 D, while fellow eyes progressed by a mean 1.5 D for 24 months (prior to cross-over) before also demonstrating comparable reductions in Kmax after CXL. Refraction stabilised at 2 years and spectacle CDVA improved 2 ± 1 Snellen lines (mean ± SD).(Caporossi et al. 2010) Two year outcome data from an uncontrolled prospective study (Vinciguerra et al. 2012) in 40 children (mean age 14.2 ± 1.7 years) with mild disease (3 mm zone steep K ≤ 53 D) confirmed similar findings with both UDVA and CDVA improving by 2 lines (LogMAR) and a reduction in Kmax of 1.27 D.

Table 2.3 Summary of efficacy outcomes following standard (epithelium-off) corneal cross-linking

Reference	*Study design*	*n (latest follow-up)*	*Mean age (range)*	*Latest follow-up (months)*	*Mean UDVA change (logMAR)*	*Mean CDVA change (logMAR)*	*MSE change (D)*	*Cylinder change (D)*	*K max change (D)*	*Pachymetry change (microns)*	*Failure (%)*
(Agrawal 2009)	CS[a]	37	16.9 (12–39)	12	—	−0.09	—	−1.20	−2.47	—	8.1
(Arora et al. 2013)	CS	30	16 (12–18)	12	−0.18[b]	−0.12[b]	—	—	0.4[b]	−66.46[b]	—
(asri et al. 2011)	CS	64	24.12±7.58	12	0.00	−0.01	—	+0.07	−0.49	−11	9.8
(Caporossi et al. 2012)	CS	44	10–40	48	−0.37	−0.14	+2.15	−0.55	−2.26	+0.6	—
(Caporossi et al. 2012)	CS	77	10–18	36	−0.15	−0.09	—	—	−0.72	—	—
(Ghanem et al. 2014)	CS	42	22.4 (14–34)	24	−0.24	−0.12	0.39	0.46	−0.9	—	—
(Greenstein et al. 2010)	CS	31	32.3 (15–52)	12	—	—	—	—	—	—	
(Greenstein, Shah, et al. 2011)	CS	54	No data	12	—	—	—	—	—	−12.1	—
(Greenstein, Fry, Hersh, et al. 2012)	CS	64	No data	12	—	—	—	—	—	—	—
(Greenstein, Fry & Hersh 2012)	CS	46	No data	12	—	—	—	—	—	—	—
(Greenstein, Fry, et al. 2011)	CS	66	No data	12	−0.08	−0.10	—	—	−1.60	—	—
(Grewal et al. 2009)	CS	102	25.6(18–31)	12	—	−0.02	+1.43	−0.17	—	−3.7	—
(Guber et al. 2013)	CS	33	26.36 (13–40)	12	—	−0.04	—	0.73	−0.16	−11.33	—
(Hashemi et al. 2013)	CS	40	22.45 (16–35)	60	−0.02	−0.12	0.41	0.65	−0.24	2	—
(Hersh et al. 2011)	CS	49	No data	12	−0.05	−0.14	+0.85	−0.08	−2.00	—	—
(Hoyer et al. 2009)	CS	35	27.92	36	—	−0.14	—	−1.64	−2.73	—	8.6
(Ivarsen & Hjortdal 2013)	CS	28	12–38	22	—	−0.07	—	—	1.1	−0.52	—
(Jordan et al. 2014)	CS	38	21.9	12	—	—	—	—	—	—	—
(Kampik et al. 2011)	CS	46	33.5	24	—	−0.05	—	—	−1.23	−21.6	—
(Kontadakis et al. 2013)	CS	24	25 (20–36)	24	—	—	—	—	—	—	—
(Kránitz et al. 2012)	CS	25	29.92	12	−0.13	−0.09	+1.32	−0.49	−1.68	−31	—
(Kymionis et al. 2010)	CS	55	24.4 (18–36)	12	—	—	—	—	—	—	—
(Lamy et al. 2013)	CS	68	24.4 (18–33)	24	—	−0.16	—	—	−0.99	—	

(Legare et al. 2013)	CS	39	26.8 (15–56)	15.8	0.18 (12 months)[c]	0 (at 24 months)[c]	1.55 (at 24 months)[c]	1.30 (at 24 months)[c]	—	−15.58 (at 24 months)	—
(Magli et al. 2013)	CS	23	14.75 (12–18)	12	−0.01	0.01	—	0.11	−1.14	−1.98	—
(Mastropasqua et al. 2013)	RCT	20	23 (16–23)	12	—	—	—	—		37	—
(Mazzotta et al. 2008)	CS	44	No data	36	—	—	—	—	—	—	—
(Mazzotta et al. 2012)	CS	44	No data	12	−0.19	−0.11	—	—	−0.30	+14.5	—
(Mencucci et al. 2012)	CS	54	26.2	12	—	—	—	—	—	+1	—
(O'Brart et al. 2011)	RCT)	24	29.6 (21–42)	18	−0.08	+0.06	+0.82	−0.5	−0.62	+3.4	—
(O'Brart et al. 2013)	CS	30	26.3 (12–40)	53.3	0.03	0.05	0.82	0.28	—	3	
(Poli et al. 2013)	CS	45	26 (15–46)	21.7	−0.2 (at 12 months)	−0.23 (at 36 months)	—	—	−0.14 (at 2 years)	−0.24	—
(Raiskup-Wolf et al. 2008)	CS	33	30.04	36	—	−0.15	—	−1.45	−2.57	—	33.3
(Raiskup et al. 2009)	CS	163	31.53	12	—	0.05	—	—	−0.75	—	—
(Raiskup & Spoerl 2011)	CS	32	27.4	12	—	−0.04	—	—	−0.7	—	—
(Rechichi et al. 2013)	CS	28	28.8 (18–41 years)	12	0.25	−0.05	0.96	0.99	—	−15	—
(Sloot et al. 2013)	CS	53[b]	21.5 (12–49)	12	—	−0.13[b]	—	—	−1.5[b]	−9[b]	9
(Spoerl et al. 2011)	CS	50	29.4 (16–45)	12	—	—	—	—	—	—	—
(Toprak & Yildirim 2013)	CS	59	28.7	12	—	−0.13	—	—	−0.84	—	—
(Vinciguerra, Albè, Trazza, Seiler, et al. 2009)	CS	28	24–52	24	−0.24	−0.15	+0.81	−0.34	−1.35	−8.1	—
(Vinciguerra, Albè, Trazza, Rosetta, et al. 2009)	CS	28	24–52	12	−0.20	−0.14	+0.41	−0.26	−6.16	−14.9	—
(Vinciguerra et al. 2010)	CS	24	15–36	12				—	−0.73	+11.0	—
(Vinciguerra et al. 2012)	CS	40	14.2 (9–18)	24	−0.21	−0.19	+1.57	−1.31	−1.27	+14.0	—
(Wittig-Silva et al. 2014)	RCT	46	25.6	36	−0.15	−0.09	−0.61	−0.90	−1.03	5.86	

CDVA, Corrected Distance Visual Acuity; DALK, deep anterior lamellar SD, standard deviation; RCT, randomised controlled trial; UDVA, uncorrected visual acuity. [a] Case series; [b] Mean of all eyes in all groups; [c] Extrapolated from graphical data. — indicates data not provided in published article.

Table 2.4 Summary of safety outcomes following standard (epithelium-off) corneal cross-linking

Reference	Eyes at latest follow-up (n)	Latest follow-up (months)	Failure to re-epithelialise (%)	Stromal oedema (%)	Sterile infiltrate (%)	Haze (%)	Scar (%)	Infection (%)	Loss of CDVA (%)	ECC change (/mm^2)
(Agrawal 2009)	37	12	—	—	—	—	—	—	18.9 (7 of 37 eyes at 1 year)	—
(Arora et al. 2013)	30	12	—	27 (8 of 30 eyes)[a]	3 (1 of 30 eyes)[a]	3 (1 of 30 eyes)	—	—	—	4 (at 1 year)
(asri et al. 2011)	64	12	—	1.56 (1 of 64 eyes at 1 month)	—	1.5% (1 of 64 eyes at 1 year)	0.96%(1 of 104 eyes at 1 month)	—	7.8%(5 of 64 eyes at 1 year)	−110 (at 1 year)
(Caporossi et al. 2012)	44	48	—	70 (31 of 44 eyes within 6 weeks)	—	9.8% (4 of 44 eyes within 3 months)	—	—		−19 (at 2 years) (mean loss of 2%per year)
(Caporossi et al. 2012)	152	36	—	55	—	9.80	0	0	—	—
(Ghanem et al. 2014)	42	24	—	—	2% (1 of 42 eyes)	—	—	—	—	—
(Greenstein et al. 2010)	31	12	—	—	—	—	—	—	—	—
(Greenstein, Shah, et al. 2011)	54	12	—	—	—	—	—	—	—	—
(Greenstein, Fry, Hersh, et al. 2012)	64	12	—	—	—	—	—	—	—	—
(Greenstein, Fry & Hersh 2012)	46	12	—	—	—	—	—	—	—	—
(Greenstein, Fry, et al. 2011)	66	12	—	—	—	—	—	—	—	—
(Grewal et al. 2009)	102	12	—	—	—	—	—	—	—	—
(Guber et al. 2013)	33	12	—	—	—	—	6 (2 of 33 eyes)	—	6 (2 of 33 eyes)	—
(Hashemi et al. 2013)	40	60	—	—	—	—	—	—	—	—
(Hassan et al. 2013)	38	36	—	—	—	—	—	—	—	—

Reference	Eyes at latest follow-up (n)	Latest follow-up (months)	Failure to re-epithelialise (%)	Stromal oedema (%)	Sterile infiltrate (%)	Haze (%)	Scar (%)	Infection (%)	Loss of CDVA (%)	ECC change (/mm^2)
(Hersh et al. 2011)	49	12	—	—	—	—	—	—	—	—
(Hoyer et al. 2009)	35	36	0	—	No data but seen in few eyes	—	—	3% (1 of 35eyes)	—	—
(Ivarsen & Hjortdal 2013)	28	22±8 (10–43)	—	—	—	—	—	—	0	—
(Jordan et al. 2014)	38	12	—	—	—	—	—	—	—	—
(Kampik et al. 2011)	46	24	0% (46 eyes at 1 week)	—	—	100%(46 eyes within 3 months)	—	—	27%(12 of 46 eyes at 2 years)	55 (at 2 years)
(Kontadakis et al. 2013)	24	24	—	—	—	—	—	—	—	—
(Kránitz et al. 2012)	25	12	—	—	—	—	—	—	—	—
(Kymionis et al. 2010)	55	12	0 (0 of 55 eyes)	—	—	—	—	—	—	—
(Lamy et al. 2013)	68	24	—	—	—	—	—	—	—	—
(Legare et al. 2013)	39	24	0	—	—	—	—	0	—	—
(Magli et al. 2013)	23	12	0	8 (2 of 23)	—	—	—	—	—	−24 (at 1 year)
(Mastropasqua et al. 2013)	20	12	—	1.68	—	—	—	—	—	No significant change-
(Mazzotta et al. 2008)	44	36	—	—	—	11.4%(5 out of 44 eyes.	—	—	—	—
(Mazzotta et al. 2012)	44	12	0 (0 of 44 eyes)	—	—	—	—	—	—	0 (at 12 months)
(Mencucci et al. 2012)	54	12	—	—	—	—	—	—	—	—
(O'Brart et al. 2011)	24	18	0% (24 eyes at 1 week)	—	—	100%(24 eyes within 6 months)	0% (at 18 months)	0% (at 18 months)	—	—
(O'Brart et al. 2013)	30	48–72	—	—	—	—	—	—	17%(5 of 29 eyes)	
(Poli et al. 2013)	45	21.7±6.14	—	—	—	—	—	—	—	No significant change

Reference	Eyes at latest follow-up (n)	Latest follow-up (months)	Failure to re-epithelialise (%)	Stromal oedema (%)	Sterile infiltrate (%)	Haze (%)	Scar (%)	Infection (%)	Loss of CDVA (%)	ECC change (/mm^2)
(Raiskup-Wolf et al. 2008)	33	36	—	—	—	—	—	—	—	—
(Raiskup et al. 2009)	163	12	—	—	—	8.6%(14 of 163 eyes at 1 year)	—	—	—	—
(Raiskup & Spoerl 2011)	32	12	0	0	0	0	0	0	—	—
(Rechichi et al. 2013)	28	12	—	—	—	—	—	—	—	−15 (at 1 year)
(Sloot et al. 2013)	53[a]	21.5 (12–49)	—	—	2% (1 of 53)[a]	—	—	2% (1 of 53)[a]	—	—
(Spoerl et al. 2011)	50	12	—	—	—	—	—	—	—	—
(Toprak & Yildirim 2013)	59	12	—	—	—	—	—	—	—	—
(Vinciguerra, Albè, Trazza, Seiler, et al. 2009)	28	24	0	—	—		—	—	—	−53 (at 1 year) −131 (at 2years)
(Vinciguerra, Albè, Trazza, Rosetta, et al. 2009)	28	12	—	—	—	12.7 (4 of 28 eyes at 1 year)	—	—	—	−53 (at 1 year)
(Vinciguerra et al. 2010)	24	12	—	—	—	—	—	—	—	−22 (at 1 year)
(Vinciguerra et al. 2012)	40	24	—	—	—	6.9 (3 of 40 eyes)	—	—	—	−32 (at 1 year) −12 (at 2 years)
(Wittig-Silva et al. 2014)	50	36	—	—	4% (2 of 46 eyes)	—	—	—	—	28 (at 1 year) 13 (at 2 years) −35 (at 3 years)

CDVA, corrected distance visual acuity; ECC, endothelial cell count. — indicates data not provided in published article. a Mean of all eyes in all groups.

Further evidence for the efficacy of standard, epithelium-off CXL is found in 3 randomised-controlled trials (RCTs) with fellow eye controls that have published 12-month results.(O'Brart et al. 2011; Hersh et al. 2011; Wittig-Silva et al. 2014)(Figure 2.2) Excluding one study (Hersh et al. 2011) in which control eyes were crossed over to treatment after just 3 months, we combined 1 year post-CXL keratometric and acuity outcome data for patients (n = 31) in the remaining 2 trials.(Gore et al. 2012) Clinically significant ectatic progression (increase in Kmax ≥ 1 D at 12 months) was observed in 32% untreated control eyes and 3% eyes treated with CXL ($p = 0.01$, z-test); whereas significant regression (decrease in Kmax ≥ 1 D at 12 months) was seen in 45% of CXL treated eyes and 10% untreated control eyes ($p = 0.005$, z-test). (Gore et al. 2012) After conversion of 12-month acuity data to LogMAR values, combined data showed a statistically significant improvement in CDVA for patients treated with CXL ($p = 0.04$, z-test).

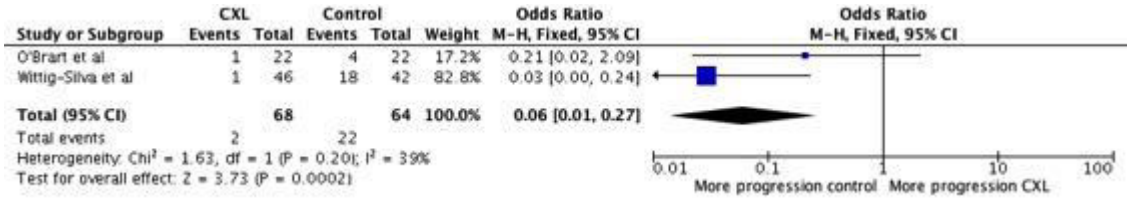

Figure 2.2 Forest plot of CXL meta-analysis

This Forest plot is a graphical representation of the above meta-analysis. The right-hand column is a plot of the measure of effect (i.e. an odds ratio) for each of the two studies (represented by the blue squares), with horizontal black lines representing the confidence intervals. The size of the blue squares is proportional to the study's weight in the meta-analysis. The black diamond represents the meta-analysed measure of effect of the two studies combined. The lateral points of the diamond represent the confidence intervals for this estimate. If the confidence interval horizontal lines for any individual study (or the points of the diamond for the meta-analysed effect) cross the vertical black line, it demonstrates that at the given level of confidence the result can not be said to differ from no effect.
This meta-analysis of 12-month results from two placebo controlled randomised trials shows disease progression (defined in these trials by an increase in maximum keratometry (Kmax) ≥1D) is significantly less likely after collagen cross-linking (black diamond does not cross the vertical line of no effect). Following recent correspondence with Melbourne study authors I have updated the above forest plot to include additional patients from that included in the original meta-analysis (Gore et al. 2012)

Spontaneous disease regression does not normally occur in keratoconus, and apparent disease regression (decrease in Kmax ≥ 1 D) in 10% of control eyes in RCTs may simply reflect limitations in measurement accuracy for contemporary topographers (Szalai et al. 2012) – a problem compounded by corneal warpage in rigid contact lens wearers. These limitations and varying inclusion criteria (Table 2.2) in contemporary studies underline the problem of defining disease progression and the thresholds for intervention in keratoconus.

2.4.4 Complications of corneal cross-linking

Although generally safe, (O'Brart et al. 2011; Hersh et al. 2011; Wittig-Silva et al. 2014; Caporossi et al. 2010; Koller et al. 2009) a range of complications is seen after standard, epithelium-off CXL. Sterile corneal infiltrates, thought to be an immune reaction to bacterial antigen deposition, were observed in 7.6% of patients in a prospective series of 117 eyes with 12 month follow-up after CXL.(Koller et al. 2009) Culture-proven bacterial keratitis with permanent loss of vision has also been reported.(Snibson 2010) Mild stromal haze is common after CXL and typically resolves within a year without detriment to visual acuity; but mid-stromal scarring was observed in 3% of cases by Koller et al, and 3% (95% confidence interval [CI] 1-9%) lost 2 or more lines of Snellen CDVA. Although the mechanism of visual loss was not identified, risk factors for loss of vision in this study were age > 35 years and pre-operative CDVA > 20/25.

Rates of endothelial cell loss similar to background age-related change were recorded in the Siena Cross Study (Caporossi et al. 2010) where treated corneas had ≥ 400 µm central thickness after epithelial removal, but significant cell loss and corneal endothelial failure have been reported in thinner corneas, or where corneas thinned intra-operatively following application of dextran-containing riboflavin solution.(Gokhale 2011; Kymionis et al. 2012; Lange et al. 2012; Sharma et al. 2012) Shielding by riboflavin-saturation in a 400 µm-thick cornea reduces irradiance at the endothelial level to 0.18 mW/cm^2, (Spoerl et al. 2007) well below the cytotoxic threshold of 0.35mW/cm^2 previously established in porcine endothelial cell

cultures.(Wollensak, Spörl, et al. 2003) Hypotonic riboflavin can be used to increase corneal thickness prior to UVA exposure in thinner corneas. This technique was originally described in 2009, with no reported complications or progression of ectasia at 6 months in a series of 20 eyes with > 320 µm initial corneal thickness after epithelial removal.(Hafezi et al. 2009) Similar encouraging 1 year results for CXL using hypotonic riboflavin in thinner corneas were reported by in a prospective series of 32 eyes.(Raiskup et al. 2011)

2.4.5 Keratocyte apoptosis and the demarcation line

An indirect qualitative outcome of CXL is a demarcation line within the stroma commonly interpreted as representing the border between treated tissue (anterior to the line) and untreated tissue (posterior to the line). This line is demarcated at the slit-lamp within the first few months following CXL by anterior stromal haze abruptly clearing posteriorly. The line can be quantitatively imaged (at a typical depth of 300 – 350 µm following standard CXL) by either optical coherence tomography (OCT) or confocal microscopy.(Spoerl et al. 2007; Seiler & Hafezi 2006) The latter imaging modality has the additional advantage of quantifying UVA-mediated keratocyte apoptosis. Using this technique in a prospective study, Jordan et al. identified complete absence of keratocyte nuclei in 86% of corneas 1 month post-CXL (Jordan et al. 2014), with a return to baseline by 12 months. The authors described the demarcation between treated and untreated corneal stroma appearing as ‘a region where normal keratocytes

transitioned into elongated, hyper-reflective, needle-like structures and then into large hyper-reflective stromal bands.'

Keratocyte apoptosis and demarcation line depth have additionally been used as a surrogate means of comparing treatment efficacy between different CXL protocols. Touboul et al observed, by confocal microscopy, that the demarcation line following accelerated CXL (30mW/cm^2 for 3 minutes, total energy 5.4 J/cm^2) lay more superficial, at a mean depth of 100-150 mm. (Touboul et al. 2012) Bouheraoua et al systematically investigated this in a prospective study of 45 patients with progressive keratoconus equally divided (n = 15) into standard CXL, accelerated CXL and iontophoretic transepithelial CXL.(Bouheraoua et al. 2014) They observed the demarcation line was visible 1 month after surgery in 93%, 87.5% and 47.7% of standard, accelerated and iontophoresis CXL corneas respectively. The depth of the demarcation line similarly differed for the same respective groups: 303 µm, 184 µm and 212 µm. The investigators additionally documented mean anterior stromal keratocyte densities remained significantly lower at 6 months (compared to baseline) in the standard and accelerated CXL groups, whereas they had returned to preoperative values in the iontophoresis CXL group. While tempting to extrapolate these differences to compare treatment efficacy, such tissue changes do not supersede the principle outcome measure of CXL which is to stabilise the corneal shape.

2.4.6 Accelerated cross-linking

Accelerated treatment protocols for CXL based on shorter UVA exposure times and higher irradiances are emerging. The underlying premise is that delivering a similar total energy over a shorter period of time will not compromise safety or efficacy in comparison with the standard protocol (30minutes at 3mW/cm^2). Stress–strain measurements on porcine corneal strips using a accelerated protocol (9 minutes at 10mW/cm2) demonstrated equivalent increases in corneal stiffness in comparison with the standard protocol.(Schumacher et al. 2011) In a recent prospective randomized trial,(Kanellopoulos 2012a) contralateral eyes of 21 patients with progressive keratoconus were randomized to either conventional or accelerated CXL (7 mW/cm^2 for 15 minutes). A halt in ectasia progression was seen in all cases at a mean follow-up of 46 months. Both groups responded similarly: CDVA improved from 20/60 to 20/40, UDVA from 20/30 to 20/25, mean sphere reduced by 2.4D and Kmax reduced from 49.5D to 46.1D. Endothelial cell loss was less in the accelerated CXL group (-100 cells/mm^2) than in the conventional CXL group (-250 cells/mm^2).

2.4.7 Transepithelial cross-linking

Transepithelial CXL, in which riboflavin is delivered through an intact epithelium (rather than epithelial debridement), promises to deliver the benefits of standard epithelium-off treatments without the painful rehabilitation and complications of epithelial removal. Epithelial-toxic agents used include benzalkonium chloride (BAC), sodium ethylenediaminetetraacetic acid

(EDTA), tetracaine, proparacaine, ethanol and gentamicin. A non-toxic reversible synthetic nonselective ion channel-forming peptide, NC-1059, has also been shown in a chick corneal model to enhance riboflavin permeability across an intact epithelium.(Zhang et al. 2012) In addition to novel formulations, iontophoresis is an alternative trans-epithelial methodology in which the negatively-charged riboflavin molecules can be driven through an intact epithelium across an electrical gradient. (Bikbova & Bikbov 2013; Vinciguerra et al. 2014; Buzzonetti et al. 2015) Finally, a hybrid technique has been described by Stojanovic et al. using of a riboflavin-soaked polyvinyl acetal pledget (Merocel sponge, Medtronic, Inc., Minneapolis, MN) inserted into the conjunctival sac (with proparacaine, genatmicin and BAC) to produce microabrasions of the superficial epithelial layers with eyelid blinking.(Stojanovic et al. 2012)

Results from preliminary clinical case series (Table 2.6, Table 2.7) using non-iontophoretic transepithelial riboflavin preparations have been equivocal, with some showing similar efficacy to epithelium-off CXL,(Filippello et al. 2012; Magli et al. 2013) whilst most have demonstrated less pronounced effects.(Leccisotti & Islam 2010; Caporossi et al. 2013; Koppen et al. 2012a; Soeters et al. 2015; Kocak et al. 2014) The earliest prospective (paired-eye) studies in humans documented small, but significant improvements in CDVA over fellow untreated eyes at 12 and 18 months respectively, with a trend towards

Table 2.5 Summary of efficacy outcomes of non-iontophoresis transepithelial corneal cross-linking

Reference	*Study design*	*Eyes at latest follow-up (n)*	*Age (years) (mean±SD) (Range)*	*Latest follow-up (months)*	*UDVA change (logMAR)*	*CDVA change (logMAR)*	*MSE change (D)*	*Cylinder change (D)*	*K max change (D)*	*Pachymetry change (microns)*
(Caporossi et al. 2013)	CS	26	22 (11–26 years)	24	0.08	0	0	0	1.55	−32
(Filippello et al. 2012)	CS	20	27 (12–42 years)	18	−0.23	−0.11	—	—	−1.17	−4.00
(Koppen et al. 2012a)	CS	37	24.02± 7.29 (12–46 years)	12	—	−0.04	+0.21	+0.04	1.33	−8.06
(Leccisotti & Islam 2010)	CS	51	26.9±6.3 (18–39 years)	12	—	−0.04	+0.36		0.51	—
(Mastropasqua et al. 2013)	RCT	20	23±2.5 (16–23 years)	12	—	—	—	—	—	0.51
(Gupta et al. 2015)	RCT	40	18-30 years	6	—	-0.09	-1.3	—	-3.25	+15
(Soeters et al. 2015)	RCT	33	18-48	12	-0.06	-0.14	0.3	+1.5	0.3	0
(Stojanovic et al. 2012)	CS	61	32±10 (15–52 years)	12	−0.30	−0.12	+0.74	−1.15	−0.57	+9.00

CDVA, corrected distance visual acuity; CS, case series; K, keratometry; MSE, mean spherical equivalent; RCT, randomised controlled trial; SD, standard deviation; UDVA, uncorrected visual acuity. — indicates data not provided in published article.

Table 2.6 Summary of safety outcomes of non-iontophoresis transepithelial corneal cross-linking

Lead Author	*Eyes at latest follow-up (n)*	*Latest follow-up (months)*	*Stromal oedema*	*Sterile infiltrate*	*Haze (%)*	*Scar (%)*	*Infection (%)*	*Loss of CDVA (%)*	*ECC change (/mm^2)*
(Caporossi et al. 2013)	26	24	—	—	—	—	—	—	—
(Filippello et al. 2012)	20	18	—	—	0 (0 of 20 eyes)	0 (0 of 20 eyes)	0 (0 of 20 eyes)	—	−34 (at 1.5 years)
(Koppen et al. 2012a)	37	12	—	—	0 (0 of 37 eyes)	0 (0 of 37 eyes)	0 (0 of 37 eyes)	0 (0 of 37 eyes)	—
(Leccisotti & Islam 2010)	51	12	—	—	4 (2 eyes 51)	0 (0 of 51 eyes)	0 (0 of 51 eyes)	0 (0 of 51 eyes)	+27 (at 1 year)
(Mastropasqua et al. 2013)	20	12	0	—	—	—	—	—	No significant change
(Gupta et al. 2015)	40	6	0 (0 of 40 eyes)	0 (0 of 40 eyes)	0 (0 of 40 eyes)	0 (0 of 40 eyes)	0 (0 of 40 eyes)	0 (0 of 40 eyes)	-2
(Soeters et al. 2015)	33	12	0 (0 of 33 eyes)	0 (0 of 33 eyes)	0 (0 of 33 eyes)	0 (0 of 33 eyes)	0 (0 of 33 eyes)	0 (0 of 33 eyes)	+1
(Stojanovic et al. 2012)	61	12	—	—	0 (0 of 61 eyes)	0 (0 of 61 eyes)	0 (0 of 61 eyes)	—	−130 (at 1 year)

CDVA, corrected distance visual acuity; ECC, endothelial cell count. — indicates data not provided in published article.

deterioration in topographic and acuity measures in non-treated control eyes.(Leccisotti & Islam 2010; Filippello et al. 2012) Improvements in corneal curvature (approximately 2 D mean reduction in Kmax) were similar to those seen after epithelium-off CXL. Filippello et al did, however, observe a difference in tissue effect by optical coherence tomography with a more superficial demarcation line typically visible at around 100 µm depth as opposed to 250-300 µm after epithelium-off CXL. (Filippello et al. 2012) Statistically significant improvements in CDVA were also observed (retrospectively) at 12-months by Stojanovic's hybrid technique (Stojanovic et al. 2012) as well as in an uncontrolled prospective study (Koppen et al. 2012b) though the authors recorded conflicting keratometric results depending on the imaging device used (progression by Scheimpflug, no change by Placido disc). The best evidence to date is 12-month results from one recently published randomised controlled trial (Soeters et al. 2015) which concluded that transepithelial CXL using Ricrolin TE (Sooft Italia S.p.A. Montegiorgio, Italy) was not effective at stabilising corneal shape compared with epithelium-off treatment.

For iontophoresis, up to 15 month follow-up data have been published (Table 2.7, Table 2.8), with reported cessation of disease progression and improvements in keratometric and visual parameters.(Bikbova & Bikbov 2013; Vinciguerra et al. 2014; Buzzonetti et al. 2015; Bouheraoua et al. 2014) However, the relative efficacy of this technique compared to epithelium-off CXL remains to be determined especially over longer term follow-up, and current randomized prospective studies comparing the two techniques

(clinicaltrials.gov.uk NCT02117999, NCT01868620, ISRCT 04451470) have yet to be reported.

Table 2.7 Summary of efficacy outcomes of iontophoresis transepithelial corneal cross-linking

Reference	*Study design*	*Eyes at latest follow-up (n)*	*Age (years) (mean±SD) (Range)*	*Latest follow-up (months)*	*UDVA change (logMAR)*	*CDVA change (logMAR)*	*MSE change (D)*	*Cylinder change (D)*	*K max change (D)*	*Pachymetry change (microns)*
(Bikbova & Bikbov 2013)	CS	22	32.15 ± 9.12	12	-0.13	0.05	0	0	2.35 (Kmean)	-6
(Bouheraoua et al. 2014)	CS	15	32.4 ± 6.6	6	—	−0.06	—	—	1.33	+0.4
(Vinciguerra et al. 2014)	CS	20	27.7 ± 6	12	—	-0.12	+1.11	0.66	-0.55	—
(Bonnel et al. 2015)	CS	15	27.75 ± 6.2 (17–37 years)	—	—	—	—	—	—	—
(Buzzonetti et al. 2015)	CS	14	13 ±2.4 (10–18 years)	15	−0.30	−0.1	+0.70	+0.70	+0.40	-4

Bonnel et al study reporting depth of demarcation line only with no other results. — indicates data not provided in published article.

Table 2.8 Summary of safety outcomes of iontophoresis transepithelial corneal cross-linking

Lead Author	*Eyes at latest follow-up (n)*	*Latest follow-up (months)*	*Stromal oedema*	*Sterile infiltrate*	*Haze (%)*	*Scar (%)*	*Infection (%)*	*Loss of CDVA (%)*	*ECC change (/mm^2)*
(Bikbova & Bikbov 2013)	22	12	—	—	0 (0 of 22 eyes)	—	—	0 (0 of 22 eyes)	+6
(Bouheraoua et al. 2014)	15	6	—	—	—	—	—	—	—
(Vinciguerra et al. 2014)	20	12	—	—	0 (0 of 20 eyes)	—	0 (0 of 20 eyes)	0 (0 of 20 eyes)	—
(Buzzonetti et al. 2015)	14	15	0	—	—	—	—	—	-3

— indicates data not provided in published article.

2.5 Visual rehabilitation

In the future, early intervention with CXL should greatly reduce the numbers of patients dependent on rigid contact lenses and corneal transplantation for visual rehabilitation in keratoconus. For the present, many patients are already past the point at which they still have good spectacle corrected or unaided acuity. Current strategies for contact lens fitting in keratoconus are discussed on page 21. Whilst transplantation remains the principal treatment for contact lens intolerant patients with stage IV keratoconus, newer interventions can be combined for earlier stage disease with the aim of restoring good spectacle corrected or unaided vision.

2.5.1 Gross corneal shape adjustment – intracorneal ring segments

Intrastromal corneal ring segments (ICRS) are effective in flattening the corneal shape and improving vision for most recipients with keratoconus (Table 2.10, Table 2.11), but the magnitude of effect is highly variable; and inclusion of different implantation techniques, different types of ICRS, and patients with late stage disease in earlier studies makes the existing evidence base for ICRS harder to interpret.(Piñero et al. 2009; Kubaloglu, Cinar, et al. 2010; Rabinowitz et al. 2006; Kubaloglu, Sari, et al. 2010) Many surgeons now use smaller diameter ICRS designs (Table 2.9) and femtosecond laser assisted implantation. Earlier case series reporting manual implantation of the original Intacs ICRS (designed for simple myopic rather than keratoconus correction) are therefore not considered here. Femtosecond laser channel

cutting has, by ensuring a consistent cut depth, both facilitated and enhanced safety in ICRS implantation.(Coskunseven et al. 2011)

Table 2.9 Characteristics of available intracorneal ring segments (ICRS)

Name	Manufacturer	Internal diameter/mm	External diameter/mm	Arc length /degree	Profile	Thickness/mm
Intacs	Addition Technology Inc. Sunnyvale, CA, USA	6.8	8.1	150	Hexagonal	0.25-0.45 (0.05 increments)
Intacs SK	Addition Technology Inc. Sunnyvale, CA, USA	6.0	7.3	150	Oval	0.4 & 0.45
Ferrara	Mediphacos Ltd, Belo Horizonte, Brazil	4.4	5.6	160	Triangular	0.2-0.35
KeraRing SI5	Mediphacos Ltd, Belo Horizonte, Brazil	5.0	-	90, 120, 160 & 210	Triangular	0.15-0.35
KeraRing SI6	Mediphacos Ltd, Belo Horizonte, Brazil	5.5, 6.0	-	90, 120, 150 & 210	Triangular	0.15-0.35
MyoRing	Dioptex GmbH, Linz, Austria	5-8	-	360	Triangular[a]	0.2-0.4 (0.02 increments)

[a]Convex anterior and concave posteriorly

Table 2.10 Summary of outcomes using Intacs ICRS

Reference, ring design	No. of eyes	Follow-up (mths)	Surgery	Mean change SE (D)	Mean change cylinder (D)	Mean change keratometry (D)	% gaining CDVA, mean gain	Complications
(Rho et al. 2013),Intacs SK	25	3	Femtosecond	2.25	0.76	1.91	-, 0.19 LogMAR	-
(Kotb & Hantera 2013), Intacs SK	37	6	Femtosecond	1.8	-	4.1	55%, 0.06 LogMAR	5.4% oedema 2.7% segment overlap
(Niknam et al. 2012), Intacs SK	37	6	Mechanical	-	-	4.48	-, 0.79 LogMAR	2.7% explantation
(Khan et al. 2011), Intacs SK	31	12	Mechanical	3.73	0.51	6.7	-, 0.15 LogMAR	19.3% extrusion 6.4% vascularisation 3.2% infection
(Haddad et al. 2012), Intacs SK	66	12	Femtosecond	2.9	0.99	1.97	-, 0.12 LogMAR	-
(Fahd et al. 2012),Intacs SK	24	6	Femtosecond	6.50	1.65	5.08	-	None
(Sansanayudh et al. 2010), Intacs SK	10	6	Femtosecond	3.0	1.1	6.8	0%, 0.26 LogMAR	None
(Kubaloglu, Sari, Cinar, Cingu, et al. 2010), Intacs	68	12	Mechanical/ Femtosecond	1.87	1.17	3.5	82%, 1.61 Snellen lines	4.4% decentration 5.8% extrusion
(Shetty et al. 2009), Intacs	12	6	Mechanical	2.98	1.5	3.6	83%, 0.13 LogMAR	0.8% vascularisation 25% deposits
(Ertan & Kamburoğlu 2008), Intacs	306	10	Femtosecond	3.0	0.2	2.7	72%, 0.20 LogMAR	0.9% extrusion
(Shetty et al. 2008), Intacs	14	12	Mechanical	5.0	1.8	3.9	69%, 0.17 LogMAR	-

(Zare et al. 2007), Intacs	30	6	Mechanical	3.6	0.7	2.1	73%, 0.12 LogMAR	13% exposure, 3.3% keratitis
(Colin & Malet 2007), Intacs	100	24	Mechanical	3.13	1.31	3.3	68%, -	4% explantation 2% extrusion
(Kymionis et al. 2007), Intacs	17	67	Mechanical	2.52	-	1.57	59%, -	71% vascularisation
(Alio et al. 2006), Intacs	13	48	Mechanical	1.4	2.0	3.3		15% vascularisation 30% deposits
(Ertan & Kamburoğlu 2008), Intacs	118	12	Femtosecond	3.8	1.7	3.9	74%, 1.6 Snellen lines	9% deposits
(Colin 2006), Intacs	57	12	Mechanical	1.5	2.8	3.7	62%, -	12% explanted
(Kanellopoulos et al. 2006), Intacs	20	12	Mechanical	3.4	2.5	2.9	-	5% perforated 30% exposure
(Alió et al. 2005, p.2), Intacs	26	12	Mechanical	3.2, 1 ring 1.9, 2 rings	2.4, 1 ring 2.3, 2 rings	4.6, 1 ring 5.2 2 rings	82%, 0.22 LogMAR 1ring 87%, 0.24 LogMAR 2 rings	None
(Hellstedt et al. 2005), Intacs	50	6	Mechanical	2.78	0	4.2	77%, 0.21 LogMAR	8% unsuccessful
(Levinger & Pokroy 2005), Intacs	58	12	Mechanical	2.84	1.37	3.44	12%, -	10% additional segment implantation
(Boxer Wachler et al. 2003), Intacs	74	20	Mechanical	2.4	-	-	45%, 0.17 LogMAR	1.3% extrusion
(Siganos et al. 2003), Intacs	33	11	Mechanical	1.3	-	3.2	76%, 0.17 LogMAR	3% vascularisation
(Colin et al. 2001), Intacs	10	12	Mechanical		2.7	4.6	-	None
(Colin et al. 2000), Intacs	10	6	Mechanical	2.1	1.5	4.8	-	8% explanted

SE (spherical equivalent), CDVA (corrected distance visual acuity), D diopter, mths months, dash (-) indicates not reported

Flattening of central curvature with ICRS implantation increases with smaller ring diameter and greater segment thickness. The penalty for using a smaller diameter ring is a greater potential for dysphotopsia. The triangular profile used in Ferrara and KeraRing ICRS is designed to reduce forward light scatter by total internal reflection of incident light, but further clinical studies are required to quantify dysphotopsia associated with ICRS implantation.

In a series with 12-month postoperative results of 50 consecutive femtosecond laser KeraRing ICRS cases reported from Turkey,(Coskunseven et al. 2008) approximately two-thirds of patients gained spectacle CDVA compared with pre-implantation levels (1 - 4 Snellen lines). Only 2 patients lost 2 lines of spectacle CDVA, and neither wanted the implants removed because of gains in UCVA. Overall improvement in mean keratometry was approximately 3D (50.6 ± 4 D pre ICRS; 47.6 ± 4.5 D post-ICRS) with larger gains for cases with a steeper initial shape (stage III, 3mm zone steep K > 53 D) in which thicker ICRS were implanted. Asymmetric ICRS implantation (asymmetric arc length and thickness in superior and inferior ICRS) or single ring implantation can be used in patients with reduced spectacle CDVA associated with high pre-operative coma (cone decentration). Results in a smaller series of 21 cases of femtosecond laser KeraRing ICRS implantation reported similar significant gains in overall higher order aberration levels for patients with high starting levels of coma (> 3 µm).(Shabayek & Alio 2007) A retrospective series of 173 femtosecond laser cut eyes comparing

Intacs SK and KeraRing SI6 (both with a 6mm diameter optical zone) observed comparable improvements in vision and keratometry, with no statistically significant differences between the two ICRS models.(Haddad et al. 2012)

Femtosecond ICRS implantation has a good safety profile. A recent multicenter retrospective review of 850 eyes with femtosecond KeraRing ICRS implantation using an Intralaser femtosecond laser for ring channel creation reported a 5.7% overall complication rate.(Coskunseven et al. 2011) Intraoperative complications did not result in failure to complete ICRS implantation. Incomplete ring channel formation was the commonest complication (2.7%). In these cases, ring channels can be completed manually allowing ICRS implantation to proceed. Endothelial perforation was evident in 0.6% cases. In this circumstance, channel creation 90µm superficial to the initial attempted depth can be completed 1 month after surgery. The target depth for femtosecond KeraRing implantation is 80% of corneal thickness at the location of the ring channel (5mm diameter). Ultrasound pachymetry was used in this study. Availability of more accurate regional pachymetry methods, OCT tomography in particular, may eliminate the risk of perforation. Postoperative complications occurred in 1.6% of cases. Within-channel migration of ring segments was noted in 7 eyes and treated successfully with repositioning and a sutured vertical incision closure. 4 cases of stromal thinning over the ICRS and 2 cases of corneal melting required implant removal. As with endothelial perforation, melting was attributed to inaccurate regional pachymetry and superficial channel creation in relatively

thin corneas. Infection (an infiltrate at the entry site) was seen in one case in this series and treated without ICRS explantation. Problems for this study are lack of acuity, refractive and keratometric outcome data. The authors also do not state the follow-up period studied or whether these were consecutive cases. Nonetheless, data from this and smaller prospective series indicate that sight-threatening complications are rare.(Coskunseven et al. 2011; Shabayek & Alio 2007)

Table 2.11 Summary outcomes using Keraring or Ferrara ICRS

Author, year, ring design	No. of eyes	Follow -up (mths)	Surgery	Mean change SE (D)	Mean change cylinder (D)	Mean change keratometry (D)	% gaining CDVA, mean gain	Complications
(Torquetti et al. 2014),Ferrara	36	120	Mechanical	-	-	2.99	67%, 0.16 LogMAR	_
(Alfonso et al. 2013), Keraring	41	6	Femtosecond	-	-	1.62	49%, 0.06 LogMAR	None
(Tunc et al. 2013), Keraring	30	12	Mechanical	5.16	-	4.95	93%, 0.34 LogMAR	None
(Alfonso et al. 2012), Keraring	56	6	Femtosecond	-	-	-	60%, 0.1 LogMAR	None
(Haddad et al. 2012), Keraring	107	12	Femtosecond	2.65	1.93	1.44	-, 0.08 LogMAR	-
(Gharaibeh et al. 2012), Ferrara	55	6	Mechanical	0.06	1.05	5.75	87%, 0.21	1.8% extrusion 3.6% infection
(Coimbra et al. 2012), Keraring	35	3	Femtosecond	2.58	3.92	3.07	82%, 0.15 LogMAR	None
(Ameerh et al. 2012), Ferrara	79	6	Mechanical	3.36	1.32	4.59	-, 0.14 LogMAR	-
(Ferrara et al. 2011), Ferrara	1073	23	Mechanical I 160° arc II 210° arc	I 1.72 II 4.58	-	I 3.46 II 3.82	I 80%, - II 69%, -	3.8% complication rate
(Kubaloglu et al. 2011), Keraring	96	6-18	Mechanical	3.62	-	5.01	91%, 0.42 LogMAR	58% deposits 1% extrusion
(Hamdi 2011), Ferrara	100	6	Mechanical	1.08	2.28	3.05	64%, -	13% complication rate
(Alfonso et al. 2011), Keraring	219	6	Femtosecond	-	-	-	57%, 0.11 LogMAR	None
(Kubaloglu, Sari, Cinar, Koytak, et al. 2010), Keraring	100	12	Femtosecond	2.83	1.33	2.76	85%, 3 Snellen lines	4% decentration 1% extrusion 1% perforation
(Pesando et al. 2010), Ferrara	130	37	Mechanical	5.51	-	3.59	98%, 0.19 LogMAR	3% explantation 0.76% perforation

(Torquetti et al. 2009),Ferrara	35	60	Mechanical	-	-	5.98	74%, 0.21 LogMAR	-
(Kwitko & Severo 2004),Ferrara	51	13	Mechanical	1.53	1.66	5.59		20% extrusion 2% infection

SE (spherical equivalent), CDVA (corrected distance visual acuity) dash (-) indicates not reported

2.5.2 Combined ICRS and CXL

ICRS implantation can be combined with CXL,(Coskunseven et al. 2009; Saelens et al. 2011; El-Raggal 2011; Chan et al. 2007; Ertan et al. 2009) but the treatment sequence is important: ICRS appears more effective in improving corneal shape before the cornea is stiffened with CXL. Coskunseven et al, in an RCT comparing CXL first and ICRS later (group 1) with ICRS first and later CXL (group 2), showed significantly greater improvements (mean 7 months follow-up) in spectacle CDVA (3 line gain [group 1]; 2 line gain [group 2], $p < 0.01$) and manifest astigmatism (2.48D mean absolute cylinder reduction [group 1]; 1.76 D reduction [group 2], $p < 0.05$) where ICRS was performed first.(Coskunseven et al. 2009) Simultaneous CXL and ICRS may be equally effective. El-Raggal showed a trend towards greater improvement at 12 months in mean K values where simultaneous ICRS and CXL was performed versus CXL 6 months after ICRS (50.2 ± 3.8 D to 44.9 ± 2.9 D simultaneous treatment; 50.4 ± 3.8 D to 47.3 ±3.5D delayed CXL, $p = 0.046$), although there were no differences in UDVA, CDVA or refractive error.(El-Raggal 2011) But this study was underpowered ($n = 8$ each arm). More evidence is required to determine the optimum interval between ICRS and CXL in combined treatment; but the practical advantages to combining ICRS with transepithelial treatment in particular are clear. An interesting variation here has been described by Selans et al who augmented stromal riboflavin penetration by injection into the ring channels prior to transepithelial CXL. (Saelens et al. 2011)

Table 2.12 Summary outcomes for combined ICRS and CXL

Reference, ring design	No. of eyes	Follow-up (mths)	Surgery	Mean change SE (D)	Mean change cylinder (D)	Mean change keratometry (D)	% gaining CDVA, mean gain	Complications
(El-Raggal 2011), Keraring	16	12	Femtosecond	-2.52	0.86	3.88	-	100% haze (CXL)
(Coskunseven et al. 2009), Keraring	48							
Group 1*	NR	13	Femtosecond	-4.15	1.76	4.26	-, 1.5 lines	-
Group 2	NR	13	Femtosecond	-4.24	2.48	3.98	LogMAR -, 3 lines LogMAR	-
(Saelens et al. 2011), Ferrara	7	12	Mechanical	-3.5	-	2.84	-, 0.26 (decimal)	Explantation n=1
(Chan et al. 2007), Intacs	12	3	Mechanical	-	1.25	1.13	-, 1 line (unspecified)	None
(Ertan et al. 2009), Intacs	25	5	Femtosecond	-	0.63	2.44	-, -	-

* Group 1: CXL then ICRS; group 2: ICRS, then CXL. NR, not recorded (numbers in each group). ICRS, intrastromal corneal ring segments; CXL, corneal cross-linking; D, diopter, dash (-) indicates not reported

2.5.3 ICRS implantation protocols

Inclusion criteria in Coskunseven's recent prospective series of femtosecond KeraRing ICRS implantation include a minimum central corneal thickness of 350 µm and 450 µm at the incision site.(Coskunseven et al. 2008) No upper limit for keratometry values was specified. Neovascularisation has not been reported after femtosecond KeraRing ICRS implantation and 5 mm diameter ICRS are within the block of tissue normally removed in any subsequent transplantation procedure. Where corneal thickness is adequate and there is no central scar, it is probably reasonable to consider ICRS implantation with CXL in patients with advanced stage III disease since there should be no increased risk of failure in any subsequent corneal transplant. But a stratified analysis of patients with contact lens fitting problems associated with steep keratometry is required to determine whether ICRS is a viable alternative to corneal transplantation for this group or whether there is an upper limit to the Kmax for ICRS. For the present, limits for ICRS implantation are probably best defined by Coskunseven's pachymetric inclusion criteria above.(Coskunseven et al. 2008)

2.5.4 Thermal keratoplasty

Thermal keratoplasty has been proposed as a possible alternative to ICRS for gross corneal shape correction in advanced keratoconus. The underlying principle is that above heat causes corneal collagen fibers to undergo a degree of shrinkage and reformation, resulting in a change in corneal

curvature. Conductive keratoplasty (CK) was the original method of thermokeratoplasty, involving a thin probe penetrating to 90% corneal depth delivering radiofrequency energy to the stroma. The resistance to current flow within the stroma generates the required heat and tissue effect. CK was previously described as a treatment for simple hyperopia in which mid-peripheral stromal shrinkage caused central corneal steeping.(McDonald et al. 2002) As a treatment in pathological corneas, Kato et al treated 21 advanced keratoconic eyes using pre-operative topography to guide CK spot application (with intraoperative keratometric monitoring). Although large initial shape improvements were obtained, almost complete regression was seen within 3 months: mean keratometry values were 55 ± 8 D at baseline, 45 ± 9 D at 1 week, 50 ± 7 D at 1 month and 54 ± 7 D at 3 months.(Kato et al. 2010)

A non-contact method of thermokeratoplasty was reported more recently by Celik et al using a radiofrequency-generating device held just above the eye to deliver of a ring of microwave energy to the stroma.(Celik et al. 2015) In this study, 24 eyes with progressive keratoconus were treated with microwave thermokeratoplasty following by immediate accelerated CXL (30 mW/cm^2 irradiation for 3 minutes; total dose of 5.4 J/cm^2). Although the desired reduction in keratometry was produced without significant side-effects, there was early and complete regression of the thermokeratoplasty effect by 12-months post-operatively.

2.5.5 Fine corneal shape adjustment – photorefractive keratectomy

Combination with CXL may allow safe application of surface excimer laser ablation techniques to fine tune corneal shape in keratoconus. To date, topography guided photorefractive keratectomy (PRK) has been studied in combined therapy (Table 2.13). But wavefront ablation would be a viable alternative in cases with good aberrometry data.

For simultaneous combined treatment, in which CXL is applied immediately after PRK, the aim is to improve CDVA by reducing irregular astigmatism rather than to correct spherocylindrical error fully. Reasons for this are the requirement for a 400µm residual stromal bed *after ablation* to allow safe CXL, and the danger of hypermetropic overcorrection if spherical equivalent reductions induced by CXL are not anticipated. Simultaneous combined treatment has clear advantages for patient comfort (the epithelium is only removed once), but takes no account of improvements in corneal regularity and spectacle CDVA that might normally be produced by CXL alone.

In a large comparative case series with minimum 2 year postoperative follow-up, Kanellopoulos (Kanellopoulos 2009) compared outcomes of 198 eyes treated with topography guided PRK followed immediately by CXL (simultaneous combined treatment) with an earlier series of 127 eyes treated with topography guided PRK a minimum of 6 months after CXL (sequential combined treatment). Simultaneous combined treatment produced greater improvement across a range of measures: LogMAR CDVA improved from 0.39 ± 0.3 D to 0.11 ± 0.2 D, with a reduction in spherical equivalent of -3.2 ±

1.4 D and mean keratometry of -3.5 ± 1.3 D. This compares with the sequential group's CDVA improvement from 0.41 ± 0.3 D to 0.16 ± 0.2 D, spherical equivalent reduction of -2.5 ± 1.2 D and mean keratometry reduction of -2.75 ± 1.3 D. Haze scores were also significantly better for simultaneous combined treatment. 20 second intraoperative applications of mitomycin C were used throughout, and the maximum ablation depth was limited to 50 µm. The essential problem for this comparison is that the time interval between CXL and PRK for sequential treatment was not specified, and may have been considerably shorter than the 2 year period in which refractive results typically continue to improve after CXL alone.(Caporossi et al. 2010) Further study is required to quantify any gain in spectacle CDVA over CXL alone for simultaneous combined CXL and PRK, and to determine whether increased haze scores for sequential combined treatment observed by Kanellopoulos, are still evident where PRK is performed later in the post CXL wound healing cycle, a minimum of 2 years after treatment.

Table 2.13 Summary outcomes for combined photorefractive keratectomy and CXL

Author	Study Design	No. of eyes	Surgical Procedures	Follow-up	% eyes gain ≥ 1 line CDVA	Mean gain CDVA (LogMAR)	Remarks
(Shetty et al. 2015)	CS	29	Simultaneous topography-guided PRK followed by CXL	12 months	45%	0.21	No complications
(Sherif et al. 2015)	CS	20	Simultaneous topography-guided PRK followed by CXL	12 months	75%	0.19	30% haze at 3 months
(Fadlallah et al. 2014)	CS	140	Simultaneous non-topography-guided PRK followed by CXL	24 months	N/A (Aiming to correct UDVA)		_
(Alessio et al. 2014)	CS	17	Simultaneous topography-guided PRK followed by CXL	48 months	Confocal outcomes only	_	_
(Sakla et al. 2014)	CS	31	Simultaneous topography-guided PRK followed by CXL	12 months	100%	0.22	No complications
(Mukherjee et al. 2013)	CS	22	Simultaneous transepithelail (manifest-guided) PTK followed by CXL	12 months	95%	0.11	No complications
(Kymionis et al. 2009)	CS	14	Simultaneous topography-guided PRK followed by CXL	Range: 3 -16 months	44 % (Snellen)	0.10	No complications
(Kanellopoulos 2009)	CS	127 sequential 198 simultaneous	Sequential (> 6 months after CXL) and simultaneous topography-guided PRK followed by CXL	Range: 24 - 68 months	Sequential: 0.25 Simult.: 0.28	_	Significant haze in 19 eyes (17 of sequential and 2 of simultaneous group)
(Kanellopoulos & Binder 2011)	CS	32	Simultaneous topography-guided partial transepithelial PRK and CXL	27 months	_	_	2 of 32 eyes had corneal progression, corneal haze grade 2 in 2 of 32 eyes
(Tuwairqi & Sinjab 2012)	CS	22	Simultaneous topography-guided PRK and CXL	12 months	N/A (Aiming to correct UDVA)	-0.01	No complications
(Lin et al. 2012)	CS	217 (only 72	Simultaneous topography-	12 months	64%	_	2 eyes had sufficient haze,

		completed 12 months f/u)	guided PRK and CXL				1 eye had herpetic keratitis, 2 eyes had PKP, 2 eyes had re-treatment
(Kymionis et al. 2012)	Nonrandomized, clinical trial	17 (PRK and CXL), 17 (CXL)	Transepithelial topography-guided PRK and CXL/CXL	24 months	42.1%	0.11	No ocular adverse events
(Kapasi et al. 2012)	Prospective, comparative	34	t-PTK (group 1) and mechanical epithelial debridement (group 2) during CXL	1 months	-	0.03 (decimal)	No complications
(Kanellopoulos & Asimellis 2014)	CS	175	Simultaneous topography-guided PRK and CXL	36 months	Epithelial remodelling outcomes only		No complications

PTK, phototherapeutic keratectomy; PRK, photorefractive keratectomy; t, transepithelial; CXL, corneal cross-linking

2.5.6 Refractive correction – phakic intraocular lens implantation

For patients with a stable corneal shape and regular astigmatism underlying good CDVA, phakic intraocular lens (pIOL) implantation can be used to complete functional visual rehabilitation. A number of recent papers have reported effective refractive correction using pIOLs in keratoconus, (post-operative spherical equivalent range -0.08 ± 0.4 to +0.1 ± 0.4; 64-67% within 0.5 D and 84-100% within 1 D of target refraction)(Izquierdo et al. 2011; Alfonso et al. 2008; Kamiya et al. 2011; Sedaghat et al. 2011; Alfonso et al. 2010; Kato et al. 2011) and for post-keratoplasty ametropia.(Alfonso et al. 2009) Of the pIOLs available,(Kohnen et al. 2010) the Visian ICL (Staar Surgical, Monrovia, CA) offers the longest safety track record for an injectable pIOL and is available in a wide range of powers (including toric correction up to 6 D). Pesando et al reported retrospective 10-year follow-up data in 59 ICL-implanted hypermetropic eyes, showing a mean endothelial cell loss of 4.7%, mostly occurring within the first few weeks of implantation and remaining almost unchanged thereafter.(Pesando et al. 2007) Edelhauser et al reported prospective, multicenter, 4-year follow-up data on 526 eyes with a 2%-3% cell loss rate over the first 3 years, followed by a cell increase of 0.1% between years 3 and 4, suggesting that endothelial remodeling and stability may have been achieved.(Edelhauser et al. 2004)

Combined ICRS and pIOL implantation has been described,(Moshirfar et al. 2011; Cakir & Utine 2010; El-Raggal & Abdel Fattah 2007) but refractive correction with pIOLs is highly predictable,(Huang et al. 2009) whereas the

refractive effect of ICRS implantation is highly variable.(Piñero et al. 2009; Kubaloglu, Cinar, Sari, Koytak, et al. 2010; Rabinowitz et al. 2006; Kubaloglu, Sari, Cinar, Cingu, et al. 2010; Coskunseven et al. 2009; Saelens et al. 2011; El-Raggal 2011; Chan et al. 2007; Ertan et al. 2009) Gross shape correction with ICRS implantation followed by CXL (with fine shape correction with PRK if necessary) should, therefore, precede pIOL implantation as a logical pathway to visual rehabilitation in grade II-III keratoconus.

3 Shape stabilisation - quantifying epithelium-off riboflavin absorption

3.1 Introduction

Corneal collagen cross-linking (CXL) is performed by irradiating riboflavin-soaked corneal tissue with an ultraviolet A (UVA) light source (370 nm). The riboflavin acts both as a photosensitiser to encourage UVA-induced corneal stiffening (cross-linking), and a shield to reduce UVA levels at the endothelial level below the cytotoxic threshold. The original Dresden protocol described removal of the corneal epithelium with application of riboflavin 0.1% drops every 2 minutes for 30 minutes prior to, and during, UVA treatment (3 mW/cm^2 power for further 30 minutes, total energy dose 5.4 J/cm^2).(Wollensak, Spoerl, et al. 2003a)

3.2 Two-photon fluorescence microscopy

The optimum riboflavin soak duration and concentration in the cornea required to achieve effective collagen cross-linking is unknown. Originally, slit-lamp biomicroscopy was used in patients to check for riboflavin fluorescence in the aqueous as a surrogate marker of complete corneal stromal penetration. Confocal (i.e. single-photon) and two-photon fluorescence (TPF) microscopy have both been used to quantify the concentration and 3-dimensional distribution of riboflavin in feline, chick embryo and porcine corneas.(Cui et al. 2011; Zhang et al. 2012; Kampik et al. 2010; Søndergaard et al. 2010) Single-photon fluorescence microscopy describes the principle of

a single photon of light exciting a fluorophore from one state (usually the ground state) to a higher energy state. An example of single-photon fluorescence microscopy is shining blue light onto a fluorescein stained cornea to emit green light (Figure 3.1). The same energy can be delivered by the absorption of two photons of light, each of double the wavelength and half the energy (energy is inversely proportional to wavelength). The probability of the near-simultaneous absorption of two photons is very low. Therefore a high flux of excitation photons is typically required, usually from a femtosecond laser.

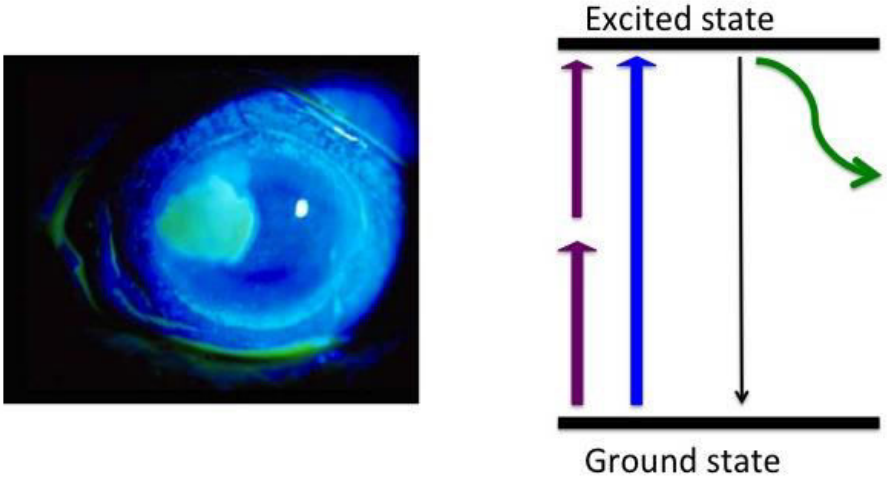

Figure 3.1 Fluorescence microscopy

Left: Photograph of single-photon fluorescence microscopy with blue light (490 nm) causing excitation of fluorescein with the subsequent emission of light with a longer wavelength (green, 520 nm) and, therefore, lower energy. Right: Two-photons of light (violet arrows) each with double the wavelength (490 x 2 = 980 nm), and therefore each with half the energy, can deliver the same total energy as a single photon of blue light. This process is called two-photon fluorescence

Advantages for TPF include reduced bleaching and phototoxicity outside the focal point (Figure 3.2), making it easier to obtain quantitative, 3D measurements, and reduced attenuation of the excitation light in the target medium due to its longer wavelength.

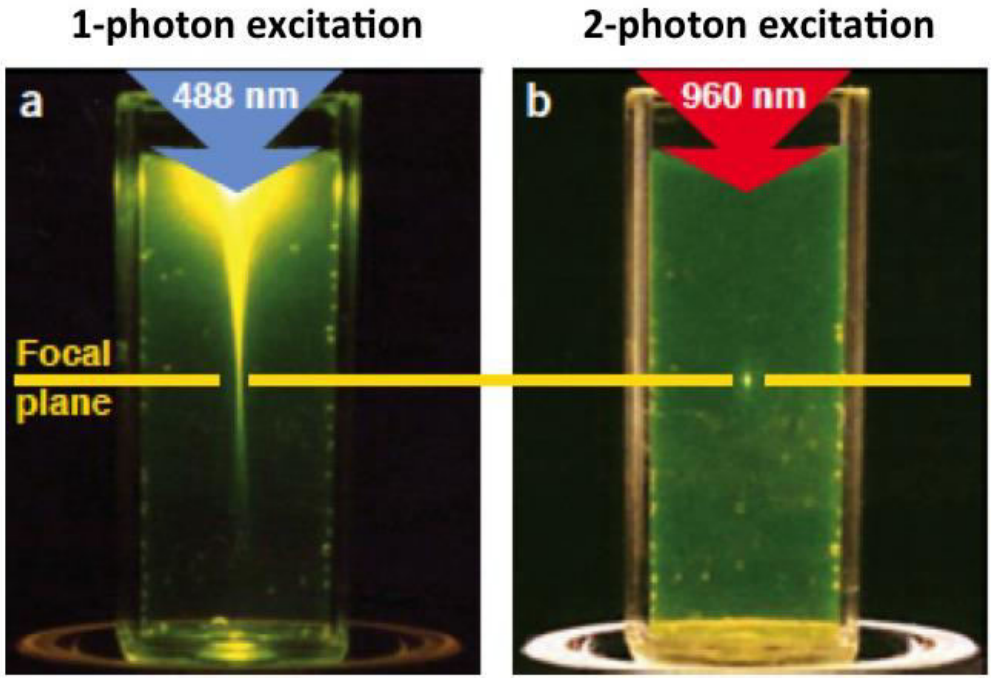

Figure 3.2 Excitation inside and outside the focal point

Localization of excitation by two-photon excitation within a cuvette filled with fluorescein solution. (a) Single-photon excitation of fluorescein by focused 488-nm light. Note the bright intensity of fluorescence at the top of the cuvette as soon as the light enters the fluorescent solution, outside of the focal plane (i.e. not where the fluorescence is intended) (b) Two-photon excitation using focused femtosecond pulses of 960-nm light. Note that fluorescence excitation is now restricted to a small localized area at the focal plane (black arrow) (Reprinted by permission from Macmillan Publishers Ltd: Zipfel et al. Nature Biotechnology 21, 1369-1377, copyright (2003))

Near-absence of TPF signal attenuation has been demonstrated within a microfluidic system imaging at depths up to 37 μm.(Schafer et al. 2007) In tissue, however, a number of additional factors, principally scattering and

aberration, may cause TPF signal loss with increasing scan depth.(Cui et al. 2011; Zhang et al. 2012; Kampik et al. 2010) While acknowledging this problem, Cui et al. made no correction for signal attenuation with increasing scan depth in their application of TPF imaging to the measurement of riboflavin concentration in (feline) corneas.(Cui et al. 2011)

In this chapter I present work investigating the use of TPF microscopy in an ex vivo whole globe animal model to measure riboflavin concentration at different depths within the cornea.

3.3 Materials and methods

Ethical approval for corneal two-photon fluorescent microscopy studies in an ex vivo model was granted by University College London Institute of Ophthalmology (ref. 10/H0106/57-2012ETR27).

3.3.1 Riboflavin spectrophotometry

The fluorescence absorption and emission spectra of 0.1% w/v riboflavin 5'-monophosphate (1.45 mg/ml) in saline and hydroxypropyl methylcellulose (HPMC) (VibeX Rapid, Avedro, Mass. USA) were measured by spectrophotometery (UV-3101PV UV-VIS-NIR; Shimadzu, Kyoto, Japan). Riboflavin exhibited a bimodal absorption spectrum with a lower peak at 374 nm, and a higher peak at 445 nm (Figure 3.3). The maximum emission wavelength was 524 nm.

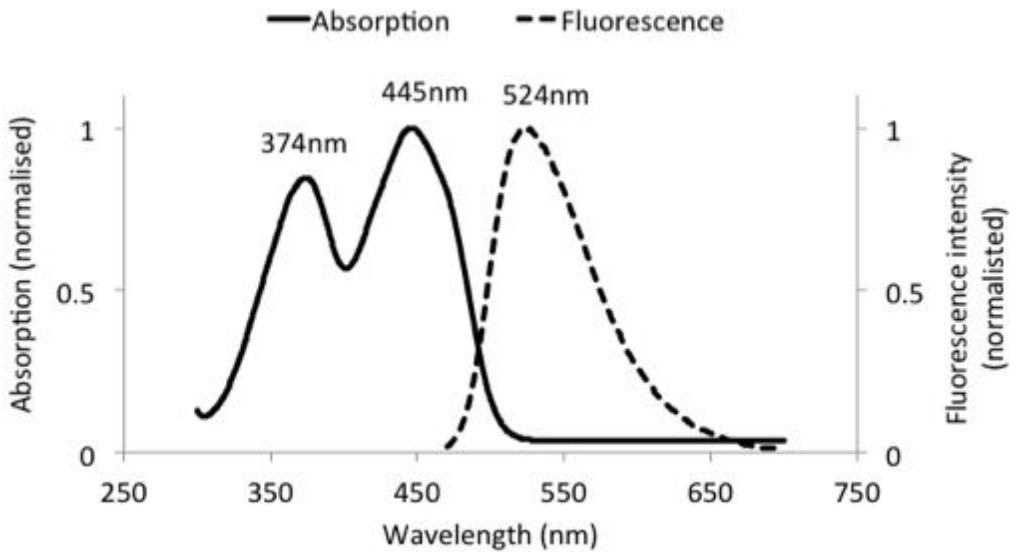

Figure 3.3 Riboflavin absorption and emission spectra

The absorption and fluorescence emission spectra of dextran-free 0.1% riboflavin 50-monophosphate in saline and HPMC (Avedro, Inc.). Absorption peaks are seen at 374 nm and 445 nm; a fluorescence emission peak is seen at 524 nm when excited at 445 nm.

3.3.2 Two-photon microscope set-up

A Ti:Sapphire laser (Chameleon Vision II, Coherent, CA, USA) equipped with a prism based Group Velocity Dispersion (GVD) compensation unit was used as the excitation laser source. The laser has a tuning range from ~680 nm up to 1080 nm, operating with a 140 femtosecond pulse duration and 80 MHz pulse repetition rate. The excitation laser beam was guided to a Leica DM6000CS upright microscope via an Electro-Optical-Modulator (EOM) to control laser output and coupled into the Leica SP8 Spectral Scan-head (Leica Microsystems, GmBH) where it passes through two galvoscanners, allowing scanning in the x-y plane, before being focused into the sample by a Leica 25X /0.95 NA water immersion objective (coverslip corrected) that

facilitated a working depth of up to 2 mm. Theoretical (full-width half-maximum) resolutions were calculated at 0.34 µm laterally and 1.4 µm axially. Employing the two-photon fluorescence principle, I used excitation light of wavelength 890 nm to correspond with the highest absorption wavelength of riboflavin (i.e. 445 x 2 = 890 nm, Figure 3.3). The emitted fluorescence passed through an 800 nm short pass dichroic filter (Chroma Technology Corp., Vermont, USA), which was then spectrally separated by a Leica Acousto-Optic-Beam Splitter (AOBS®) before passing to the Leica HyD® detectors.

3.3.3 Sample preparation

Freshly enucleated porcine eyes (First Link Ltd., Wolverhampton, UK), stored within a sealed bottle of phosphate buffered saline (0.85% NaCl, 0.01M NaPhos, pH 7.2-7.4), were transported on ice to arrive within 24 hours of death. Rabbit globes, more closely matching human corneal epithelial thickness were additionally used to confirm findings in epithelium-on experiments. Each globe was secured within a custom-made perspex cylinder to ensure stability on the microscope stage (Figure 3.4A). A custom reservoir chamber for riboflavin (a coverslip glued onto two rubber O-rings) was placed coverslip down and filled with ~400 µl of riboflavin solution. The epithelium was either left intact or debrided using a hockey stick scraper (e.janach srl, Como, Italy), the cornea of the intact globe was apposed to the O-ring and immersed in riboflavin and a timer was started (time = 0 minutes). Relying on surface tension to keep the O-ring/coverslip and cornea apposed, the assembly was then inverted, creating a bubble-free, sealed lake of riboflavin

over the cornea and beneath the coverslip ready for imaging (Figure 3.4B). The assembly was then positioned within a custom-built recessed stage to house the cylinder-supported globes beneath the objective. The first TPF z-stack was started at time = 2.5 minutes.

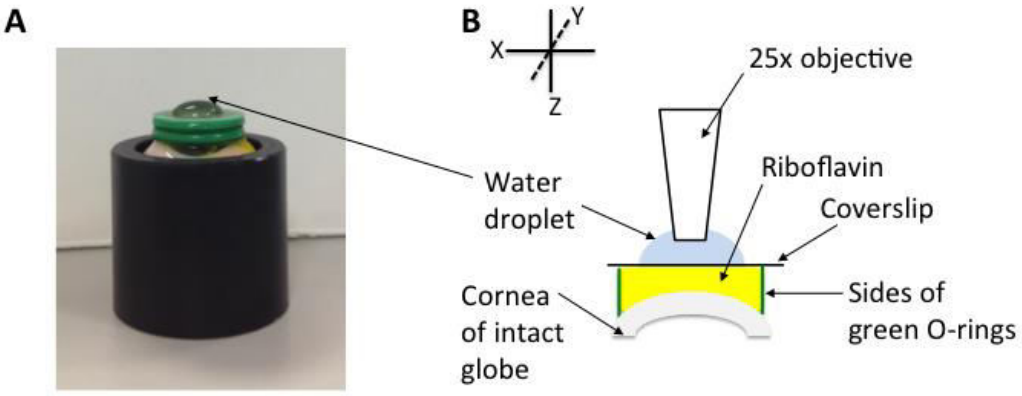

Figure 3.4 Sample and stage set-up

Intact globe set-up on microscope stage. (A) Perspex cylinder used to secure whole globe on the microscope stage with a sealed, air bubble free reservoir of riboflavin on top of the cornea (B).

3.3.4 Imaging protocol and concentration calibration

All TPF experiments were performed with the room lights at a minimum. The microscope stage and objective were enclosed in opaque Perspex casing to reduce incident light being detected. TPF excitation light of 890 nm wavelength was chosen to correspond with the highest riboflavin absorption peak (445 nm) as determined by spectrophotometry. The average laser output power at 890 nm was 33 mW at the objective with minimal fluctuation in average power being observed during the course of any given day's

experiment. Emitted riboflavin fluorescence was collected between 525 nm and 650 nm, to avoid overlap with the absorption spectrum of riboflavin. I confirmed the absence of any reabsorption of this emitted light by demonstrating no change in measured TPF signals with excitation depth in homogeneous riboflavin solutions within a well slide (Figure 3.5).

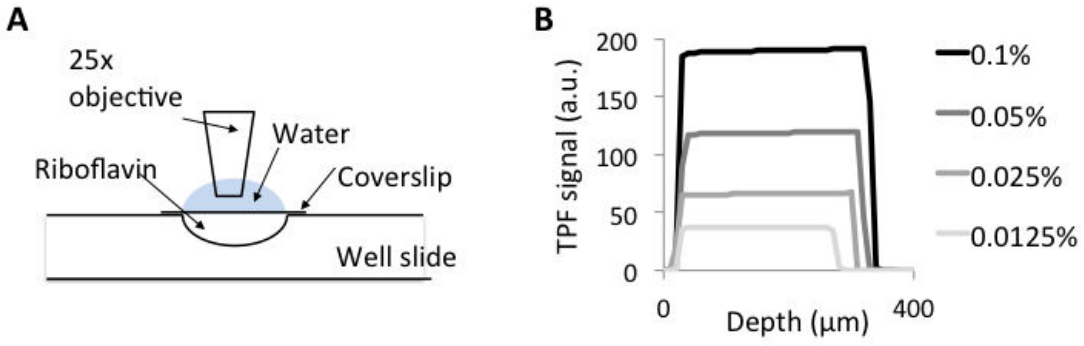

Figure 3.5 Confirming absence of reabsorption of emitted light
TPF signal calibration for riboflavin in solution. (A) Well slide setup beneath a coverslip-corrected objective. (B) Serial riboflavin dilutions from 0.1% to 0.0125% (wt/vol) produced constant TPF signals with-depth through the drop sample.

Serial z-stacks at 10 µm intervals were started within the pre-corneal riboflavin reservoir at approximately 30 µm above the corneal surface to provide a reference TPF signal level for this 0.1% w/v solution. This level provided a signal-to-concentration calibration for each eye. Z-stacks were acquired through the depth of the cornea (scan rate: 600 Hz, 512 x 512 pixels, image size: 445 µm x 445 µm, line average: 2, pinhole wide open). An iterative approach to developing this protocol was used, balancing the need for sufficient axial resolution with 10 µm stacks and a fast total acquisition time

(approximately 130 seconds) to limit the possibility to riboflavin migration during each whole corneal scan. Each run was repeated every 2.5 minutes, up to 20 minutes, and then every 5 minutes, up to 60 minutes.

3.3.5 Confirming TPF signal attenuation

To demonstrate that TPF signal attenuation must be occurring when imaging *en face*, I excised corneal strips from riboflavin-soaked intact globes. A cross-sectional (sagittal) surface of each strip was placed face-down onto a microscope slide and a coverslip was placed on top. A single TPF image (using a 10x 0.30 NA objective) was acquired of a plane approximately 50 µm below the coverslip. Excised corneo-scleral buttons were also imaged from both directions, draped over a scleral contact lens to avoid stromal folds. A coverslip was then placed directly on top, applanating a central area of the cornea without coupling fluid, and z-stacks of TPF images were acquired. No immersion fluid was used for either excised tissue experiment to minimise the migration of riboflavin within the cornea prior to imaging. The time taken to excise and mount the tissue prior to imaging was under 2 minutes. Results from both these experiments were compared with z-stacks acquired in intact globes.

3.3.6 TPF signal correction

The average raw TPF signal data for each image in a z-stack were exported in .CSV format (Excel for Mac, 2011; Microsoft Corp) and plotted against corneal depth for measurements with corneas soaked for increasing times. A

uniform concentration of riboflavin was judged to have been achieved when the posterior corneal TPF signal stopped increasing (typically after ~50 minutes). The z-stack data for this condition was then used to provide the attenuation reference for this eye (i.e. each eye provided its own internal reference). A detailed example using this methodology to correct the attenuation at earlier time points is shown in Figure 3.6.

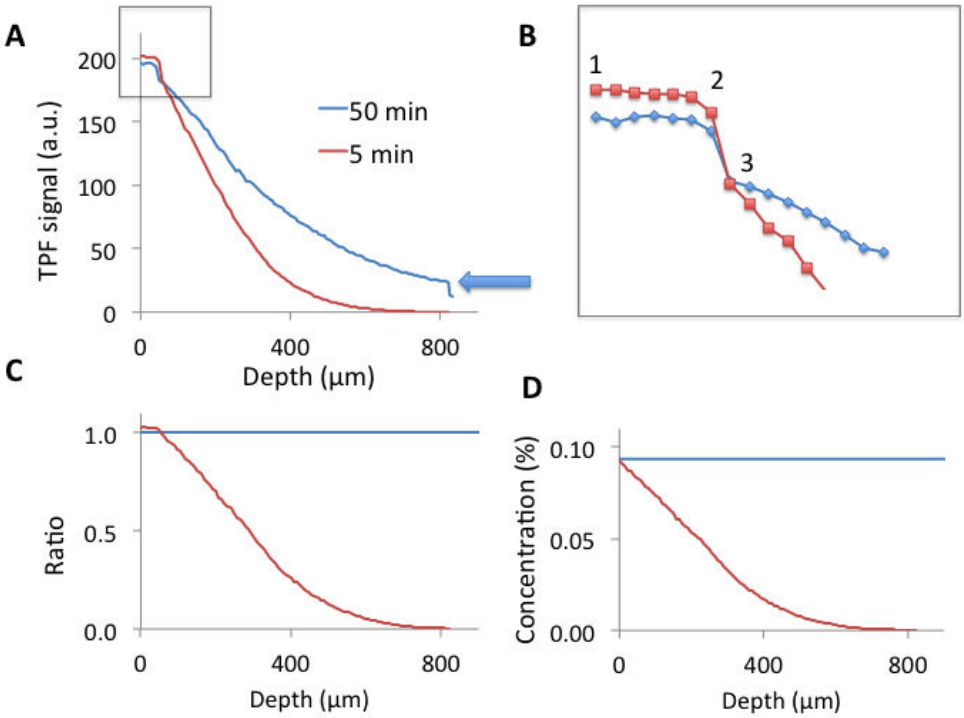

Figure 3.6 Signal attenuation correction example

Example methodology of correcting TPF signal attenuation when imaging epithelial debrided intact globes. (A) Spatially (x-y) averaged raw TPF data for 5- and 50-minute soak durations in the same eye plotted against corneal depth (z). After 50 minutes the TPF signal recorded at the back of the cornea (blue arrow) plateaued, with no further increases observed at 55 or 60 minutes (plots not shown). This indicated the tissue was completely and uniformly soaked, with attenuation of the signal preventing a flat signal plot. This 50-minute plot was used to model the signal attenuation. (B) Enlarged box insert from (A) delineating the changes in signal slope at the beginning of the z-stack: 1 to 2 is within the precorneal riboflavin reservoir; 2 to 3 is part- cornea, part-reservoir; 3 onwards, the whole of the image is within the cornea. (C) All TPF signal readings at 5 minutes were then divided by the reading for the corresponding depth in the 50-minute plot (uniformly saturated), giving a uniform corrected TPF signal level throughout the cornea for the 50-minute plot and a corrected slope for the earlier time point. (D) The y-axis of the plot was converted to riboflavin concentration by normalizing to the TPF signal level within the reservoir of 0.1% riboflavin solution. The x-axis of the plot was shifted so that a depth of 0lm corresponded with the start of the cornea.

3.4 Results

3.4.1 Proof of TPF signal attenuation

In epithelial debrided controls (i.e. no riboflavin) negligible fluorescence was detected. Cross-sectional TPF images (Figure 3.7) taken of excised corneal strips demonstrated near-uniform signals after 40 minutes' soak time. After 60 minutes' soak time to ensure uniform saturation, the TPF signal was seen to diminish with depth in the cornea in an excised corneo-scleral button (Figure 3.8). Although the relative amplitude of the TPF signal was reduced compared with the intact globe image prior to excision, reversing the tissue (i.e. endothelial side up) did not reverse the slope of the TPF signal loss, confirming that the decrease in TPF signal when imaging through the z-axis is due to signal attenuation rather than a depth-dependent drop in riboflavin concentration.

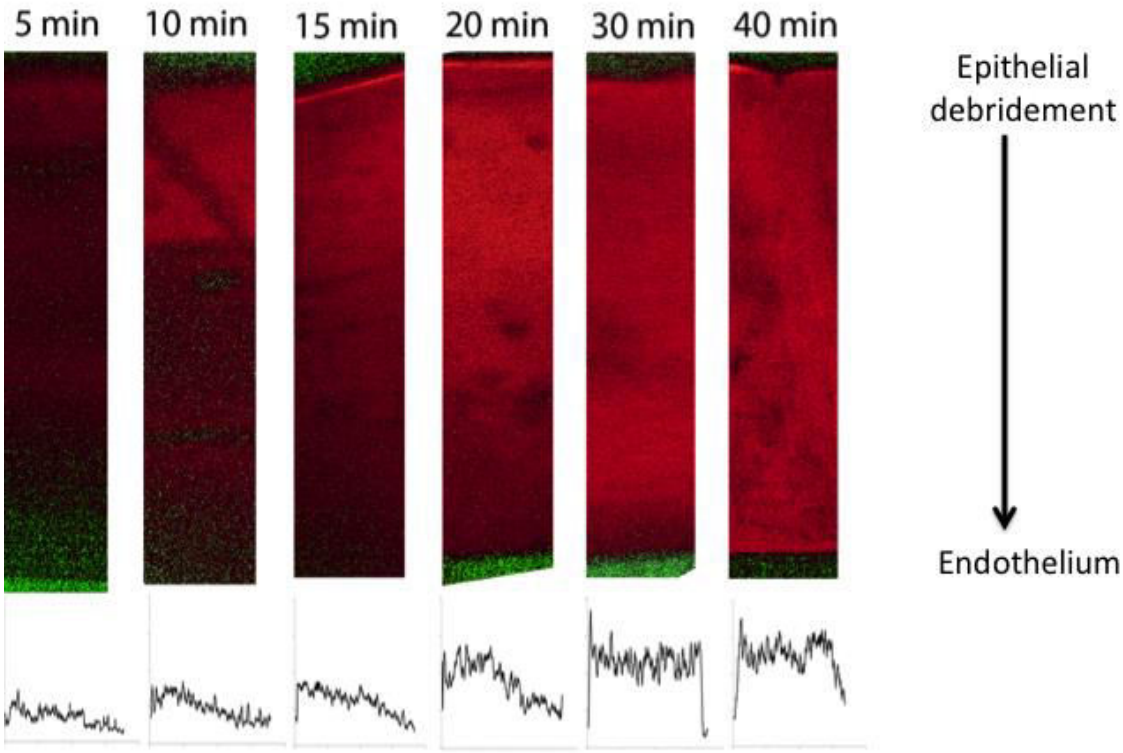

Figure 3.7 Cross-sectional TPF images

TPF images of cross-section of excised corneal strips (epithelium-off) showing increasingly uniform TPF signal with longer soak times. In the Leica imaging software the saturation spectrum increases from green (zero fluorescence) to black to orange to red]. At 5 minutes, low levels of fluorescence are detected as indicated by the dim red colour. Compare this with scans performed after more prolonged soak duration in which the signal increases (brighter red), as well as the signal remaining more uniform in the posterior cornea. Plots of TPF signal variation across the sectioned corneal specimens, produced using Java-based imaging software (ImageJ, 1.47v, http:// imagej.nih.gov.ij; provided in the public domain by the National Institutes of Health, Bethesda, MD, USA); are shown below each strip.

These images confirm that the signal drop observed with increasing depth in uniformly soaked corneal specimens on z-stack imaging was attributable to signal attenuation rather than any variation in riboflavin concentration with depth. Excising strips of cornea was inevitably complicated by aqueous loss which is likely to wash and dilute some of the riboflavin from the tissue. In addition significant distortion of the tissue was observed when laid face-up on a slide (the images presented have been rescaled to the thicknesses observed on z-stack imaging prior to excision). This method is not suitable for quantifying TPF signals.

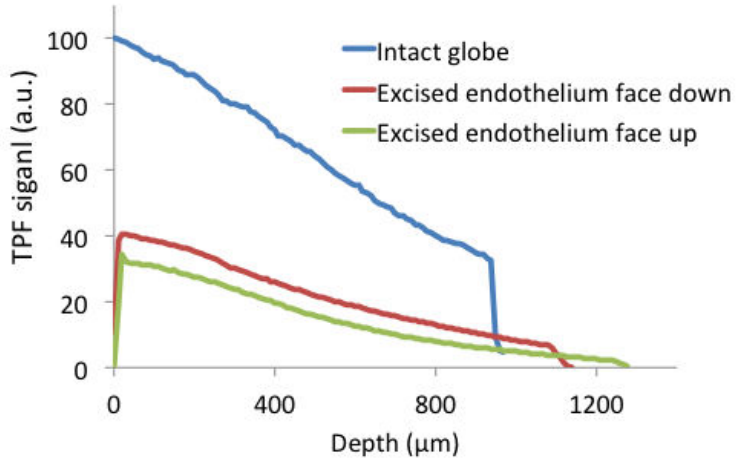

Figure 3.8 Confirming signal attenuation from both tissue sides

The aim of this figure is to show that the same signal attenuation with depth is produced whether imaging epithelium to endothelium, or upside down (endothelium to epithelium).
The blue plot shows the TPF signal achieved imaging coronally through a fully soaked epithelial-debrided whole globe. The signal is seen to decrease with increasing depth through the stroma.
The corneoscleral button was then excised from this globe and draped over a scleral contact lens (endothelium down) to maintain relative corneal curvature (with a coverslip on top) before repeating the TPF z-stack. The same decrease in signal (red plot) is produced, although at a lower signal amplitude, attributable to increased light scatter when the corneal tissue architecture is distorted, despite trying to minimize this with a contact lens support.
The button was then re-laid endothelium facing up (green plot). Note that the slope does not reverse when the same corneal specimen is reimaged endothelium face-up. This is further evidence that the drop in TPF signal level with increasing tissue depth on z-stack images of a uniformly soaked specimen is attributable to signal attenuation rather than any variation in riboflavin concentration. The further small drop in signal amplitude when the same specimen is reverse mounted (difference between red and green plots) is attributed to the same tissue distortion effects, also causing bunching of the tissue such that the thickness appeared to increase as compared to imaging the globe intact.
Note that the Y-axis TPF uses an arbitrary unit (a.u.) meaning that this particular plot should not be compared for absolute signal amplitude with other plots.

3.4.2 Time and dose-dependent corrected corneal riboflavin concentrations (epithelium-off)

In epithelial-debrided samples, after correcting for this signal attenuation, I observed that TPF signals increased with longer riboflavin soak duration, with the mean (± SD) maximum tissue concentration recorded at 0.094 (±0.001) % w/v [1.36 mg/ml] (Figure 3.9, Figure 3.10). Uniform riboflavin absorption across the entire corneal depth was achieved after a minimum 50 minutes (range 50–55 minutes). Following a 30 minute soak, as used in the standard epithelium-off CXL protocol, a mean stromal concentration of 0.086 (±0.001)% w/v [1.25 mg/ml] was achieved at a depth of 300 µm. Half this concentration (0.043 [±0.014]% w/v, 0.62 mg/ml) was observed within the first 5 minutes. Without correcting for attenuation, the concentration after 30 minutes at 300 µm was calculated at 0.06%.

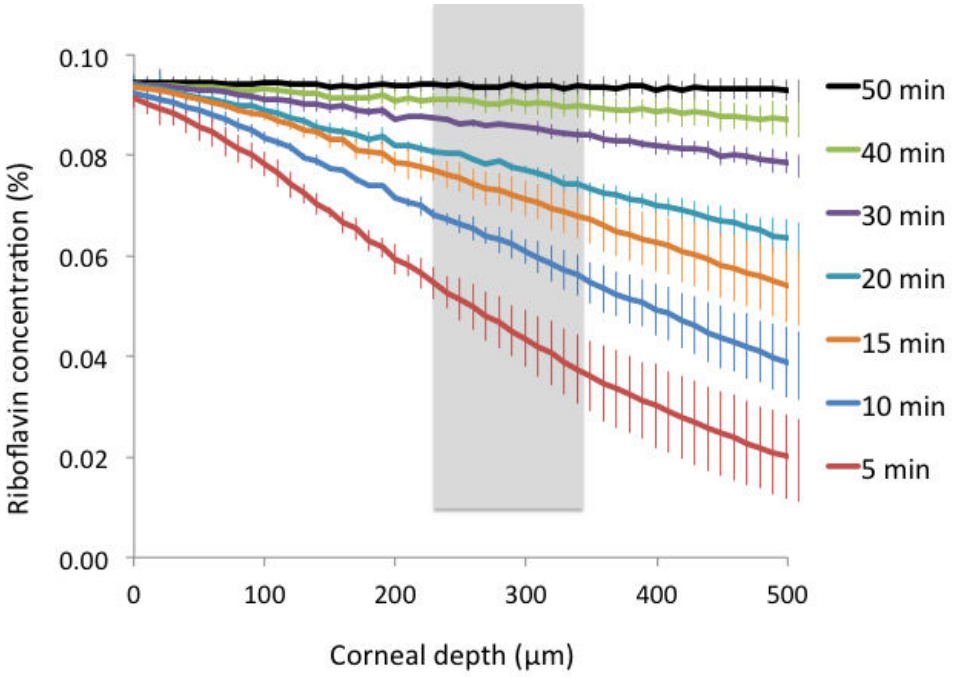

Figure 3.9 Riboflavin concentration with depth (epithelium-off)

Mean riboflavin concentrations, corrected for TPF signal attenuation, in epithelial debrided samples, presented over a 500 µm depth corresponding to the approximate thickness of a human cornea after epithelial removal (n = 4, standard deviation error bars). The shaded box highlights the demarcation zone between 250 and 350 lm commonly seen after epithelium-off corneal cross-linking in human corneas.

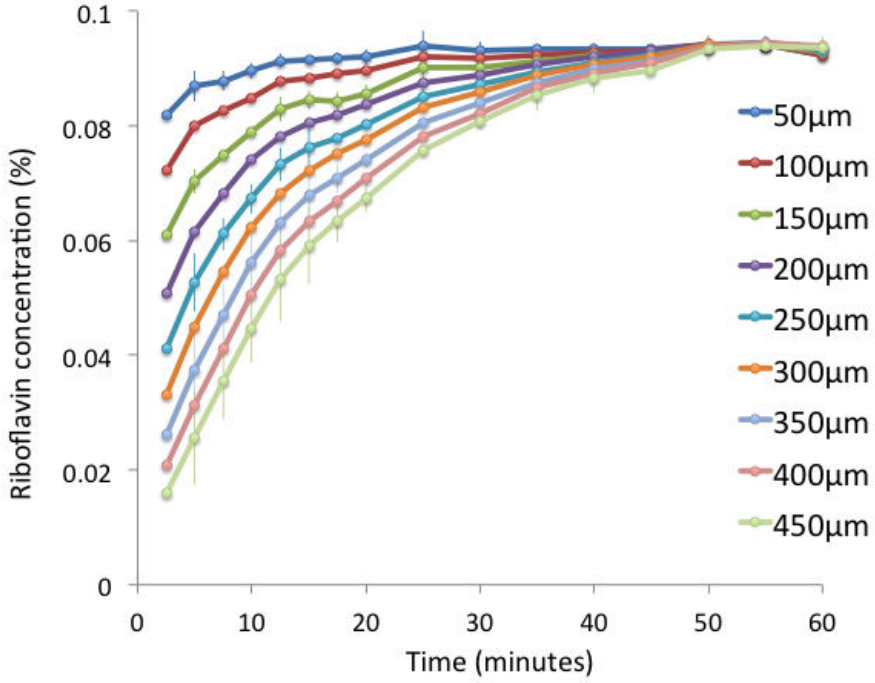

Figure 3.10 Depth-specific changes in riboflavin concentration with time

Mean changes in corneal riboflavin concentration in epithelial-debrided samples, corrected for TPF signal attenuation, at different depths (n = 4, alternate plot standard deviation error bars).

3.4.3 TPF signal attenuation through an intact epithelium

Replicating the above protocol through an intact epithelium I observed significant, and variable TPF signal attenuation from the epithelium itself. Figure 3.11 shows TPF signals achieved when imaging through a reservoir of riboflavin above the globe, mimicking my original set-up. TPF signals within the cornea can be seen to rise with increasing time, along with a drop in signal within the reservoir as the dye moves from the reservoir into the cornea. However, the peak tissue signal even after soaking for 2 hours was approximately one-tenth of that in the reservoir. Removing the epithelium from the same globe and immediately reimaging the underling stroma yielded an almost 4-fold increase in TPF signal (Figure 3.11, epithelium-off plot). This epithelial-masking effect was observed in all imaged eyes. There was no

consistent ratio between the signal achieved before or after epithelial removal, nor within the same eye when imaging through varying epithelial thickness at different locations on the test corneas.

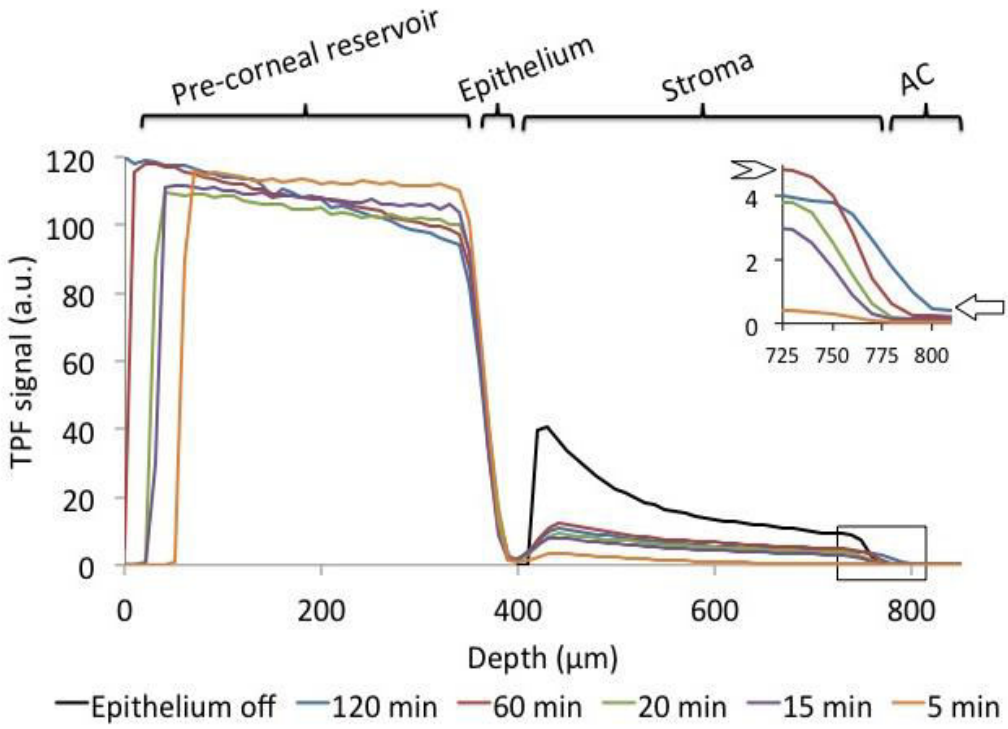

Figure 3.11 TPF signal attenuation through an intact epithelium

Two-photon fluorescence (TPF) signal of ParaCel riboflavin solution (Avedro Inc., Waltham, MA, USA) imaged through an intact rabbit epithelium. Insert magnifies the transepithelial signals at the back of the cornea revealing a peak at 60 minutes (chevron), before dropping by 120 minutes. Rising TPF signal within the anterior chamber (arrow) confirms the presence of a third compartment for riboflavin. AC, anterior chamber. NB. Absolute TPF signal varies depending on laser power and detector gain settings, explaining the differences between Y-axis scale above compared with figures 2.6 & 2.8).

Figure 3.11 above also shows that the signal within the epithelium itself was consistently near-zero. This can also be seen graphically looking at an individual stack (Figure 3.12 below) passing obliquely through this layer.

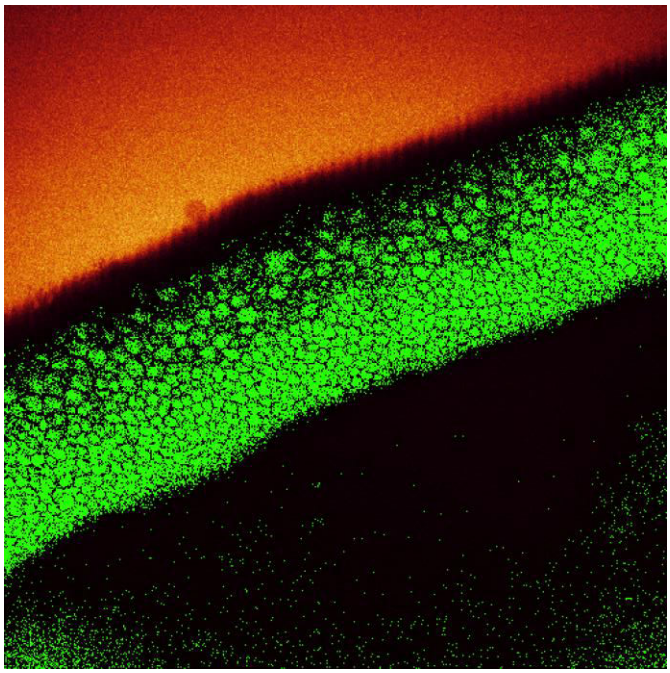

Figure 3.12 Single stack TPF image (transepithelial)
Stack oriented obliquely passing from the hyperfluorescent pre-corneal reservoir (orange, high signal), through the cellular epithelium (green, no signal) to the hypofluorescent anterior stroma (black, low signal). [In the Leica imaging software the saturation spectrum runs from green (zero fluorescence) to black to orange to red]. This image shows that the TPF signal within the epithelium itself was near-zero. passing obliquely through this layer. This apparent epithelial hypofluorescence proved to be false – the methodology I describe in chapter 3 imaging sagittal corneal sections confirms that the concentration of riboflavin within the epithelium at least equals that that within the underling stroma.

I was additionally unable achieve a steady signal at the back of the cornea. In Figure 3.11 above (insert), the posterior corneal signal can be see to peak at approximately 60 minutes, before dropping at 120 minutes. Soaking for these extended durations resulted in an approximate 10% drop in reservoir signal, as well as riboflavin moving intraocularly, with a rising TPF signal detected within the anterior chamber, confirming the presence of a third compartment for riboflavin. Despite soaking for more than 3 hours I was unable to equalise the riboflavin concentration within the cornea to that of the reservoir.

3.5 Discussion

I have shown that riboflavin TPF signal is attenuated with increasing depth in corneal tissue and demonstrated a correction method designed to increase measurement accuracy for epithelium-off ex vivo comparisons of riboflavin absorption for different soak protocols.

There are a number of potential causes of increased TPF signal attenuation with depth, including absorption and scattering of both excitation and emission radiation and aberration of the excitation beam focus. Fluorescence photons emitted at wavelengths corresponding to the overlap between the absorption and emission spectra (Figure 3.3) can be reabsorbed. This 'inner-filter' effect is more pronounced the higher the concentration of fluorescence photons in the sample. As such, when fluorescence microscopy is used to determine fluorophore concentration, fluorescence intensity will only be proportional to the concentration at less concentrated solutions. I initially observed this effect at the highest (0.1%) riboflavin concentration, with an increasingly attenuated signal when imaging through calibration drops on a well slide. By shifting the microscope detector range beyond the riboflavin absorption spectrum (>525 nm), I minimized this phenomenon, obtaining near-flat TPF signals with increasing depth through the drop (Figure 3.5B).

Previous studies using TPF microscopy to quantify corneal riboflavin absorption ignore the inner-filter effect. Cui et al measured both fluorescein and riboflavin absorption in feline corneas, and while the effects of reabsorption of the fluorescence emitted from fluorescein were mitigated by a

bandpass filter of appropriate wavelength, no such detection filter was used for the riboflavin measurements.(Cui et al. 2011) By way of a signal attenuation correction factor, Kampik et al. used the intensity loss in collagen fiber second-harmonic generation (SHG) signals taken simultaneously during the same z-scan.(Kampik et al. 2010) However, the SHG detector wavelength channel used (420-460 nm), and to a lesser extent that used for riboflavin (505-555 nm), overlap with the absorption spectrum of riboflavin (300-525 nm, Figure 3.3). This would be expected to cause significant re-absorption of the emitting SHG light, compromising its use as a reference to correct TPF signal attenuation.

My calibration method is based on 2 assumptions: firstly, that the concentration within the riboflavin reservoir above the cornea remains constant throughout the entire soak; and secondly, that in a fully soaked cornea the riboflavin concentration within the cornea equals that of the reservoir. For epithelium-on samples, the utility of this two-compartment model was fatally undermined by the failure to achieve a fully soaked cornea. Even when imaging epithelium-off, neither of these two assumptions may be strictly correct. Figure 3.6B reveals that the TPF signal within the reservoir does decrease with time, albeit by only a few per cent. With a finite (small) volume, the reservoir is potentially susceptible to photobleaching. I investigated this by repeating the above z-stack protocol through the same custom chamber reservoir of riboflavin placed on a slide (i.e. no cornea). Over 50 minutes I observed near-identical TPF signal plots over a depth of 1200 µm, with no evidence of photobleaching. I have additionally investigated

the possibility of photobleaching within the corneal tissue, by performing a final z-stack at the end of the full 60 minute protocol in a new adjacent axial location (i.e. un-irradiated tissue). I observed near identical TPF signal plots over a depth of 800 μm, with no evidence of photobleaching. As graphically demonstrated in Figure 3.2, fluorescence excitation restricted to the focal plane is a key advantage of multi-photon microscopy, explaining the lack of photobleaching demonstrated. An alternative explanation could be that the reduction in TPF signal with time is due to loss of fluorescent riboflavin molecules as they diffuse into the cornea. However, as illustrated in Figure 3.6B, this decrease over 50 minutes was small, with a mean of 2.5 (±1.1)% for all imaged eyes. For future work, this small effect could be reduced by increasing the volume of the reservoir. The assumption that the concentration in a fully soaked cornea is the same as that in the reservoir also appears to be not quite correct. I consistently observed a step-like decrease in TPF signal as the imaged plane transitioned from the fluid-filled reservoir into the cornea (Figure 3.6B), measured to be 6.1 (± 1.6)% after 50 minutes soak. This small loss of signal may result from optical aberrations encountered as the laser light crosses the curved surface of the cornea or it may reflect a true difference in concentration between the reservoir and the fully soaked cornea.

The percentage transmission of light of wavelengths between 600 nm and 1000 nm has been previously measured in early post-mortem eyes between 95% and 98%.(Beems & Van Best 1990) Scattering of light may still occur in an otherwise healthy optical system, becoming more prevalent in disease (for example cataract, corneal oedema or corneal scarring). Oedema is likely to

be particularly relevant in the porcine corneas used in this current study which, although optically clear to the naked eye, were regularly over 800 µm in central corneal thickness (pre-riboflavin soak), compared with published in vivo measurements of 666 ± 68 µm.(Hatami-Marbini et al. 2013) This is presumed to be due to early endothelial failure within the first 24 hours after harvest and is a limitation of this animal model. I did not attempt to deturgesce the porcine corneas with a dextran solution (as is used clinically prior to transplantation) due to the infrared absorption properties of dextran (see below paragraph for further discussion of dextran).

There is a lack of consensus regarding the exact nature and location of CXL-induced collagen cross-links.(Hayes et al. 2013; Wollensak et al. 2004) Two-photon microscopy of corneal collagen has been used in an in vivo rabbit model to quantify corneal collagen cross-links after treatment.(Krüger et al. 2011) In this study, the investigators identified a well-demarcated change in both autofluorescence and SHG signal down to a depth of 250 µm. This correlates well with a demarcation line visible by optical coherence tomography (OCT) in human patients, typically around 250 – 300 µm after epithelium-off CXL.(Seiler & Hafezi 2006; Doors et al. 2009) At this depth (300µm), following a standard 30 minute soak, I measured a mean stromal concentration of 0.086%. It is, however, not possible to make any absolute correlation between the concentrations reported in this study (using an HPMC-based riboflavin preparation) and demarcation line tissue changes observed in vivo on OCT (using a dextran-based riboflavin preparation). I attempted to apply this methodology to determine concentration depth profiles

using 0.1% riboflavin in 20% dextran (500 kDa) as used in the original CXL study,(Wollensak, Spoerl, et al. 2003a) in both well-slide and soaked corneas, but was unable to achieve any consistent TPF signals. Dextran has previously been shown to strongly absorb near-infrared light (Xu et al. 2003) and absorption of the TPF excitation beam may have been raising the temperature of dextran and affecting its optical properties. This is likely to have been the cause of variations in the TPF signal levels I measured. TPF microscopy may therefore not be suitable to investigate corneal riboflavin absorption for dextran-based preparations, although these are increasingly being replaced by HPMC-based preparations.

Replicating this whole-globe imaging technique through an intact epithelium was not successful. Besides the variable signal-attenuating effect of the epithelium itself, the principle problem I could not resolve was the failure to achieve a full stromal riboflavin soak through the epithelium, thereby breaking a principle assumption of my calibration method, that in a fully soaked cornea the riboflavin concentration within the cornea equals that of the reservoir. I was also unable to achieve a steady state signal at the back of the cornea which I interprete as being due to riboflavin migration from the stroma into the anterior chamber over such extended soak durations. Lastly, I was unable to explain the apparent epithelial hypofluorescence which proved to be false – the methodology I describe in chapter 3 imaging sagittal corneal sections confirms that the concentration of riboflavin within the epithelium at least equals that that within the underling stroma.

In conclusion, this work describes a method for accurately measuring stromal riboflavin absorption in an ex vivo epithelium-off whole-globe animal model. I present evidence that TPF microscopy of corneas is affected by significant signal attenuation when imaging at depth. To account for this, I have presented a new time-lapse measurement approach carried out during the riboflavin soak in which each cornea acts as its own internal reference. I additionally conclude that while suitable for epithelium-off imaging, this whole-globe technique is unsuitable when imaging through an intact corneal epithelium. In the next chapter I describe an alternative method to resolve this issue by imaging cross-sections of corneal tissue.

4 Shape stabilisation – quantifying transepithelial riboflavin absorption

4.1 Introduction

Riboflavin is a key ingredient in the UV-driven photochemical CXL process.(McCall et al. 2010) Whilst riboflavin is hydrophilic with a molecular weight of 340 Dalton (Da), the corneal epithelium is lipophilic and has a reduced permeability to molecules larger than 180 Da.(Huang et al. 1989; Spoerl et al. 1998) Thus standard CXL requires debridement of the central epithelium to facilitate stromal riboflavin absorption and achieve adequate efficacy.(Spoerl et al. 1998) Epithelial debridement, however, is associated with post-operative pain, delayed visual recovery and increases the risks of infection, corneal melt and scarring.(Koller et al. 2009) As a result, CXL is normally reserved for patients with documented disease progression.

Transepithelial (epithelium-on) CXL aims to avoid the pain, delayed recovery and complications of epithelial removal inherent in epithelium-off CXL. A number of formulations of riboflavin designed to facilitate absorption across an intact corneal epithelium are currently available.(Filippello et al. 2012; Magli et al. 2013; Leccisotti & Islam 2010; Caporossi et al. 2013; Koppen et al. 2012b; Soeters et al. 2015; Kocak et al. 2014) Most contain toxic agents to increase epithelial permeability, including benzalkonium chloride (BAC), high concentration sodium chloride, sodium ethylenediaminetetraacetic acid (EDTA) or trometamol.(Filippello et al. 2012; Magli et al. 2013) A non-toxic reversible synthetic nonselective ion channel-forming peptide, NC-1059, has

also been shown in a chick corneal model to enhance riboflavin permeability across an intact epithelium.(Zhang et al. 2012) Despite these permeability enhancers, results in clinical studies with current commercial transepithelial riboflavin preparations have been equivocal: some studies report similar efficacy to epithelium-off CXL, but most report inferior results.(Leccisotti & Islam 2010; Caporossi et al. 2013; Koppen et al. 2012b; Soeters et al. 2015; Kocak et al. 2014) Iontophoresis, in which an electrical gradient is used to drive negatively-charged riboflavin molecules across the intact epithelium, may further enhance riboflavin absorption in transepithelial CXL.

Previous studies to quantify riboflavin penetration through an intact epithelium have used high-performance liquid chromatography (HPLC)(Baiocchi et al. 2009; Ostacolo et al. 2013; Cassagne et al. 2014) and fluorescence microscopy.(Zhang et al. 2012; Gore et al. 2014; Cui et al. 2011; Kampik et al. 2010; Søndergaard et al. 2010) HPLC, in which the sample is dissolved in a solvent for analysis, can accurately quantify the concentration of riboflavin in a whole block of tissue, but is unable to provide information about the concentration at different depths within the corneal stroma (unless lamella sections are prepared and separately dissolved).(Mastropasqua et al. 2014) Fluorescence microscopy, both single-photon excitation (i.e. confocal) and multi-photon excitation(Gore et al. 2014; Zhang et al. 2012; Cui et al. 2011; Kampik et al. 2010; Søndergaard et al. 2010) has the added advantage of quantifying concentration at depth within the cornea; both excitation techniques, however, suffer from signal attenuation with increasing scan depth, principally attributable to scattering and aberration.(Gore et al. 2014;

Cui et al. 2011; Kampik et al. 2010) In chapter 2 I described a novel time-lapse measurement approach to correct for two-photon fluorescence (TPF) signal attenuation;(Gore et al. 2014) although applicable to epithelium-off absorption, this method has not proven suitable when imaging through an intact epithelium.(Gore et al. 2015)

In this chapter I describe an alternative method for quantifying riboflavin penetration in an epithelium-on ex vivo animal model and compare the efficacy of different transepithelial protocols with standard epithelium-off absorption.

4.2 Materials and methods

Ethical approval for corneal two-photon fluorescent microscopy studies in an ex vivo model was granted by University College London Institute of Ophthalmology (ref. 10/H0106/57-2012ETR27).

4.2.1 Sample preparation

Adult pigmented rabbit heads transported on ice in a phosphate buffered saline (PBS) bath were received within 5 hours post-mortem (First Link Ltd., Wolverhampton, UK). Intact globes were enucleated and examined under a low-magnification light microscope to rule out obvious epithelial trauma or scars. The globes were warmed to room temperature in balanced salt solution before different commercially-available riboflavin solutions (Table 4.1) were applied to the corneas of intact globes according to the manufacturers' protocols (Protocols tested, section 4.2.3).

4.2.2 NC-1059 solution preparation

NC-1059 is a synthetic non-selective ion channel-forming peptide. A 200 µM NC-1059 peptide solution (amino acid sequence KKKK-AARVGLGITTVLVTTIGLGVRAA; *LifeTein LLC, New Jersey, USA*) was prepared by dissolving it in either 0.25 % or 0.1 % w/v riboflavin 5'-monophosphate solution (Ricrolin +, Table 4.1)

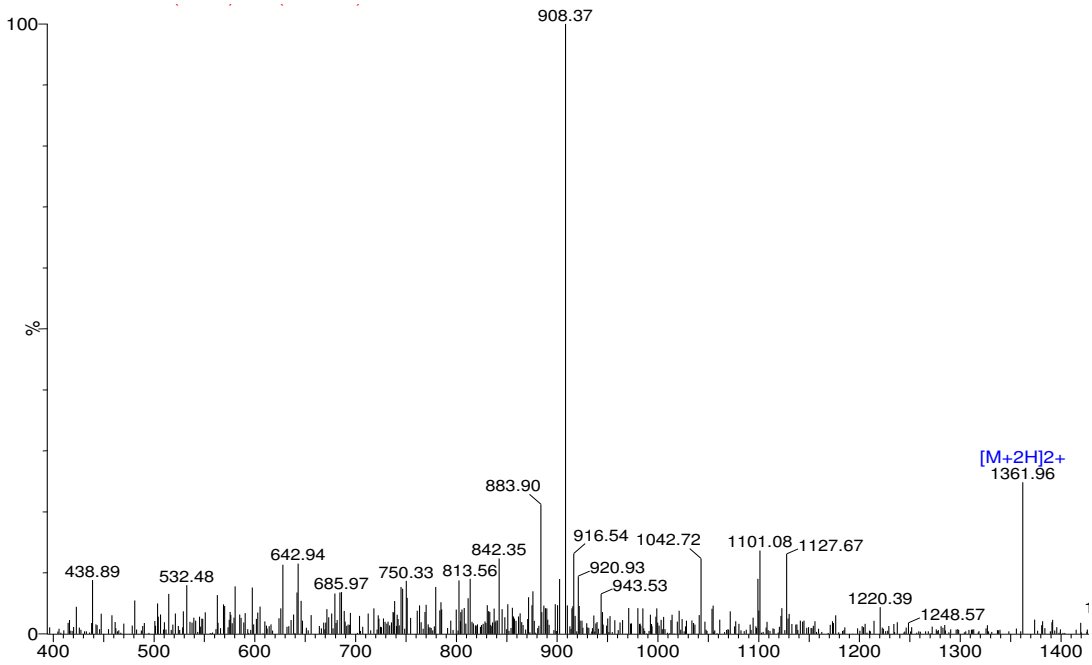

Figure 4.1 Mass spectrometry report of NC-1059 peptide

Analysis and report provided by manufacturer, *LifeTein LLC, Hillsborough, New Jersey, USA*

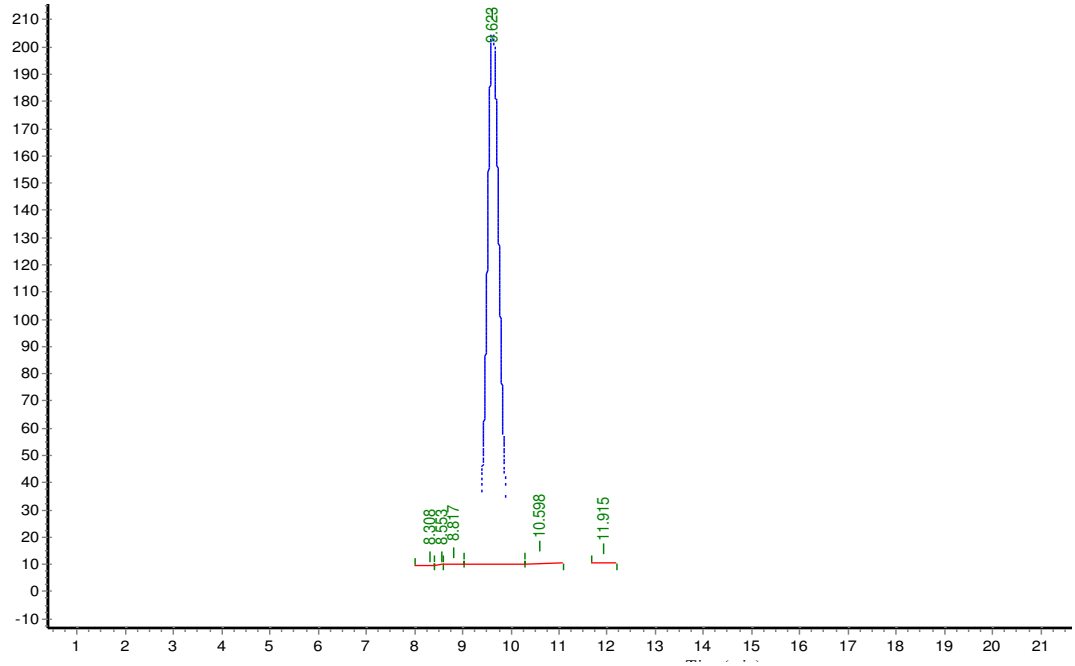

Figure 4.2 High performance liquid chromatography (HPLC report for NC-1059 peptide

Purity 95.95%. Analysis and report provided by manufacturer,

Table 4.1 Commercially prepared riboflavin solutions

Formulation	Manufacturer	Composition
Vibex Rapid	Avedro, Inc., MA, USA	0.1% wt/vol riboflavin 5'-monophosphate, saline, HPMC
Ribocross TE	IROS Srl, Napoli, Italy	0.125% wt/vol riboflavin 5'-monophosphate, D-alpha-tocopheryl poly(ethylene glycol) 1000 succinate
Medio-Cross TE	Peschke Meditrade GmbH, Germany	0.25% wt/vol riboflavin 5'-monophosphate, HPMC, benzalkonium chloride 0.01%
Ricrolin + 0.1%	Sooft Italia S.p.A. Montegiorgio, Italy	0.1% wt/vol riboflavin 5'-monophosphate, sodium edetate, trometamol, sodium dihydrogen phosphate dihydrate, sodium phosphate dibasic dehydrate
Ricrolin + 0.25%	Sooft Italia S.p.A. Montegiorgio, Italy	0.25% wt/vol riboflavin 5'-monophosphate, sodium edetate, trometamol, sodium dihydrogen phosphate dihydrate, sodium phosphate dibasic dehydrate
ParaCel	Avedro, Inc., MA, USA	0.25% wt/vol riboflavin 5'-monophosphate, HPMC, sodium edetate, trometamol, benzalkonium chloride, saline
VibeX Xtra	Avedro, Inc., MA, USA	0.25% wt/vol riboflavin 5'-monophosphate, saline

All the above solutions (except Vibex Rapid) are designed for transepithelial use. HPMC, hydroxypropyl methylcellulose

4.2.3 Protocols tested

Positive controls were prepared using a 9 mm vacuum well secured to epithelial-debrided corneas of whole globes filled with 0.1 % w/v riboflavin in HPMC and saline (Vibex Rapid) for 30 minutes (n = 5). Unsoaked globes (i.e. no riboflavin) served as negative controls (n = 5).

4.2.3.1 Non-iontophoresis protocols

1. Medio-Cross TE

A 9 mm vacuum well secured on the cornea was filled with approximately 0.5 ml of Medio-Cross TE solution for 30 minutes. Riboflavin was not rinsed from the cornea (n = 5).

2. Ribocross TE

A 9 mm vacuum well secured on the cornea was filled with approximately 0.5 ml of Ribocross TE solution for 30 minutes. Riboflavin was not rinsed from the cornea (n = 5).

3. ParaCel and VibeX Xtra

ParaCel drops were applied at a rate of 1 drop every 90 seconds for 4 minutes. The cornea was then rinsed with VibeX Xtra completely coating the cornea. Additional VibeX Xtra was applied at a rate of 1 drop every 90 seconds for 6 minutes (total riboflavin soak time 10 minutes). Riboflavin was not rinsed from the cornea (n = 5).

4. 200 µM NC-1059 peptide in 0.1 % w/v Ricrolin +

A 9 mm vacuum well secured on the cornea was filled with approximately 0.5 ml of 200 µM NC-1059 peptide in 0.1 % w/v Ricrolin + solution for 30 minutes. Riboflavin was rinsed from the cornea with PBS for 1 minute (n = 3).

5. 200 µM NC-1059 peptide in 0.25 % w/v Ricrolin +

A 9 mm vacuum well secured on the cornea was filled with approximately 0.5 ml of 200 µM NC-1059 peptide in 0.1 % w/v Ricrolin + solution for 30 minutes. Riboflavin was rinsed from the cornea with PBS for 1 minute (n = 3).

4.2.3.2 Iontophoresis protocol

The iontophoresis system comprised 2 electrodes: a negatively-charged metal grid housed within the corneal applicator and a positively-charged 20G needle inserted through the sclera into the vitreous (Figure 4.3A). The corneal applicator was vacuum-attached to the cornea. The reservoir was filled with differing riboflavin formulations to above the level of the metal grid before beginning the iontophoresis treatment. Protocols varied either by iontophoresis dosage, soak time or riboflavin formulation (n = 4, Table 4.2). After the iontophoretic procedure, the applicator was removed and the corneas were rinsed with PBS to both remove any riboflavin on the corneal surface and to try to reduce riboflavin concentration within the epithelium.

Table 4.2 iontophoresis protocols

Protoco	Solution	Curre	Soak I	Current	Soak	Rinse
Negative control	None	None	-	-	-	-
Positive Control	Vibex Rapid	None	30 min	-	-	-
A	MedioCross TE	1mA 5 min	5 min	0.5 mA 5 min	5 min	5 min *
B	MedioCross TE	1mA 5 min	15 min	-	-	1 min
C	Ricrolin+ 0.25%	1mA 5 min	5 min	0.5 mA 5 min	5 min	5 min *
D	Ricrolin+ 0.25%	1mA 10 min	-	-	-	5 min
E	MedioCross TE	1mA 5 min	-	-	-	1 min
F	Ricrolin + 0.1%	1mA 5 min	-	-	-	1 min
G	Vibex Rapid	1mA 5 min	-	-	-	1 min
H	Vibex Rapid	1mA 5 min	5 min	0.5 mA 5 min	5 min	5 min

Min, minute; * St. Thomas'/Cardiff Iontophoresis protocol (unpublished)

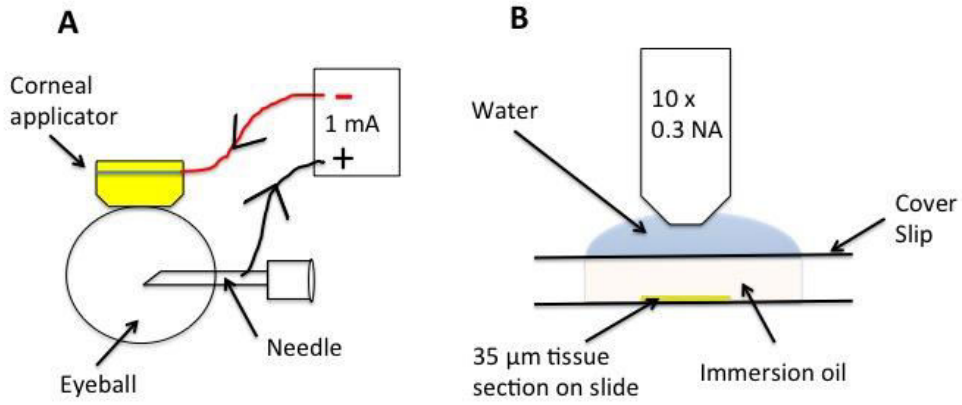

Figure 4.3 Sample preparation and image acquisition

(A) Iontophoresis schematic showing a riboflavin-filled corneal well housing a negative electrode with the return electrode connected to a needle passed into the vitreous cavity. The riboflavin solution acts as an electrical contact between the electrode and the eye. The generator self-checks the continuity and a warning signal sounded in case of current disruption. (B) Slide mounted 35µm tissue sections were covered in immersion oil with a coverslip placed on top and coupled to the microscope objective with distilled water.

4.2.4 Section preparation

At the end of the riboflavin soak, the globes were immediately immersed in liquid nitrogen for 5 minutes and stored overnight at -25 degrees Celsius. A broad incision across the posterior globe was made just before immersion to prevent the cornea from splitting open on freezing. For each globe, three 35 µm corneal cross-sections were cut on a cryostat 1 mm apart (Figure 4.5). With the frozen section on the blade platform (maintained at -21°C), a knife was used to cut the cornea free and the remaining tissue was brushed away. The cornea itself was meticulously brushed to ensure no ice remained attached that might allow riboflavin to leak out once thawed (transparent images of processed sections during the development of the methodology confirmed the epithelium itself was not removed by this brushing; see Figure 4.4 below). Colour photographs were taken of the sagittally-exposed globe and free corneal section.

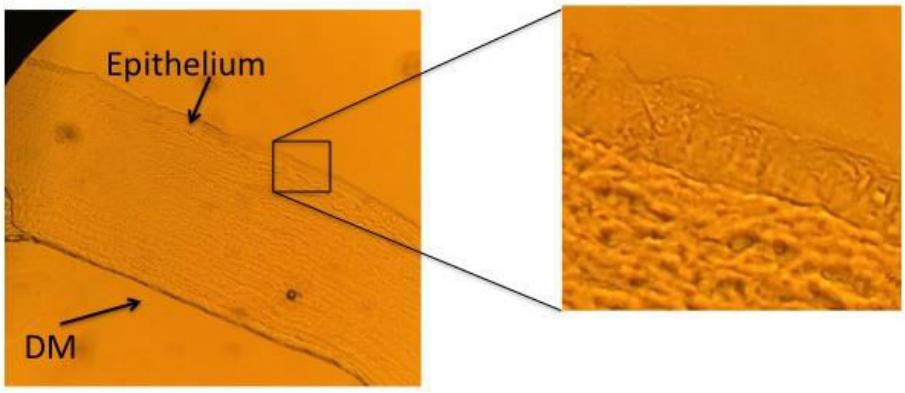

Figure 4.4 Epithelial detail in corneal section

Transparent image confirming epithelial integrity in processed rabbit corneal section. Columnar basal epithelial and flatter superficial structures visible

The corneal section was then mounted on a slide and covered with fluorescence-free immersion oil (Immersol 518 F, Carl Zeiss Ltd.) to prevent any leakage of riboflavin out of the tissue. No dye leakage was observed over several minutes during protocol development using immersion oil. This compared with prompt dye leakage when either water-based optimal cutting temperature (OCT) compound or water itself was used as an immersion medium. A coverslip was placed on top prior to imaging under the microscope objective (Figure 4.3B). The time taken from the tissue thawing onto the slide to image acquisition on the microscope was approximately 1 minute, and I refer to this earliest imaging time point as t = 0 minutes. To investigate riboflavin migration within the thawed slide-mounted tissue, serial images were captured every minute for selected samples. For all other measurements, data was acquired as soon as possible following tissue thawing, i.e. after approximately 1 minute.

4.2.5 Two-photon microscope set-up and imaging protocol

The two-photon microscope set-up is based on that described in chapter 2. A Ti:Sapphire laser, operating at a wavelength of 890 nm with a 140 femtosecond pulse duration and 80 MHz pulse repetition rate, was used as the excitation laser source. The excitation laser beam was guided to a Leica DM6000CS upright microscope where it passes through two galvoscanners, allowing scanning in the x-y plane, before being focused into the sample by a Leica 10 X /0.3 NA water immersion objective. Theoretical (full-width half-maximum) axial and lateral resolutions were calculated at 16 µm and 1.1 µm

respectively. TPF excitation light of 890 nm wavelength was chosen to correspond with the highest riboflavin absorption peak (445 nm) as determined by spectrophotometry. Emitted riboflavin fluorescence was collected between 525 nm and 650 nm to avoid overlap with the absorption spectrum of riboflavin. 553 µm x 553 µm (512 x 512 pixel) images were captured at a scan rate of 600Hz (line average 16) with the pinhole wide open.

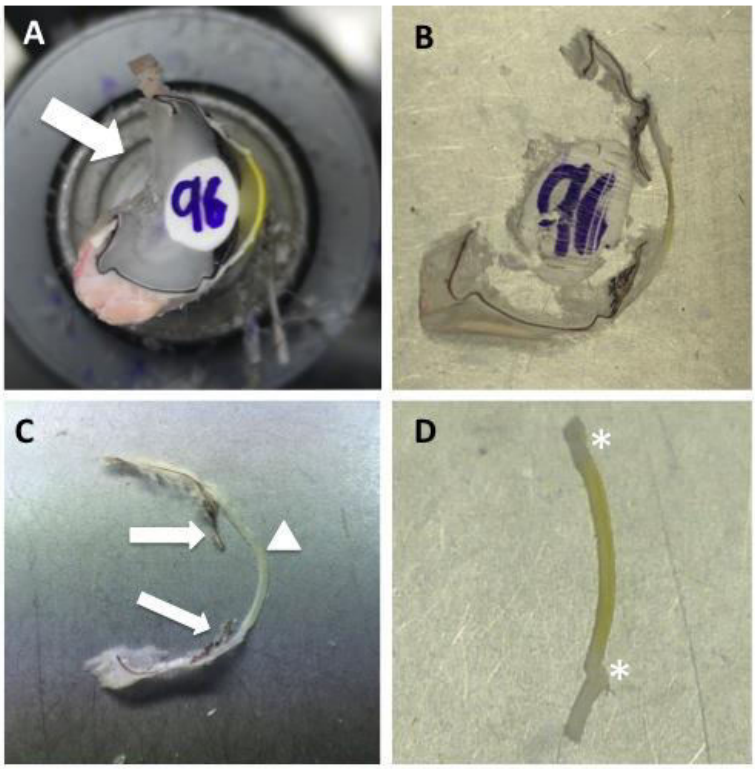

Figure 4.5 Tissue sectioning

Section preparation. (**A**) Globe adhered onto specimen stage (with optimal cutting temperature (OCT) compound) and secured within cryostat chuck. Yellow cornea visible with white crystalline lens marked with '96.' Note disrupted posterior segment from relieving incision made prior to immersion in liquid nitrogen to prevent anterior globe splitting (white arrow). (**B**) 35 µm whole-globe section laid on blade platform. (**C**) Lens and aqueous brushed away leaving sclero-corneal shell (arrow-head) and iris (arrows). (**D**) Blade used to cut cornea out before meticulously brushing away attached ice on the back. Note slight corneal crimp from suction well (*). The surface riboflavin film - measured by Wollensak et al.(Wollensak et al. 2010) at up to 300 µm in cellulose-containing formulations - was also brushed away (Ribocross TE film was particularly adherent to the epithelium and was still present on imaging (Figure 4.9) despite attempts to remove it).

4.2.6 Image analysis

Grey scale images (Figure 4.6A) were exported and analysed using Java-based imaging software (ImageJ, 1.48v, http:// imagej.nih.gov.ij; provided in the public domain by the National Institutes of Health, Bethesda, MD, USA).

For each image, three separate rectangular regions of interest each 40 pixels wide in the x-direction were manually selected. The intensity profiles along the z-direction for each region of interest were then exported to a .txt file (Excel for Mac, 2011; Microsoft Corp, Redmond, WA, USA) (Figure 4.6B). The epithelial/stromal junction was then identified in each trace by the abrupt change in signal and confirmed with reference to the corresponding image region of interest. This information was then used to align all three plots along the z-axis and a mean intensity plot was then generated representing the average TPF signal for that image as a function of depth (z). TPF signals were converted to riboflavin concentration by normalizing to the TPF signal achieved in a well-slide reservoir of 0.1 % riboflavin solution during the same experimental session. Mean (SD) concentrations were calculated from 5 globes tested for each protocol. Unpaired Student *t*-tests were used to compare riboflavin concentrations achieved at a depth of 300 µm. A *p* value less than 0.05 was considered significant. Analyses were performed in Excel for Mac, 2011; Microsoft Corp, Redmond, WA, USA).

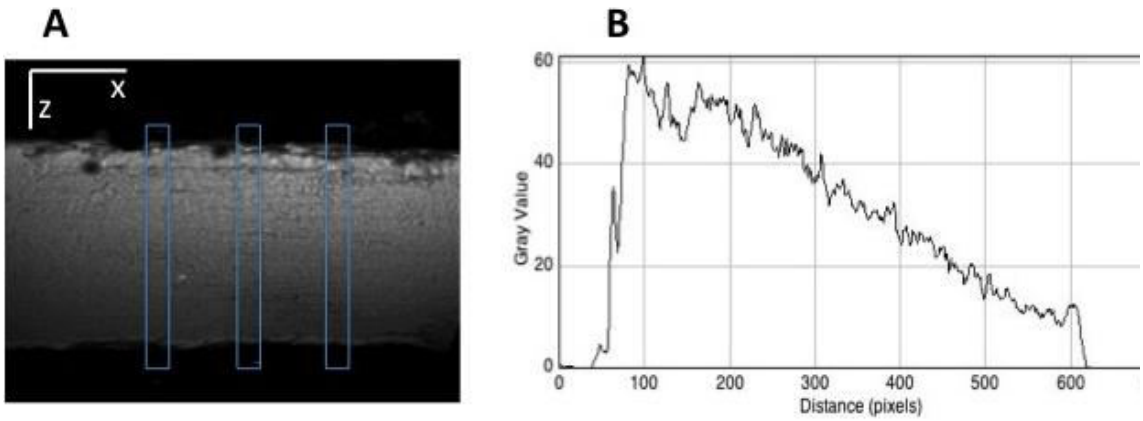

Figure 4.6 Image analysis

(A) Grey scale two-photon fluorescence image were exported and analysed in ImageJ. For each image, three regions of interest (blue rectangles) each 40 pixels wide in the x-direction, were manually selected. The intensity profiles along the z-direction for each region of interest were then exported to a .txt file. The epithelial/stromal junction was then identified in each trace by the abrupt change in signal and confirmed with reference to the corresponding image region of interest. This information was then used to align all three plots along the z-axis and a mean intensity plot (B) was then generated representing the average TPF signal for that image as a function of depth (z). The edges of the images were not analysed to avoid areas of vignetting (grey scale image formatted to increase brightness and clarity

4.3 Results

4.3.1 Riboflavin migration within thawed tissue

Serial images were captured at time = 0, 1 and 2 minutes (t = 0 being the first scan approximately 1 minute after the tissue had thawed on the slide). Figure 4.7 confirms fluorophore migration within the sample, redistributing posteriorly with time including from the epithelium into the underlying stroma. Measured at the beginning of the stroma, this drop in signal is approximately 7 % within the first minute. Therefore, all subsequent data was acquired as soon as possible following thawing, i.e. after approximately 1 minute.

4.3.2 Depth-specific corneal riboflavin absorption for commercially available protocols

No fluorescence was detected by TPF microscopy in the negative (untreated) controls. The maximum riboflavin concentration in positive controls (epithelium-off) was 0.09 % (± 0.01). Maximum stromal riboflavin concentrations for MedioCross TE, Ricrolin +, Paracel/Xtra and Ribocross TE were: 0.054 % (± 0.01), 0.031 % (0.003), 0.021 % (± 0.001) and 0.015 % (± 0.004) respectively. Depth-specific riboflavin concentrations are displayed in Figure 4.9 and Figure 4.10. Stromal absorption of riboflavin by iontophoresis was not homogenous, with areas of relative hypo- and hyper fluorescence within each section. In all samples, the epithelial concentration was higher than that in the underlying stroma. A film of higher signal riboflavin adherent to the epithelium was detected in samples treated with Ribocross TE.

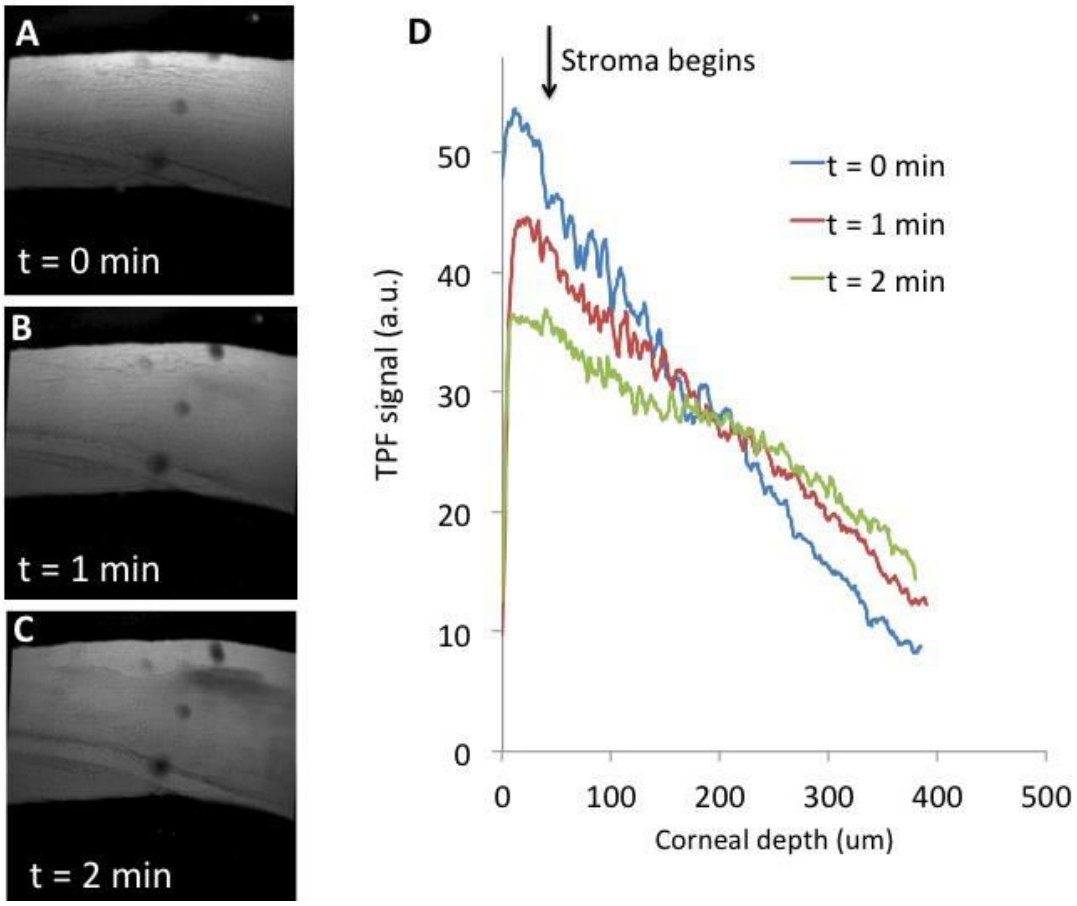

Figure 4.7 Riboflavin migration within thawed tissue

Fluorophore migration within the corneal section investigated with serial images of the same tissue location at time = 1, 2 and 3 minutes (**A-C**). Dark circles are air bubbles within the oil overlying the tissue. All images have been formatted to increase brightness by the same amount to improve view. (**D**) Corresponding TPF signal across samples. Note the loss of the epithelial peak as riboflavin moves into the stroma.

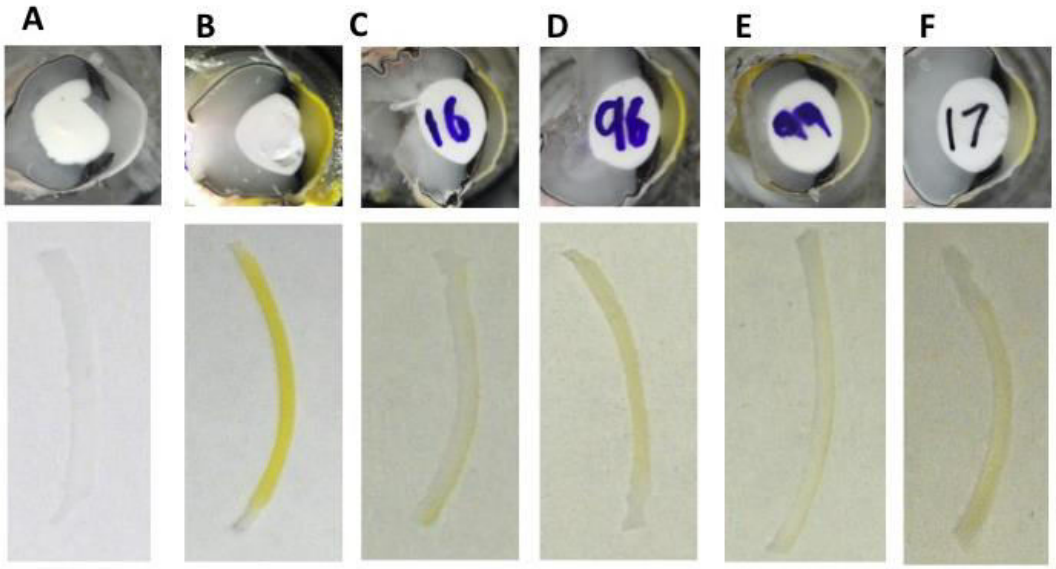

Figure 4.8 Colour photographs of corneas soaked with commercially-available protocols

Colour photographic globe and section examples from each group tested allowing macroscopic comparative view of riboflavin penetration through the cornea into the anterior chamber. Upper row: Sagittal sections of treated globes mounted on a cryostat during section preparation. Lower row: 35 µm corneal sections prepared and laid on white paper for photographic contrast (visible shadows indicate section lifting off paper). (**A**) negative control; (**B**) positive control (epithelium-off) 0.1% riboflavin 30 minutes; (**C**) Ribocross TE 0.125% 30 minutes; (**D**) MedioCross TE 0.25% 30 minutes; (**E**) ParaCel 0.25% 4 minutes, VibeX Xtra 0.25% 6 minutes; (**F**) Ricrolin + 0.1% 1 mA 5 minutes iontophoresis.

At a depth of 300 µm (within the demarcation zone commonly seen after corneal cross-linking), the stromal concentration in epithelium-off positive controls was 0.075 % (± 0.006), while at the same depth MedioCross TE and Ricrolin + achieved 0.018 % (± 0.006) and 0.016 % (0.002) respectively (Figure 4.10). None of the remaining transepithelial protocols achieved concentrations above 0.005% at this same 300 µm depth.

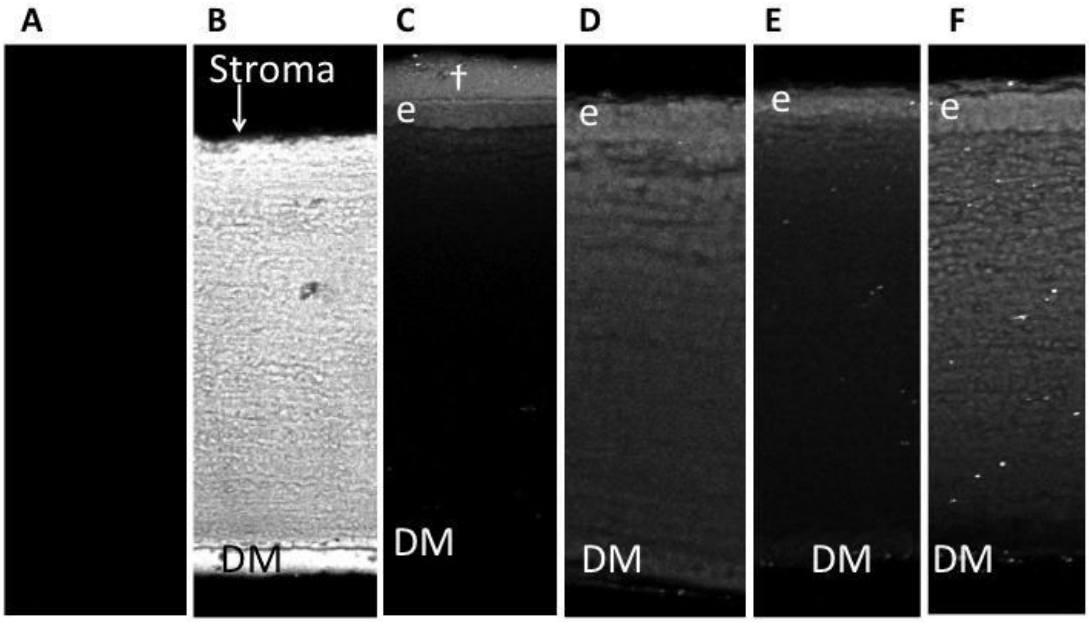

Figure 4.9 TPF images for commercially-available protocols

Two-photon fluorescence images of tissue sections (grey scale). (**A**) negative control (B) positive control (epithelium-off) 0.1% riboflavin 30 minutes; (**C**) Ribocross TE 0.125% 30 minutes; (**D**) MedioCross TE 0.25% 30 minutes; (**E**) ParaCel 0.25% 4 minutes, VibeX Xtra 0.25% 6 minutes; (**F**) Ricrolin + 0.1% 1 mA 5 minutes iontophoresis. e, epithelium; DM Descemet's membrane; †, Ribocross TE 'riboflavin film' on top of epithelium. All images have been formatted to increase brightness by the same amount to improve view. DM scroll artifact visible in some preparations.

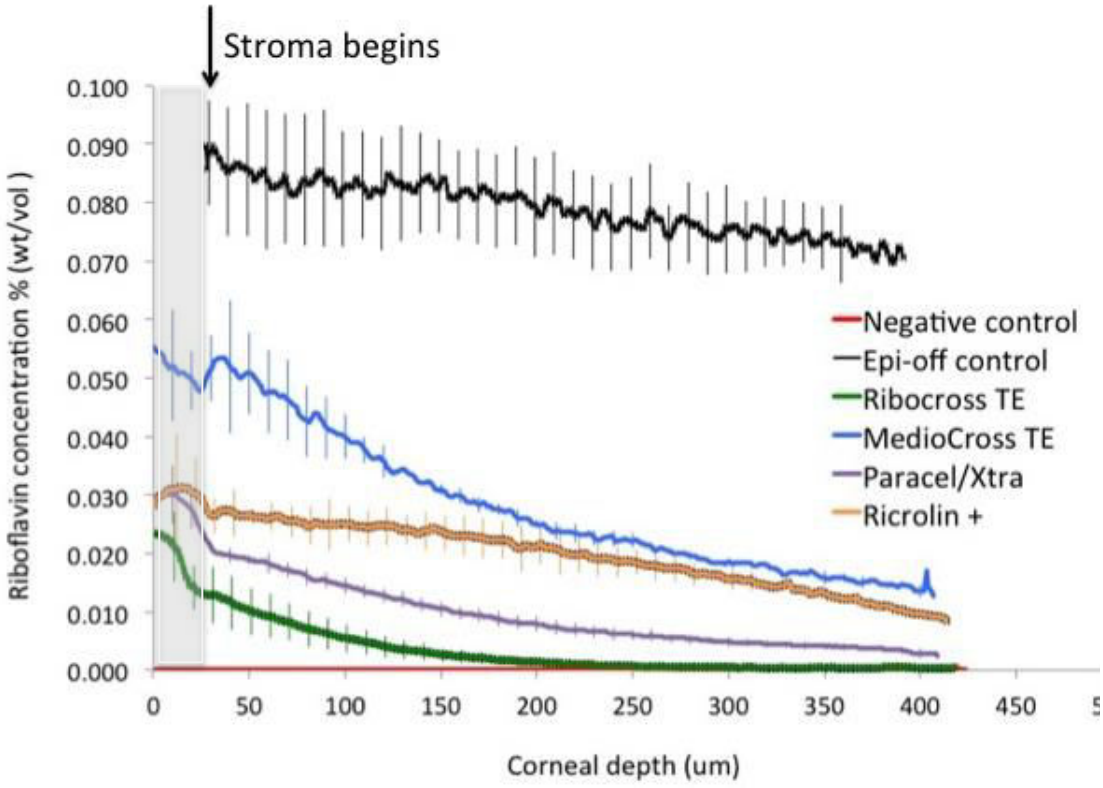

Figure 4.10 Depth-specific riboflavin concentrations for commercially-available protocols

Mean concentrations (standard deviation error bars) of riboflavin achieved using different transepithelial protocols, compared with epithelium-off absorption. Shaded area denotes epithelium.

4.3.3 Depth-specific corneal riboflavin absorption for NC-1059 peptide

The maximum riboflavin concentration in positive controls (epithelium-off; 0.1 % w/v riboflavin, *Vibex Rapid*) was 0.09 % (± 0.01). The maximum stromal riboflavin concentration for 200 µM NC-1059 peptide solution in 0.25 % w/v Ricrolin + was 0.043 (± 0.01) % w/v riboflavin. The maximum stromal riboflavin concentration for 200 µM NC-1059 peptide solution in 0.1 % w/v Ricrolin + was 0.015 (± 0.003) % w/v riboflavin. Macroscopic globe sections (Figure 4.11), TPF images (Figure 4.12) and depth-specific riboflavin concentrations (Figure 4.13) are displayed below.

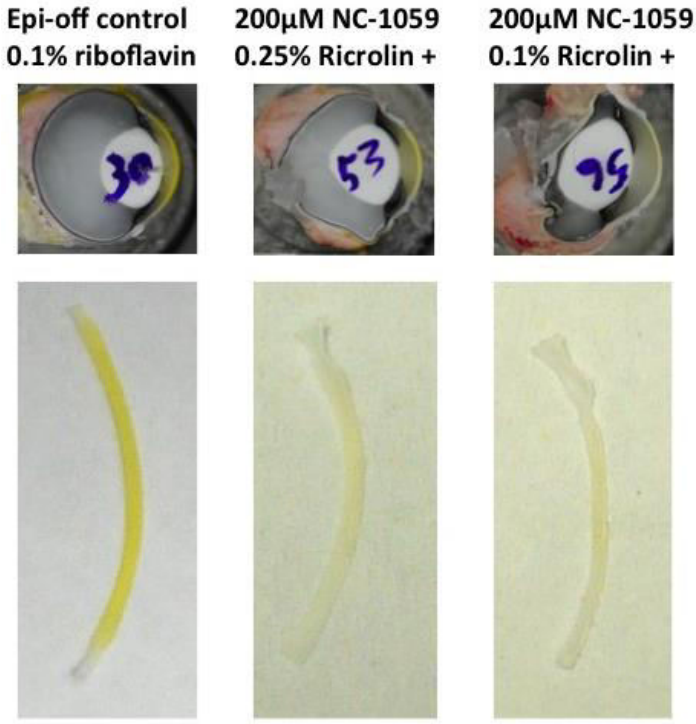

Figure 4.11 Colour photographs of corneas soaked with NC-1059 peptide and riboflavin

Macroscopic view of riboflavin absorption through the cornea into the anterior chamber. Upper row: Sagittal sections of globes mounted on a cryostat during section preparation. Lower row: 35 µm corneal sections laid on paper

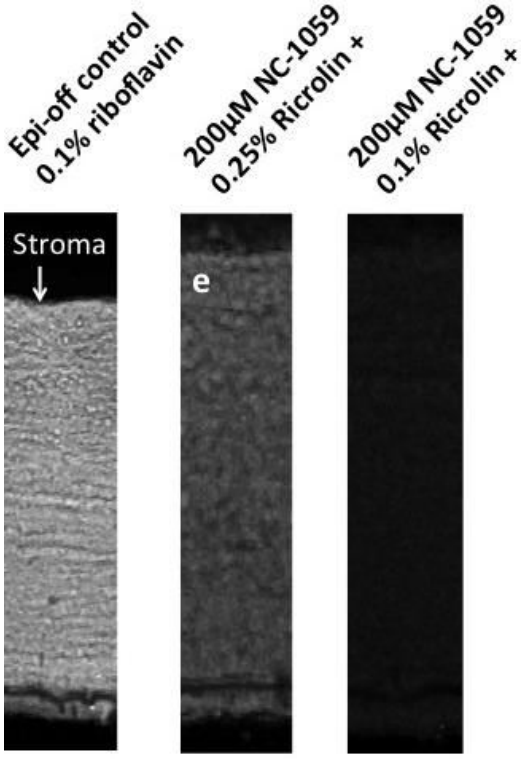

Figure 4.12 TPF images for NC-1059 peptide

Two-photon fluorescence images of tissue sections (grey scale). The right-hand image (0.1% Ricrolin +) shows very low levels of fluorescence, but is not zero (just over 0.01% w/v). The corresponding colour photograph in Figure 4.11 is not intended to be quantitative due to differences in background lighting and contrast (note colour of background paper also differs)
e, epithelium. Note Descemet's membrane scroll processing artifact.

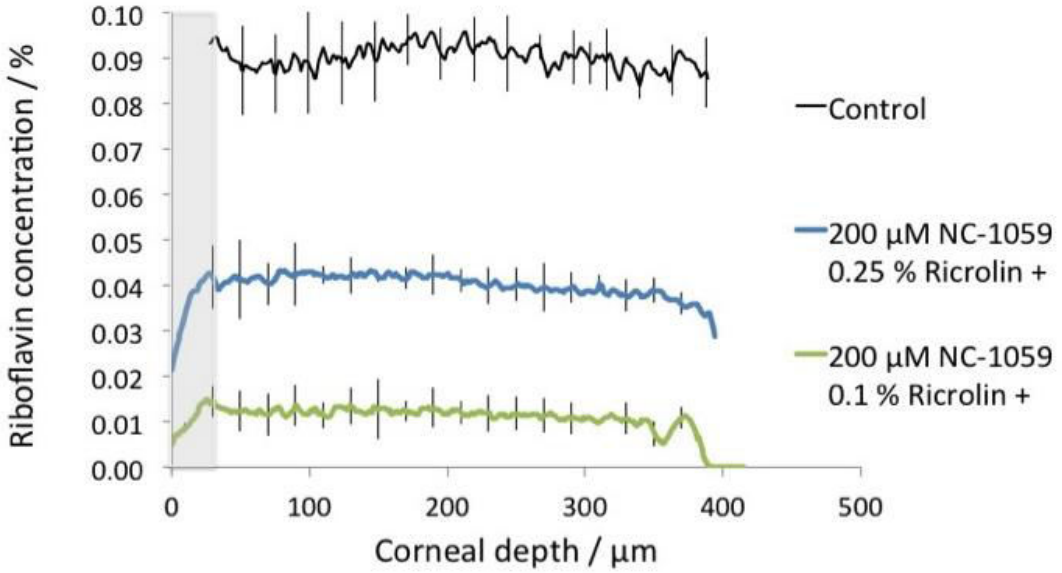

Figure 4.13 Depth-specific riboflavin concentrations for NC-1059 assisted riboflavin absorption

Mean concentrations (standard deviation error bars) comparing epithelium off controls (0.1% w/v riboflavin) with 200 µM NC-1059 peptide dissolved in two concentrations of Ricrolin +. Shaded area denotes epithelium. Note the near-uniform concentration with depth which is presumed a result of the long soak duration (30 minutes) allowing the riboflavin to near-evenly distribute across the stroma.

4.3.4 Depth-specific corneal riboflavin absorption for modified iontophoresis protocols

Higher concentrations were achieved with longer iontophoretic dosage and longer solution contact (diffusion) time with the cornea (Figure 4.14, Figure 4.15, Figure 4.16; Table 4.3). The best protocol (A), utilizing 0.25 % w/v riboflavin with BAC and two separate iontophoretic treatments followed by soak periods of 5 minutes to allow diffusion of riboflavin from the sub-epithelial tissues deeper into the stroma (the 'St. Thomas'/Cardiff Iontophoresis protocol', total time 20 minutes), was not significantly different with respect to stromal riboflavin concentrations compared with epithelium-off controls (0.089 [± 0.006] % w/v vs. 0.083 [± 0.013] % w/v at a depth of 300 µm, $p = 0.8$, Table 4.3). The best performing protocol (C) not containing BAC but with 0.25 % w/v

riboflavin and the same iontophoresis treatments and soak times as protocol A, achieved a mean stromal concentration of 0.056 (± 0.011) % w/v at 300 µm.

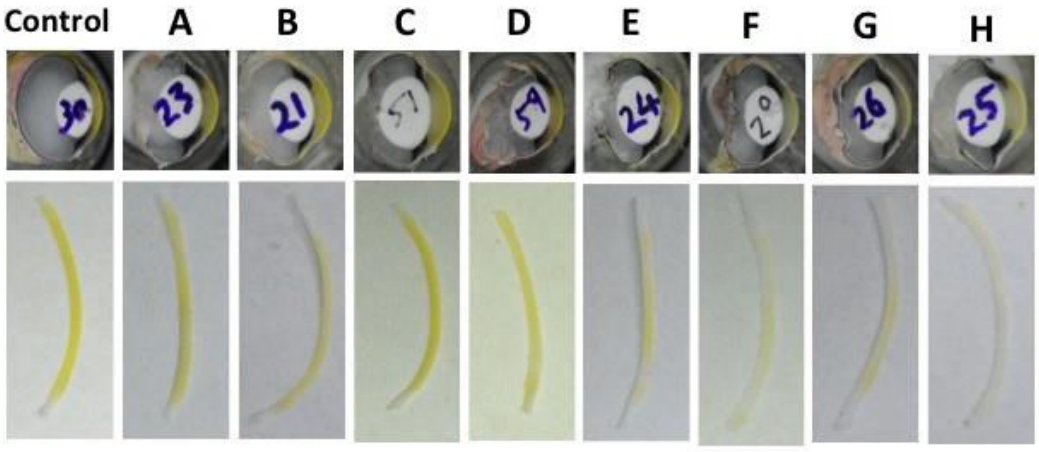

Figure 4.14 Macroscopic absorption images for modified iontophoresis protocols

Color photographic globe and section examples from each group tested allowing macroscopic comparative view of riboflavin absorption through the cornea into the anterior chamber. Upper row: Sagittal sections of treated globes mounted on a cryostat during section preparation. Lower row: 35 µm corneal sections prepared and laid on white paper for photographic contrast (visible shadows indicate section lifting off paper). **A-H** protocols as per Table 4.2.

Near-uniform stromal riboflavin absorption with depth was observed in longer-duration protocols (A-C), as compared with shorter treatments in which the concentration fell by up to 40 % within the anterior 300 µm (protocols D-F). Riboflavin solutions containing saline (protocols G, H), resulted in minimal stromal absorption (maximum 0.01 %). Of note, corneal thickness was observed to increase by approximately 60 µm following these saline-based iontophoretic applications (Figure 4.15 & Figure 4.16).

Table 4.3 Iontophoresis corneal riboflavin concentrations

Protocol*	Riboflavin concentration ± SD % w/v			P value[1]
	Epithelium	Peak stroma	300 µm*	
Control	-	0.095 ± 0.002	0.089 ± 0.006	-
A	0.069 ± 0.008	0.086 ± 0.012	0.083 ± 0.013	0.74
B	0.046 ± 0.013	0.059 ± 0.011	0.058 ± 0.01	0.007
C	0.051 ± 0.012	0.06 ± 0.009	0.056 ± 0.011	0.001
D	0.049 ± 0.005	0.053 ± 0.007	0.038 ± 0.004	< 0.001
E	0.041 ± 0.003	0.041 ± 0.002	0.025 ± 0.004	< 0.001
F	0.031 ± 0.006	0.027 ± 0.002	0.017 ± 0.002	< 0.001
G	0.008	0.011	0.009	< 0.001
H	0.008	0.01	0.008	< 0.001

* See Table 4.2, page 105 for protocol details. [1]Unpaired Student t-test comparing 300µm riboflavin concentration vs. control. 300µm depth chosen to correlate with demarcation zone commonly seen after corneal cross-linking.

The concentration of riboflavin within the epithelium was equivalent to or higher than that in the immediate underlying stroma. Extended rinsing of the surface effectively washed away any pre-corneal riboflavin film but did not selectively reduce the fluorophore load within the epithelium itself. A 5 minute corneal rinse after protocols A and B (MedioCross TE) resulted in a wash-out effect of both the epithelium and anterior stroma up to an approximate depth of 200 µm.

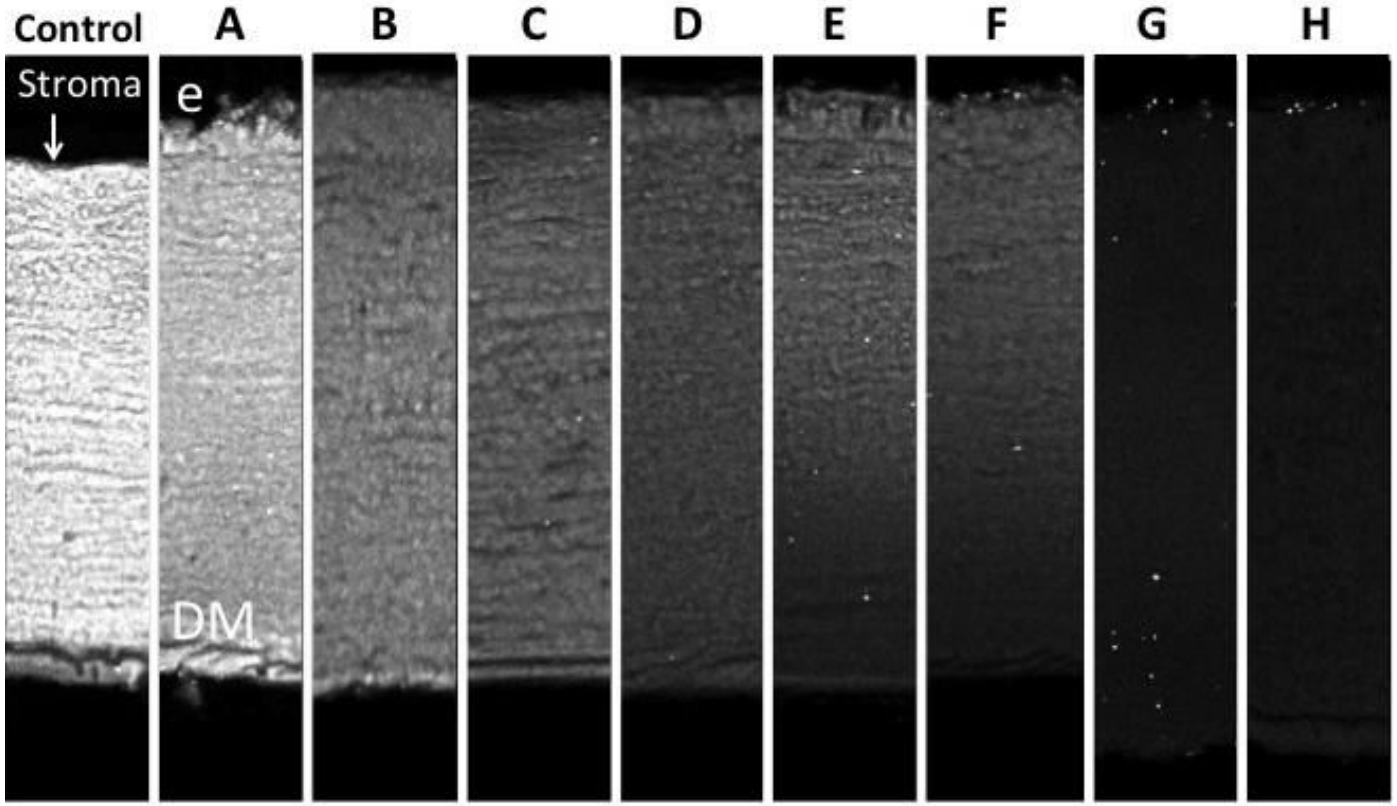

Figure 4.15 Two-photon fluorescence images of tissue sections

A-H protocols as per Table 4.2. e, epithelium; DM, Descemet's membrane. All images have been formatted to increase brightness by the same amount to improve view. DM scroll artifact visible in some preparations. Apparent epithelial damage with BAC-containing protocol A should not be inferred as a treatment effect - this TPF methodology was not designed to qualify epithelial structural changes and a processing-induced artefact cannot ruled out.

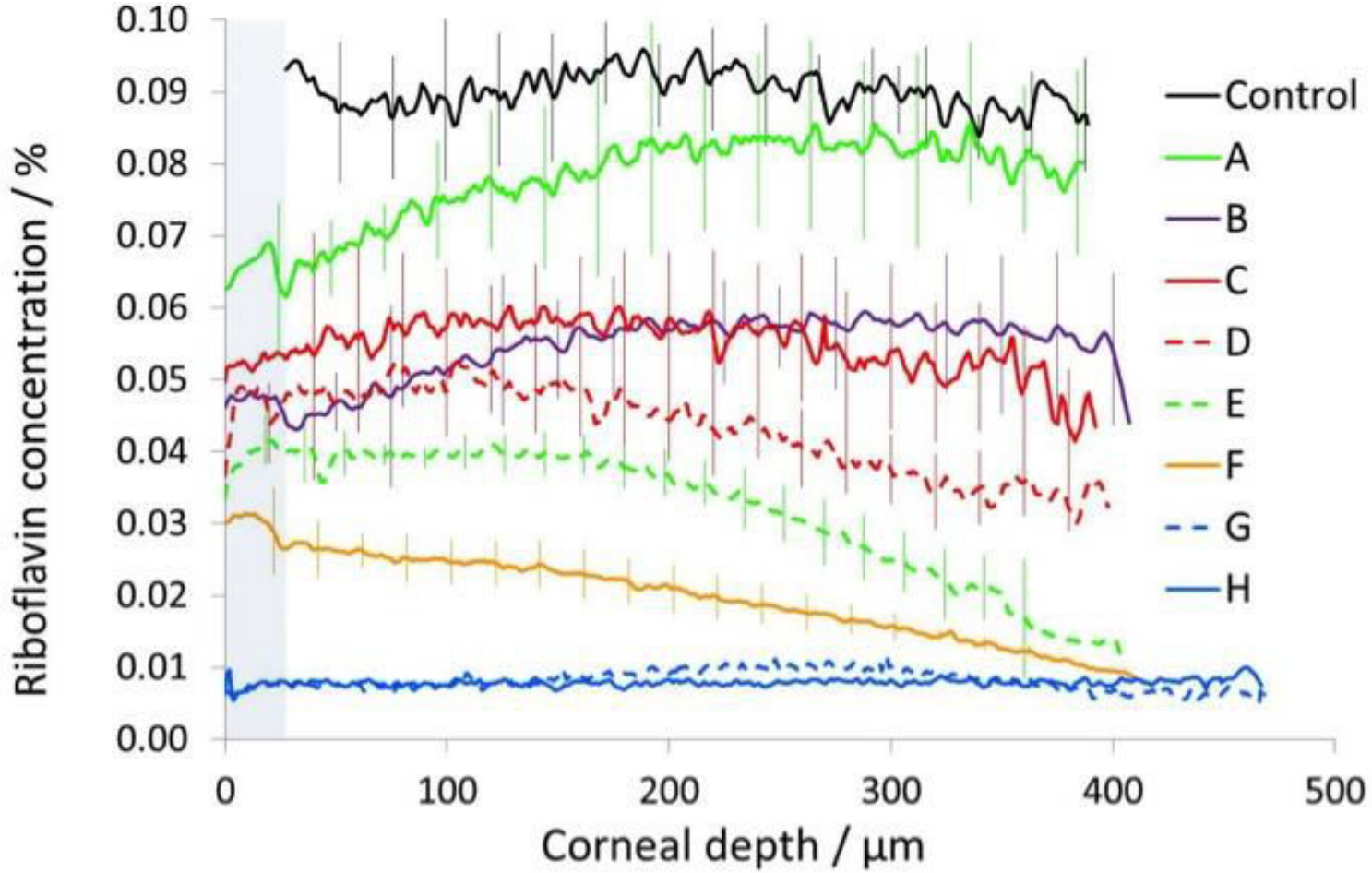

Figure 4.16 Depth-specific riboflavin concentrations for iontophoresis protocols

Mean concentrations (standard deviation error bars) of riboflavin achieved using different transepithelial protocols, compared with epithelium-off absorption. Shaded area denotes epithelium. A-H protocols as per Table 4.2. Note the increased concentrations achieved at 300um with protocols A and C compared to B and D due to the second iontophoresis/soak cycle.

4.4 Discussion

These results reveal that, compared with epithelium-off CXL, absorption of riboflavin into the corneal stroma is significantly reduced in all non-iontophoretic transepithelial CXL protocols. I also demonstrate that stromal riboflavin absorption in iontophoretic transepithelial CXL can match that achieved 'epithelium-off,' by increasing solution formulation, soak time and iontophoretic dosage

4.4.1 Methodological advantages

Since most tissue cross-linking is thought to take place in the anterior cornea,(Lombardo, Pucci, et al. 2014) determining the availability of key photochemical ingredients (riboflavin, UV light, oxygen) at specific depths may add useful additional information. The method I describe above provides these depth-specific measurements of riboflavin, with the microscope objective and image size determining the resolution available. An additional advantage of this technique, as compared to whole-tissue analysis (high-performance liquid chromatography, HPLC;(Baiocchi et al. 2009; Ostacolo et al. 2013; Cassagne et al. 2014) spectrophotometry(Samaras et al. 2009; Hayes et al. 2008; Alhamad et al. 2012)) is the ability to quantify riboflavin concentration within the epithelium which, as my results demonstrate, often exceeds that in the underlying stroma.(Gore et al. 2015) In clinical practice, the consequences of loading the corneal epithelium with riboflavin in transepithelial CXL could include epithelial toxicity and UV light shielding. The normal epithelium filters out an average 20% of UVA light radiation passing

through the cornea.(Lombardo, Pucci, et al. 2014) This UV light attenuation is increased by riboflavin absorption within the epithelium in transepithelial CXL, and stromal concentrations of riboflavin are reduced. Enhanced UV absorption with free radical generation within the epithelium could result in 'arc eye' type epithelial toxicity. Epithelial defects are commonly observed on day 1 after transepithelial CXL using MedioCross TE,(Taneri et al. 2014) and punctate epitheliopathy is evident in all cases (personal communication, David O'Brart, February 2015).

The inability to measure concentration at specific depths in the epithelium and stroma is a significant limitation of HPLC. Furthermore, unless this riboflavin-rich epithelium is specifically removed prior to dissolving the sample, the concentration result will be inappropriately increased. This may have contributed to the observations described by Ostacolo et al.(Ostacolo et al. 2013) in which Ribocross TE was tested using modified Franz-type diffusion cells with freshly excised porcine corneas (both with and without epithelium). After 40 minutes, riboflavin accumulation through an intact epithelium (0.394 ± 0.02 nmol/mg) matched that achieved epithelium-off (0.396 ± 0.03 nmol/mg). This contrasts with my results in which Ribocross TE performed poorly compared to other protocols tested. As demonstrated in Figure 4.15 and 3.16, I observed TFP signals within the epithelium to be higher than in the underlying stroma in all tested protocols. Furthermore, the pre-corneal film of riboflavin solution exhibited even higher fluorescence signal. Dissolving a full-thickness specimen, including a riboflavin-loaded epithelium and pre-corneal film, will lead to overestimation of corneal stromal riboflavin concentrations by

HPLC. This may explain why Ostacolo et al.(Ostacolo et al. 2013) recorded only a 4-fold reduction in stromal concentration when their control riboflavin solution (i.e. no vitamin E) was applied to an intact epithelium, compared with epithelium-off application (0.098 ± 0.04 nmol/mg epithelium-on; 0.396 ± 0.03 nmol/mg epithelium-off). Cassagne et al.(Cassagne et al. 2014) also used HPLC in an in vivo rabbit eye study of iontophoresis, testing both the dissolved cornea and aqueous sample. Again, the investigators did not remove the epithelium prior to analysis. This may, in part, explain the discrepancy in their results in which the relative difference in riboflavin concentration between treated tissue and controls was much less in the cornea, than in aqueous samples (which would not be affected by epithelial contamination).

4.4.2 Iontophoresis

Riboflavin is water soluble and negatively charged at physiological pH, and laboratory studies suggest that iontophoresis can be applied effectively to enhance riboflavin absorption in transepithelial CXL. Several groups have reported similar increases in corneal biomechanics(Cassagne et al. 2014; Lombardo, Serrao, et al. 2014; Touboul et al. 2014) in animal models as compared with epithelium-off CXL. Preliminary clinical studies have also been encouraging, with reported cessation of disease progression with up to 15 month follow-up and improvements in keratometric and visual parameters.(Bikbova & Bikbov 2013; Vinciguerra et al. 2014; Buzzonetti et al. 2015) However, the relative efficacy of this technique compared to epithelium-off CXL remains to be determined especially over longer term follow-up, and

current randomized prospective studies comparing the two techniques (clinicaltrials.gov.uk NCT02117999, NCT01868620, ISRCT 04451470) have yet to be reported.

Existing recommended protocols for iontophoresis in transepithelial CXL typically utilize riboflavin solutions of 0.1 % w/v and currents of 0.5 – 1 mA with application times of 5 to 10 minutes. Improved riboflavin absorption can be obtained by modifying these parameters. Stromal riboflavin concentrations using protocol A here were similar to epithelium-off controls ($p = 0.8$) (figure 4, table 3). This protocol utilized a solution of 0.25 % w/v riboflavin with BAC and the 'St. Thomas'/Cardiff Iontophoresis protocol'. This protocol, designed by David O'Brart, was derived in collaborative pilot experimentation at St Thomas' Hospital and Cardiff University using spectrophotometry, and comprises two cycles of iontophoresis each followed by a 5 minute soak period to allow time for riboflavin to diffuse more posteriorly. The use of the cationic surfactant BAC has been shown with percutaneous iontophoresis to have a synergistic effect on the transport of anions.(Lombardo, Serrao, et al. 2014) I similarly observed this synergistic effect with higher stromal concentrations achieved with protocol A (0.25 % w/v riboflavin, BAC) compared to protocol C (0.25 % w/v riboflavin, no BAC) (figure 4, table 3).

The ideal transepithelial protocol would load the stroma with riboflavin, while leaving the epithelium relatively clear. To this end, in this study I rinsed the surface of the globe after iontophoresis in a bid to wash out some of the riboflavin from within the epithelium. Figures 3 and 4 and table 3 show that

this approach did not work since there was no significant difference in fluorescence between the epithelium and the subjacent stroma. Extended rinsing (5 minutes) of the ocular surface in protocols A and B (MedioCross TE) also reduced corneal stromal concentrations of riboflavin up to an approximate depth of 200 µm. Stromal riboflavin elution was less evident with non-BAC containing solutions (protocols C and D), where the epithelial tight junctions were still probably largely intact. Although iontophoresis is not commercially promoted to be used with BAC-containing solutions, this stromal wash-out effect with prolonged rinsing of the ocular surface may compromise tissue cross-linking within the anterior cornea.

It is important to note that iontophoresis is ineffective with riboflavin formulations containing saline (Protocols G and H) that produced minimal riboflavin absorption and some stromal swelling.

4.4.3 NC-1059 peptide

NC-1059 peptide has been previously shown in cultured corneal epithelial cell monolayers to reversibly modulate the barrier function of intercellular tight junctions to enhance drug permeation.(Martin et al. 2009) Tight junctions within normal corneal epithelium represent a formidable barrier to the passage of molecules and ions. Most drug absorption, therefore, relies on *transcellular* passage, favouring lipophilic molecules. Riboflavin is a large (340 Da) hydrophilic molecule, underlying it poor penetration (Huang et al. 1989; Spoerl et al. 1998) NC-1059 overcomes this by forming non-selective ion channels that increase *paracellular* transport.(Martin et al. 2009) Zhang and colleagues,

using confocal fluorescence microscopy, reported significantly enhanced riboflavin diffusion across intact corneal epithelium in chick embryos.(Zhang et al. 2012) However, as discussed in chapter 2 and section 4.1, page 97 above), this method suffers from significant signal attenuation with increasing stromal scan depth in ex vivo tissue, even more so when imaging though the epithelium. This signal attenuation is clearly visible in their results in which all images, including epithelium-off controls, exhibit decreasing fluorescence with depth. Furthermore, the investigators have misinterpreted the lack of fluorescence within the epithelium itself as indicative of no riboflavin being within this layer. Our method described above imaging sagittal sections proves that it is not possible to load the stroma with riboflavin without similarly loading the epithelium.

4.4.4 Methodological limitations

There are a number of limitations to the method described above. Firstly, results in ex-vivo rabbit corneas, although a better anatomical match to human corneal epithelial thickness than porcine eyes, may be affected by post-mortem changes in epithelial layer integrity. Measures taken to minimize this compromise included a short postmortem interval, immersion in chilled PBS immediately postmortem, and warming to physiological temperature prior to preparation of corneas for experimentation. I observed no obvious stromal swelling (indicative of endothelial pump failure) in negative controls, and mean corneal thicknesses to those published for rabbit corneas in vivo (400 µm).(Riau et al. 2012) Despite this, some epithelial degradation and enhanced permeability is likely, and my results may overestimate stromal riboflavin

absorption in clinical transepithelial CXL. Secondly, migration of riboflavin within the snap frozen tissue will have started as soon as the section thawed on the slide. Even with the cryostat next to the microscope, there was still a delay of up to a minute before image acquisition. This would tend to result in an underestimation of stromal riboflavin concentrations. Finally, imaging through two media of different refractive indices (oil and water either side of the coverslip) may have increased optical aberrations as the laser light passes through. I chose oil to ensure no (water soluble) riboflavin leaked out of the tissue. When I tried to embed excised corneas in optimal cutting temperature (OCT) compound I observed very prompt dye leakage once thawed on the slide (data not shown). This may have impacted the study of Cassagne et al.(Cassagne et al. 2014). For lack of an appropriate oil-immersion objective, I placed a coverslip on top and used a water-immersion objective. Any induced aberrations may have resulted in a small absolute loss of signal; but since this same method was employed for all imaged samples, no relative drop between samples should be present.

4.4.5 Clinical relevance

Notwithstanding the above laboratory studies, results from preliminary clinical case series using non-iontophoretic transepithelial riboflavin preparations have been equivocal, with some showing similar efficacy to epithelium-off CXL,(Filippello et al. 2012; Magli et al. 2013) whilst most have demonstrated less pronounced effects.(Leccisotti & Islam 2010; Caporossi et al. 2013; Koppen et al. 2012a; Soeters et al. 2015; Kocak et al. 2014) 12-month results from one recently published randomised controlled trial (Soeters et al. 2015)

concluded that transepithelial CXL using Ricrolin TE (Sooft Italia S.p.A. Montegiorgio, Italy) was not effective at stabilising corneal shape compared with epithelium-off treatment. For iontophoresis, up to 15 month follow-up data have been published, with reported cessation of disease progression and improvements in keratometric and visual parameters.(Bikbova & Bikbov 2013; Vinciguerra et al. 2014; Buzzonetti et al. 2015) The longer-term relative efficacy of all these transepithelial techniques compared to epithelium-off CXL remains unknown.

4.4.6 Conclusion

The methodology described above provides a quantitative means of measuring riboflavin across the whole cornea in an ex vivo model.

I present evidence that the corneal epithelium represents a significant barrier to riboflavin absorption into the stroma. Existing commercial transepithelial CXL protocols load the corneal epithelium with riboflavin and achieve relatively low riboflavin concentrations in the anterior corneal stroma when compared to epithelium-off CXL. I also demonstrate that transepithelial riboflavin absorption can be improved using modified iontophoresis protocols, increasing soak time, riboflavin concentration in the soak preparation and current dosage. Although a key rate-limiting step, the absolute stromal concentration of riboflavin required for effective CXL is not known.

The St. Thomas'/Cardiff Iontophoresis protocol achieves more than 50% greater stromal absorption compared to the standard iontophoresis protocol, as well as far higher concentrations than with non-iontophoresis transepithelial protocols. Although less than that achieved with the 'gold

standard’ epithelium-off, its considerable stromal riboflavin absorption, without relying on epithelial-toxic additives, may represent the best transepithelial technique to date. Clinical trials will determine whether this level of stromal riboflavin absorption produces effective CXL.

5 Shape stabilisation - Accelerated CXL results for progressive keratoconus

5.1 Introduction

Randomised controlled studies confirming CXL works exist only for the original 'Dresden' epithelial-off protocol. (O'Brart et al. 2011; Wittig-Silva et al. 2014) This protocol (Wollensak, Spoerl, et al. 2003a) takes over 1 hour, including manual debridement of the corneal epithelium with 30 minutes application of riboflavin drops prior to UVA exposure of irradiance (power) 3 mW/cm^2 for a further 30 minutes (total energy 5.4 J/cm^2). Speeding up the procedure is attractive to both patient and practitioner, assuming treatment efficacy is not undermined. The absence of evidence has not hindered the growing popularity of alternative CXL protocols.

Accelerated protocols are emerging in which the same total UVA energy dose is delivered as a shorter, higher-power burst. The premise of shorter UVA delivery is that the same total energy can be delivered in a fraction of the time by increasing the power (energy = power x time). To date, low levels of evidence are available on accelerated CXL protocols, with evaluation of results complicated by variations in total energy, irradiance and/or treatment time. (Kanellopoulos 2012a; Celik et al. 2012; Kanellopoulos 2012b; Cınar et al. 2013; Gatzioufas et al. 2013; Tomita et al. 2014; Cinar et al. 2013; Sherif 2014) Notwithstanding this heterogeneity, keratometric and visual outcomes following accelerated CXL appear to demonstrate effective disease stabilisation.

In 2012, Moorfields Eye Hospital began treating patients with progressive keratoconus using an accelerated protocol. In this chapter, I present the outcomes of this treatment.

5.2 Methods

5.2.1 Ethics and data handling

This study design was reviewed by the Research Governance Committee and approved as an audit project by the Clinical Audit Working Group at Moorfields Eye Hospital NHS Foundation Trust. Patients were identified from a prospective electronic database of all patients aged above 15 years of age attending the *Early Keratoconus Clinic*. The database contains keratometric and refractive data entered prospectively in clinic and at the time of surgery. I extracted data from a consecutive series beginning with the first accelerated treatment in September 2012 through to April 2013. Eyes with 12-months' keratometric follow-up data were included in this study.

5.2.2 Outcomes measures

The primary outcome measure was the failure rate of CXL treatment, defined by an increase in maximum anterior keratometry (Kmax) on corneal tomography of >1.5 D at 12 months. Secondary outcome measures included anterior keratometry of the steep (K2 front) and flat (K1 front) axes in the central 3mm zone, posterior keratometry of the steep axis (K2 back), uncorrected distance visual acuity (UCVA), spectacle-corrected distance

visual acuity (CDVA), subjective refraction, corneal thickness at the thinnest point and endothelial cell density. Visual acuities were initially measured in Snellen, before the using LogMAR charts in the clinic from September 2013.

5.2.3 Monitoring for disease progression

Serial corneal tomography (Pentacam HR, Oculus GmbH, Germany) and subjective refractions were used to confirm pre-operative keratoconus progression. Progression was defined by one or more of the following: >1.5 D increase in Kmax or anterior K2 (K2 front); >0.5 D increase in posterior K2 (K2 back); >1 D increase in refractive astigmatism; >1 line loss of CDVA or >13 µm decrease in pachymetry. These criteria were based on published (Szalai et al. 2012) limits of agreement for repeated measurement using the Pentacam in patients with keratoconus, where changes >1.5 D have a >95% probability of not being simply attributable to measurement error. Exclusion criteria included pregnancy or breastfeeding, active ocular surface disease or a minimum stromal thickness less than 375 µm.

5.2.4 Specular microscopy

Corneal endothelial cell densities were measured using the Topcon SP-2000P noncontact specular microscopy and analyzed with IMAGEnet 2000 computerized analysis system (v2.5x; Topcon, Tokyo, Japan). If a clear image could not be acquired centrally, the patient was asked to look just to side of

the fixation light. Only whole cells with a continuous border (manually refined) on a frame with 75 or more cells, were accepted for planimetric analysis.

5.2.5 Surgical procedure

Following topical instillation of proxymetacaine 0.5%, tetracaine 1% and povidone-iodine 5%, the eyelashes were taped and a lid speculum inserted. The corneal epithelium was manually debrided to approximately 9mm. Dextran-free riboflavin 5'-monophosphate in saline and hydroxypropyl methylcellulose (VibeX Rapid*,* Avedro, Mass. USA) was applied every 2 minutes for either 20 minutes (if minimum pachymetry ≥ 400 µm) or 10 minutes (if minimum pachymetry < 400 µm). Continuous UVA exposure (KXL®, Avedro, Mass. USA) at 30 mW/cm^2 for 4 minutes was then applied (total energy 7.2 mJ/cm^2).

At the end of the procedure, preservative-free dexamethasone 0.1% and chloramphenicol 0.5% were instilled and a bandage contact lens applied. Post-operatively, patients were prescribed a tapered course of preservative-free topical dexamethasone 0.1%, moxifloxacin and hyaluronic acid 0.1% for 1 week, along with topical diclofenac 0.1%, cyclopentolate 1% twice a day and 50 mg oral diclofenac three times a day for 3 days. Patients were additionally provided with 3 minims of proxymetacaine 0.5% for use in the early post-operative period. The bandage contact lens was removed at 1 week after which all therapy was discontinued except topical hyaluronic acid 0.1% and fluorometholone 0.1% four times a day for 1 month.

5.2.6 Statistical analysis

For purposes of statistical analysis, I have converted Snellen visual acuities to logMAR equivalents (−log decimal acuity). I present data as means ± standard deviation. I use Paired Student t-tests to compare baseline and 12-month post-operative data, accepting a p value ≤ 0.05 as significant. Analyses were performed in Excel for Mac (2011, Microsoft Corp.).

5.3 Results

70 eyes were treated between September 2012 and April 2013. 55 eyes (79%) had complete 12-month keratometric follow-up data (45 patients, 29 male, 16 female; mean age 27 ± 7 years). All eyes had documented ectasia progression over at least a 6-month period prior to CXL, with a mean Kmax of 59.7 ± 6.8 D. Forty-five eyes had stage I-III disease (Modified Krumeich classification), with the remaining 10 eyes stage IV (K2 > 55 D).

At 12-months, the treatment failure rate was 12.7 %, with an increase in Kmax of > 1.5 D observed in 7 of 55 eyes. Despite some 12-month keratometric comparisons being statistically significant, we observed no clinically relevant changes in overall mean corneal shape or thickness. Excluding those eyes considered treatment failures, the mean reduction in Kmax was 1.07 ± 1.94 D ($p < 0.001$). Specular microscopy in 10 eyes showed a 3% reduction in endothelial cell density ($p = 0.033$). Mean UDVA and CDVA remained

unchanged, with only one (1.8%) eye losing more than 1 line of CDVA. No infective complications occurred. One (1.8%) eye developed a small peripheral sterile infiltrate that quickly responded to further topical steroids. Full baseline and post-operative data are presented in Table 5.1, Table 5.2 and Figure 5.1.

Table 5.1 Visual function data pre- and post-CXL

Parameter	Baseline (n=55)	6-months (n=38)	12-months (n=32)	P value[1]
UDVA (LogMAR)	0.80 ± 0.41	0.87 ± 0.41	0.76 ± 0.42	0.037*
CDVA (LogMAR)	0.19 ± 0.20	0.20 ± 0.29	0.19 ± 0.25	0.382
Sphere (D)	-0.49 ± 4.40	-0.32 ± 3.79	0.57 ± 3.87	0.275
Cylinder (D)	-4.91 ± 2.27	-5.24 ± 3.15	-5.38 ± 3.71	0.708
SEq (D)	-3.03 ± 4.58	-3.00 ± 3.60	-2.12 ± 3.35	0.479

UDVA uncorrected distance visual acuity; CDVA corrected distance visual acuity; D diopter; SEq spherical equivalent. [1]Paired T-test of baseline compared with 12-months; *statistically significant. Note that CDVA is spectacle-corrected acuity, not contact lens acuity).

Table 5.2 Keratometric data pre- and post-CXL

Parameter	Baseline (n=55)	6-months (n=23)	12-months (n=55)	P value[1]
Kmax (D)	59.7 ± 6.8	59.1 ± 6.2	59.1 ± 6.2	0.036*
K2 front (D)	51.5 ± 5.2	51.0 ± 4.5	51.6 ± 5.0	0.606
K1 front (D)	47.3 ± 4.3	47.6 ± 4.5	47.9 ± 4.5	0.001*
K2 back (D)	-7.9 ± 0.9	-7.8 ± 0.8	-7.9 ± 0.9	0.383
Pachymetry[2] (µm)	440 ± 39	431 ± 43	433 ± 34	0.008*
ECD (mm^2) (n=10)	3059 ± 276	-	2964 ± 257	0.058
ECV (%) (n=10)	35.9 ± 5.3	-	33.9 ± 4.8	0.359

D diopter; ECD endothelial cell density; ECV endothelial coefficient of variation. [1]Paired T-

test of baseline compared with 12-months; [2]Pachymetry at the thinnest location; *statistically significant

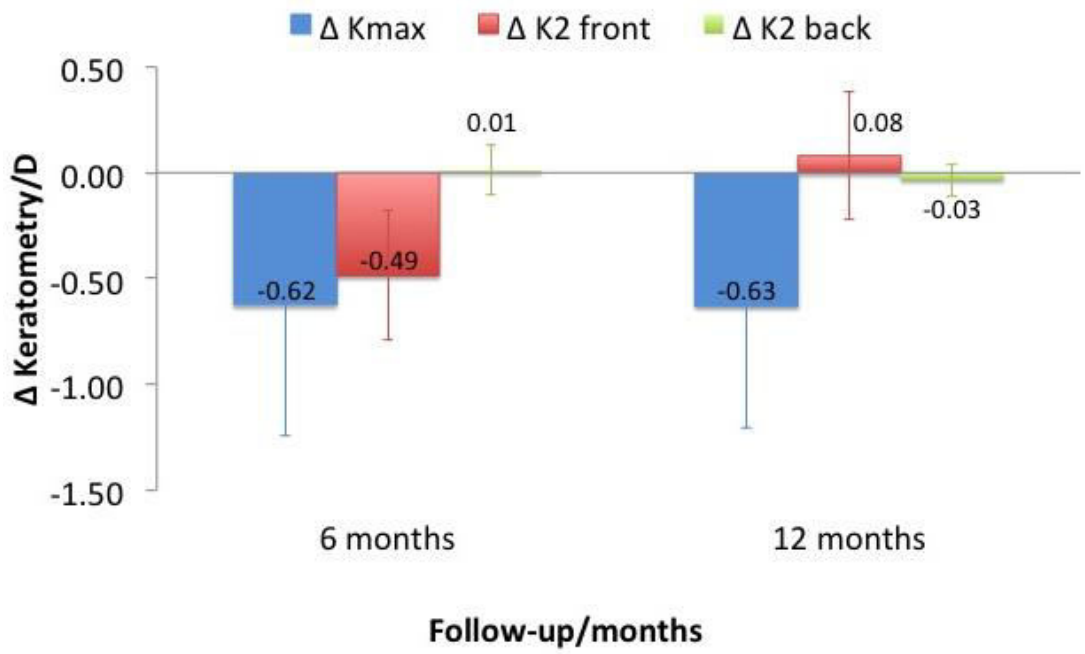

Figure 5.1 Mean keratometry changes compared with baseline (95% CI error bars)

5.4 Discussion

Overall, these data suggest that accelerated CXL irradiating at 30mW/cm^2 for 4 minutes (total energy dose 7.2 J/cm^2) is an effective and safe intervention for progressive keratoconus.

A limitation of this study is the lack a quality of life (QoL) assessment of the impact of this treatment on ocular and/or general health (e.g. 25-item National Eye Institute Vision Function Questionnaire (NEI-VFQ 25). Such

questionnaires may have provided valuable insight into whether the patients themselves felt the treatment had helped them, irrespective of the specific visual and refractive outcomes. Unfortunately, this study was approved, and undertaken, as an audit and we were therefore unable to deviate from standard clinical care. Introducing health questionnaires before and after treatment would have required separate research study approval with formal study recruitment and consent by all patients.

The benchmark comparator for all accelerated CXL protocols is the original 'Dresden' protocol. Two randomised-controlled trials (RCT) with at least 12-month results support it use in progressive keratoconus with, on average, maximum keratometry flattening by 1D and CDVA improving by 1 line. (O'Brart et al. 2011; Wittig-Silva et al. 2014) One eye in the Melbourne study demonstrated continued progression (i.e. treatment failure) at 3 years. (Wittig-Silva et al. 2014) By contrast, limited clinical data are available on accelerated CXL protocols. A prospective, paired-eye randomized trial of conventional vs. accelerated CXL (continuous 7 mW/cm^2 for 15 minutes, total energy 6.3 J/cm^2) in 21 patients reported similar results in halting ectasia progression in each group.(Kanellopoulos 2012a) For conventional and accelerated groups respectively, mean steepest keratometry (Kmax) reduced from 49.5 to 46.1 D and 48.7 to 45.8 D, while mean sphere was reduced by 2.5D and 2.1D and mean cylinder reduced by 2.9D and 2.5D. Problems with this study include the paired-eye design (for an asymmetrical disease), the lack of randomisation details, variable follow-up rate (18 to 56 months) and the lack of statistical analysis of results between the two groups. Furthermore, it is not

possible to compare this study with other published series because laser phototherapeutic keratectomy (PRK) was used to remove the epithelium. Rather than an effect of CXL, the large degree of flattening seen in both groups (> 3 D) is likely to be a result of apical stromal ablation, attributable to the masking effect of the corneal epithelium that tends to be thinnest over the cone.(Kymionis et al. 2012) Using a slightly higher irradiance (continuous 9 mW/cm^2 for 10min, total energy 5.4 J/cm^2), Cinar et al reported 6-month results in 13 progressive keratoconus eyes compared with 13 conventionally treated eyes. (Cinar et al. 2013)They reported statistically significant reductions in mean Kmax of 1.14 ± 2.08 D (accelerated) and 0.94 ± 1.86 D (conventional), although there were no overall differences in visual or refractive outcomes between the two groups. Neither of these two studies of accelerated CXL comment on any individual treatment failures.

Lack of consensus on what defines disease progression both before and after treatment complicates comparisons between CXL techniques based on the current literature. Assuming no diurnal variation in corneal shape, the coefficient of repeatability (CoR) should correspond closely to the limits of agreement for successive measures of corneal tomography indices, defining a threshold beyond which there is a 95% probability that an observed difference reflects disease progression rather than measurement inaccuracy. Pentacam measurement repeatability in stage II keratoconic eyes has been shown to be worse than in normal corneas, with a CoR for Kmax between 1.5 – 2.00 D.(Szalai et al. 2012; Hashemi et al. 2015) We based our definition of progression, and treatment failure, on this CoR value; lower thresholds (+1 D)

have been used in alternative studies.(O'Brart et al. 2011; Wollensak, Spoerl, et al. 2003a) Changes in this, and other criteria used to evaluate stability, may alter the intervention and failure rates where the observed increase in Kmax is less than +1.5 D.

Further complicating a comparison of published outcomes are the numerous permutations of accelerated protocols in which total energy, irradiance and/or treatment time can be changed. Pulsing the light is a more recent protocol variable, intended to allow a trace amount of ambient oxygen to diffuse into the cornea during the 'off' phase. Corneal tissue absorbs radiant energy during the CXL process. This can be delivered as either a 'slow-cook' (i.e. Dresden protocol, 3 mW/cm^2 for 30 minutes) or a 'short burst' (30 mW/cm^2 for 3 minutes), with the same total radiant energy dose (5.4 J/cm^2; energy = irradiance x time). This reciprocity is defined in the Bunsen-Roscoe law, which states that the induced photochemical reaction depends on the total radiant energy dose regardless of the irradiation time. However, this law appears to break down at very high irradiances, with no observed increase in Young's modulus in ex vivo pig corneas treated above 50mW/cm^2 (treatment time less than 2 minutes).(Wernli et al. 2013) Below this cut-off, the same authors observed comparable increases in stiffness between the two treatment protocols. An alternative technique (scanning acoustic microscopy) has been used to demonstrate similar increases in corneal stiffness in ex vivo human corneas treated at 9mW/cm^2 for 10 minutes (same total energy, 5.4 J/cm^2). (Beshtawi et al. 2013)

UV delivery devices differ as well, although this variable has, to date, not received the attention it warrants. The UV-X CXL device (IROC, Zurich, Switzerland), as used in the Melbourne RCT(Wittig-Silva et al. 2014) comprises an array of 7 overlapping diodes with a resultant non-homogenous beam profile of varying intensity across the treatment zone (Figure 5.2). The Gaussian beam profile of this device, working at a nominal irradiance of 5.4 J/cm^2 results in zones of central hot-spots of higher surface irradiance (up to 8.4 J/cm^2) and peripherally low irradiance zones (3.7 J/cm^2).(Marshall et al. 2013) The disparity in treatment efficacy reported in the literature may, in part, be a function of the beam profile of the treatment device used, with 'over-treatment' hot-spots over a central cone causing more flattening that areas exposed to less UV irradiance. The homogenous beam profile of the KXL device, as used in the series of patients I report in this chapter, may be expected to produce a more isotropic treatment effect with less flattening.

Besides ex vivo functional comparisons, apparent tissue changes in patients following conventional and accelerated CXL protocols have been investigated. A demarcation line, typically visible at approximately 300 µm following the Dresden protocol, is thought to represent the border between treated tissue (anterior to the line) and untreated tissue (posterior to the line). Touboul et al observed, by confocal microscopy, that the demarcation line following accelerated CXL (30mW/cm^2 for 3 minutes, total energy 5.4 J/cm^2) lies more superficial, at a mean depth of 100-150 mm. (Touboul et al. 2012) However, Kymionis et al. saw no such difference by OCT comparing Dresden and an alternative protocol (9mW/cm^2 for 14 minutes, total energy 7.56 J/cm^2), with

mean demarcation line depths of 337 and 322 µm respectively. (Kymionis et al. 2014) These conflicting findings may reflect the differences in irradiance, time and total energy exposure employed in these two studies. For the time being, the evidence-base lacks longer-term studies of corneal shape and vision using these protocols to prove whether a more superficial treatment, as suggested with 30mW/cm^2 for 3 minutes, is any less effective.

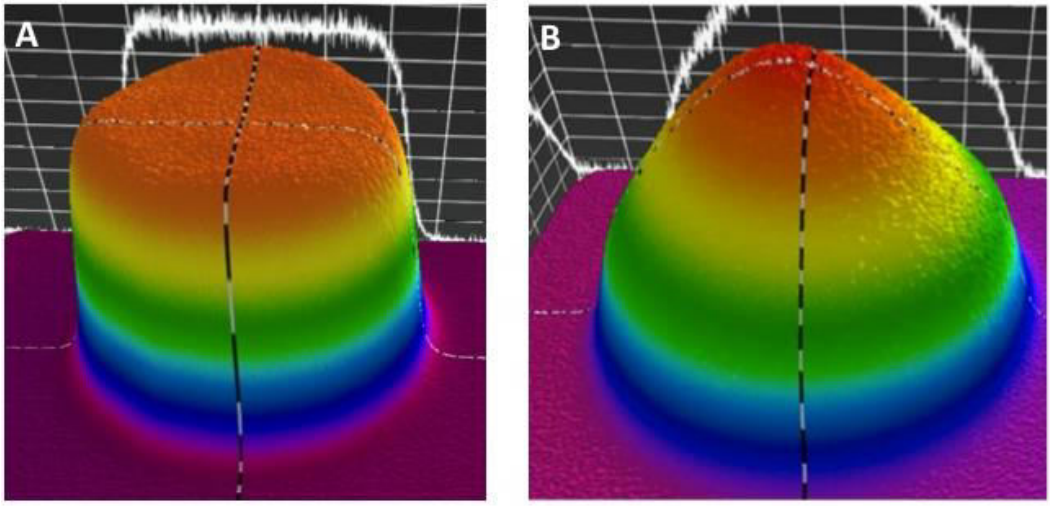

Figure 5.2 Ultraviolet light beam profile

(A) Measured beam profile of KXL device (Avedro, Inc, MA, USA) demonstrating uniform energy distribution with application of nominal 5.4 J/cm^2 dose, providing a consistent energy profile through a range of focus of more than 1cm from the image plane. **(B)** Beam profile of a multi-LED CXL device (UV-X, IROC, Zurich, Switzerland) used in early studies demonstrating uneven energy distribution and central hot spot of approximately 8.4 J/cm^2 with application of nominal 5.4 J/cm^2. (Images reprinted with permission by Avedro, Inc.)

The safety profile of high-irradiance UV exposure has yet to be established. Transient signs of endothelial stress (cell density, polymegathism and pleomorphism) have been documented by Cingü et al. in 36 keratoconic eyes within the first month after high-irradiance CXL (18 mW/cm^2 for 5 minutes) before returning to normal after 6 months. (Cingü et al. 2013) Kanellopoulos reported a drop in the endothelial cell count in both accelerated (7 mW/cm^2 for 15 minutes) and conventional CXL groups (-100 vs. -250 cells respectively) at a mean follow-up of 46 months.(Kanellopoulos 2012a) Although I only have data in 10 of 55 treated eyes, a mean reduction in cell density of 95/mm^2 (3%) does not suggest any significant increased risk associated with the accelerated protocol.

In summary, I present up to 2 year outcomes following accelerated CXL for progressive keratoconus. Practical reasons exist to support a reduction in the total treatment time for CXL, and the data presented in this study add to the growing published literature on these new accelerated protocol iterations. While the debate continues on the relative merits, (MacGregor et al. 2014; Tsatsos et al. 2014) it is not possible at present, with an incomplete evidence base, to conclude whether UVA delivery times can be reduced without compromising the efficacy of the treatment.

6 Visual rehabilitation - Gross shape correction: Femtosecond laser-assisted intrastromal corneal ring segment implantation in progressive keratoconus.

6.1 Introduction

Intrastromal corneal ring segments (ICRS) were originally developed for the correction of myopia, although gained limited popularity compared with excimer laser. They act as a spacer between corneal lamellae thereby shortening central arc length, the degree of shortening being proportional to the thickness of the implant. As an implantable means to remodel the corneal profile, interest in these devises has shifted away from the treatment of simple ammetropia to ectatic diseases, notably keratoconus.

Available ICRS differ principally in their cross-sectional profile, diameter, thickness and segment length. The original Intacs segments (Addition technologies, USA) had a hexagonal profile, available in two diameters, with a newer design (Intacs SK) available in two different thicknesses and an oval profile. Ferrara ICRS (Mediphacos, Brazil), with a triangular profile designed to reduce glare associated with other profiles, are available in small diameters (6 mm and 5 mm) and a range of thicknesses (150 – 350 µm). Similar in design, material and thickness to Ferrara, the same company subsequently marketed KeraRings, with the smallest internal diameter (4.4 mm). KeraRings are additionally available in different arc lengths (90, 120, 160 and 210

degrees), to potentially achieve better astigmatic control. Superiority amongst these rings has yet to be convincingly demonstrated, for either quality of vision (e.g. glare) or visual, refractive and topographical parameters.

In this chapter, I report 18-month results of femtosecond laser-assisted intrastromal corneal ring segment (KeraRing) implantation in keratoconus.

6.2 Methods

6.2.1 Study design

Retrospective consecutive case series.

6.2.2 Inclusion criteria

The medical records were reviewed for all keratoconic patients receiving KeraRing implantation by 3 surgeons at Moorfields Eye Hospital between 2010 and 2013 inclusive. All patients met all 4 of the following inclusion criteria before surgery:

1. Contact lens intolerance
2. Corrected distance visual acuity (CDVA) ≤ 6/9
3. Corneal thickness at the 6 mm channel site ≥ 450 µm.
4. Controlled ocular surface inflammation

6.2.3 Surgical procedure

Surgical plans based on Scheimpflug tomography and subjective refraction were obtained from the manufacturer (Mediphacos Ltd, Belo Horizonte, Brazil). Following topical instillation of proxymetacaine 0.5%, tetracaine 1% and povidone-iodine 5%, a 360-degree femtosecond laser channel of internal diameter 5mm and external diameter 5.9mm was created at a depth between 350 – 400 µm as dictated in the surgical plan (see example in Figure 6.1 below). Into this channel, either 1 or 2 ring segments were implanted. No sutures were used. At the end of the procedure, preservative-free dexamethasone 0.1% and chloramphenicol 0.5% were instilled.

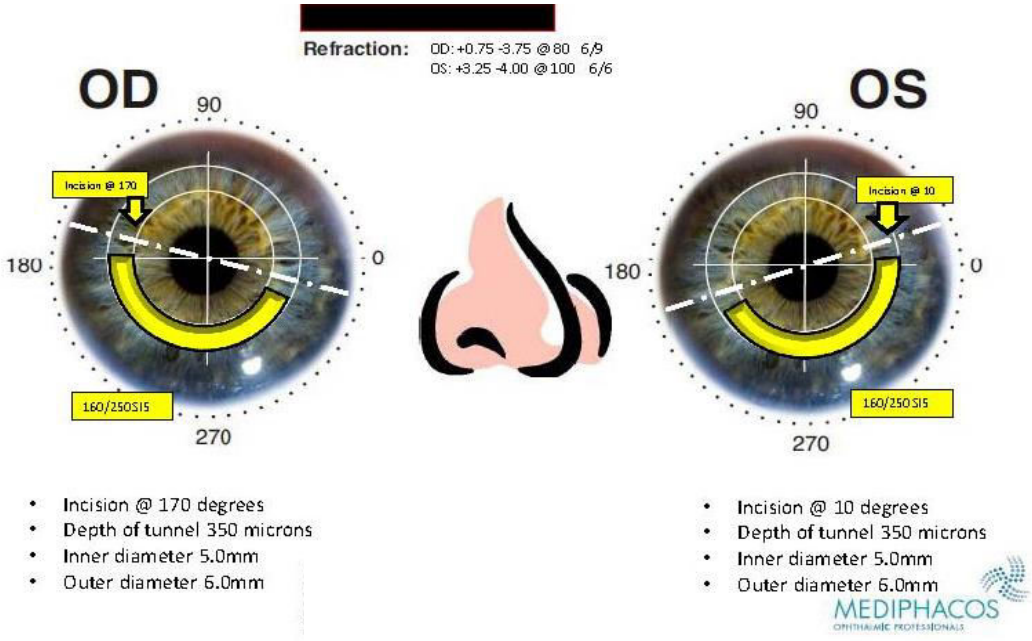

Figure 6.1 Example KeraRing surgical plan

6.2.4 Post-operative care

Post-operatively, patients were prescribed preservative-free topical dexamethasone 0.1% and chloramphenicol 0.5% four times a day for 1 week. Serial tomography and subjective refractions were performed to monitor for post-implantation ectasia progression. The first topography scan after 3 months post-surgery was used as an updated baseline with which to compare for ectasia progression.

6.2.5 Outcome measures

The main outcome measure was CDVA. Secondary outcomes measures included UDVA, manifest refraction, corneal coma, contact lens tolerance and complications. Snellen visual acuity was converted to LogMAR equivalent for statistical analysis. Mean ± standard deviation are presented.

6.3 Results

KeraRings were implanted in 26 eyes of 26 patients (mean age 33 ± 7 years) and followed-up for a mean 18 ± 6 months. Spectacle-CDVA improved (Figure 6.2; Figure 6.3) from 0.32 ± 0.21 LogMAR equivalent pre-operatively to 0.18 ± 0.20 post-operatively ($p < 0.001$), with a mean improvement of 1.5 ± 1.52 LogMAR equivalent lines of acuity (Figure 6.3). Refractive astigmatism reduced significantly by a mean 3.38 ± 2.49 D ($p < 0.001$), with a trend towards a greater post-operative response with higher pre-existing levels (Figure 6.4).

Table 6.1 summarises the changes in outcome measures.

Table 6.1 Refractive and keratometric parameters (n = 26)

Parameter	Pre-operative	Post-operative	P value*
CDVA (LogMAR)	0.32 ± 0.21	0.18 ± 0.20	< 0.001
UDVA (LogMAR)†	1.25 ± 0.29	0.66 ± 0.44	< 0.001
Sphere	-0.53 ± 4.06	-0.35 ± 2.84	0.79
Cylinder	-7.44 ± 2.67	-4.07 ± 2.10	< 0.001
Kmax	59.60 ± 4.96	58.59 ± 5.35	0.24
K2 front	52.38 ± 3.56	50.42 ± 3.64	0.001
K1 front	48.13 ± 4.14	46.92 ± 3.32	0.051

Mean ± SD; UDVA uncorrected distance visual acuity; CDVA corrected distance visual acuity; * Paired student T-test; † n = 15 due to undocumented UDVA

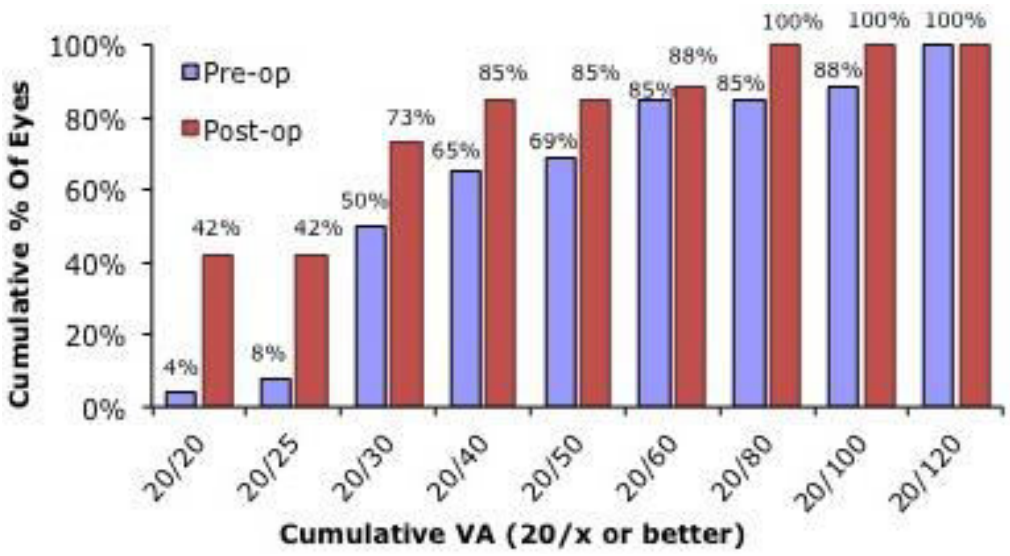

Figure 6.2 Cumulative corrected distance visual acuity (n = 26)

No intra--operative complications occurred. One eye lost 1 line of vision following KeraRing implantation. Pre-operatively, all eyes were intolerant of rigid gas permeable (RGP) contact lenses. Post-operatively, vision correction was tolerated in RGP lenses (n = 14, 54%), toric soft contact lenses (n = 6, 23%) and spectacles (n = 5, 19%). The remaining eye developed post-implantation central striae; despite achieving 6/9 CDVA, the patient elected to

undergo deep anterior lamellar keratoplasty. Corneal collagen cross-linking was performed on 4 (15 %) of 26 eyes for progressive keratoconus post-implantation.

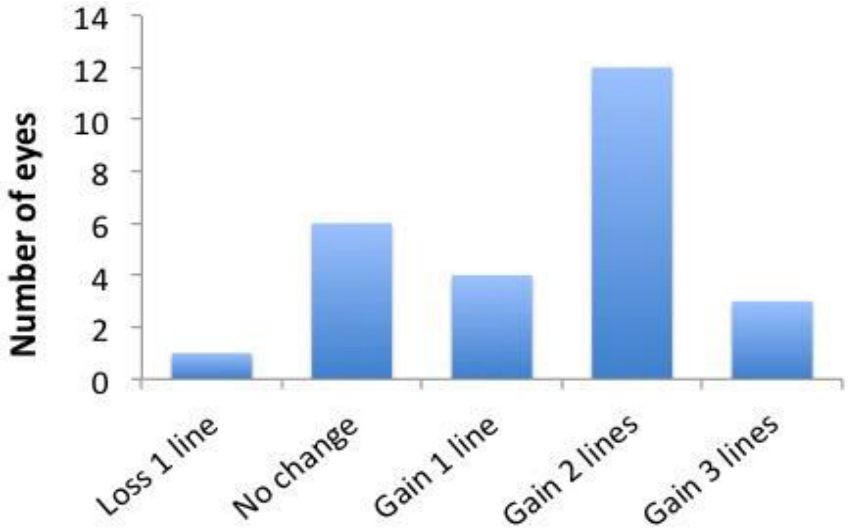

Figure 6.3 Change in CDVA (equivalent LogMAR lines), n = 26

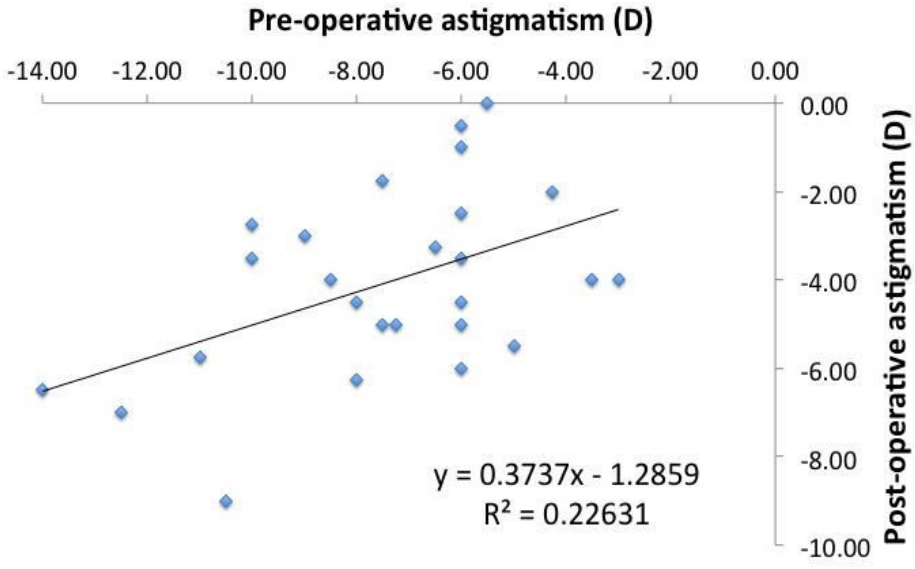

Figure 6.4 Change in manifest astigmatism

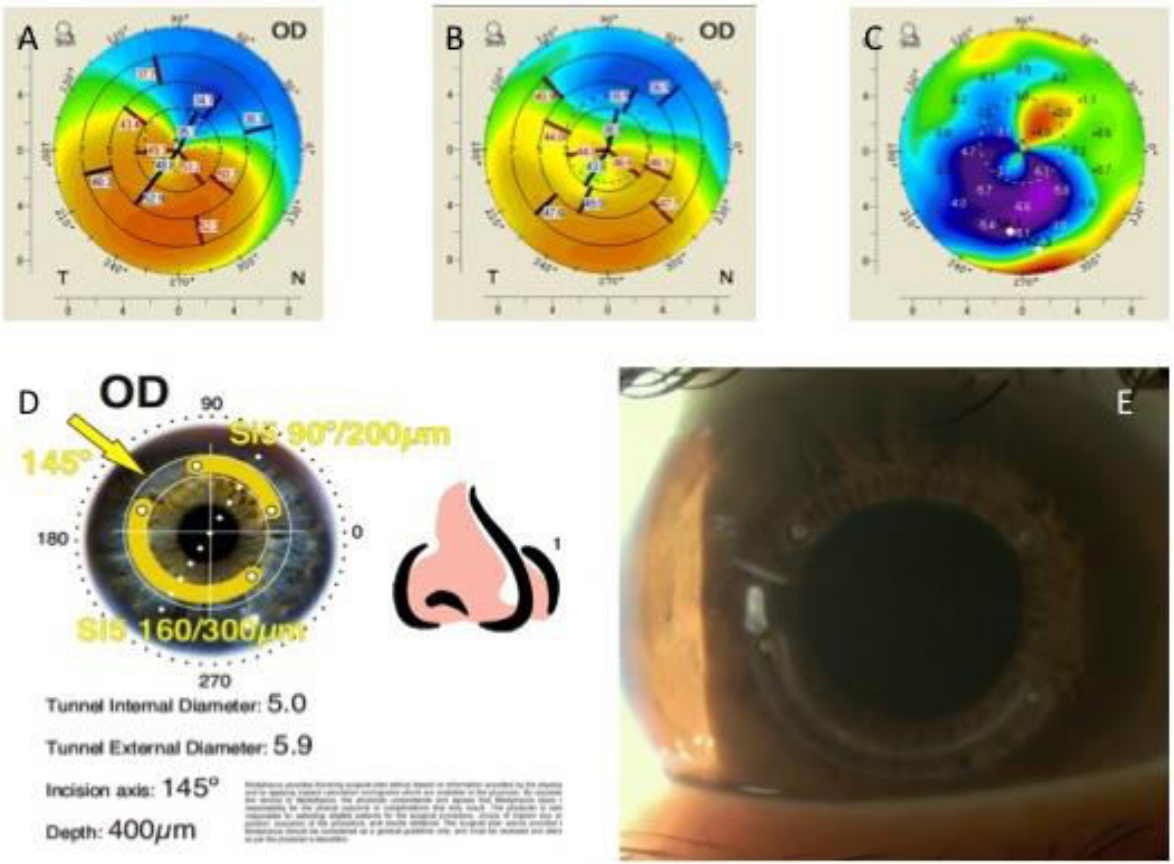

Figure 6.5 Example pre- and post-ICRS implantation

(A) Sagittal curvature pre-implantation; **(B)** sagittal curvature post-implantation; **(C)** Induced difference (A-B) showing flatting over cone, with corresponding steepening superiorly; **(D)** surgical plan; **(E)** colour photograph of ICRS in situ. Note axial misalignment compared with plan. Pre-op: -1.00/-4.25x60 6/60. Post-op: 6.00/-2.00x130 6/9

6.4 Discussion

This small retrospective series presents data showing significant gains in spectacle-corrected vision can be achieved with femtosecond laser-assisted intrastromal corneal ring implantation in keratoconus. Through improvements in CDVA and/or contact lens tolerance, keratoplasty may be avoided in these patients. I have previously detailed comparable outcomes from the literature on page 51 which I will not be duplicate here.

However, anecdotal scepticism amongst some surgeons of the benefits of ICRS in keratoconic eyes is due, in part, to the poor predictability of outcome in any given eye. Underlying this is the lack of validated nomograms for deciding optimal ICRS implantation (thickness, diameter, arc length/s etc.). The earliest studies described standardized implantation in all eyes regardless of shape (Kymionis et al. 2007), while more recent nomograms based on regression analysis of empirical data for different ring designs purport to improve predictability. Nomograms for each of the principle ICRS designs have been used to improve predictability based on preoperative spherical equivalent (Ertan & Colin 2007; Zare et al. 2007; Kanellopoulos et al. 2006), cone location and morphology, (Torquetti & Berbel 2009) and preoperative CDVA. (Vega-Estrada et al. 2013) To date there have been no direct comparisons between these various nomograms. Furthermore, data predicting which patients are least likely to do well are lacking; for example, establishing an evidence-based upper keratometry limit for successful ICRS use is not possible at present, with Kmax inclusion criteria in series to date ranging from ≤ 55 D to < 70 D. Although implantation need not adversely

compromise future lamellar graft options, (Fontana et al. 2009) avoiding ICRS in eyes with a predicted poor outcome in favour of more definitive visual rehabilitation through transplantation would be preferable.

Very little long-term data is available for ICRS, and any effect of ICRS implantation on disease progression remains uncertain. CXL was performed on 4 (15 %) of 26 eyes in the above series for progressive keratoconus post-implantation. Progression has similarly been observed up to 3 years post-Intacs insertion, indicating that disease stabilization was not achieved by ICRS alone.(Alio et al. 2006)

In conclusion, with increasing availability of femtosecond laser technology, OCT regional pachymetry, and intraoperative guidance systems to help reduce axial misplacement intraoperatively (Figure 6.5), ICRS implantation should become safer and more predictable. Several important gaps in the evidence base for this intervention exist. As a step towards visual rehabilitation (and away from corneal transplantation), there are already strong arguments for ICRS implantation for gross corneal shape correction in keratoconus patients with reduced CDVA – particularly if they are contact lens intolerant. Finer adjustments to correct surface irregularity (as detailed in chapter 6) can then be considered.

7 Visual rehabilitation - Fine shape correction: A prospective study of simultaneous transepithelial photorefractive keratectomy and corneal collagen cross-linking for keratoconus

7.1 Introduction

Irregular astigmatism (irregular corneal shape leading to irregular focus) is a common cause of failure to achieve an adequate spectacle correction for most patients with corneal disease, including keratoconus. For those affected, rigid gas permeable contact lenses are the simplest means of visual rehabilitation. Not all patients tolerate rigid contact lens wear, and those that do may experience discomfort and have a restricted wearing time. Traditionally, where contact lenses fail, a corneal transplant is required to restore vision.

Keratoconus, in which the corneal shape becomes progressively steeper and more irregular in the 2nd to 4th decades of life, is a common cause of irregular astigmatism.(Gore et al. 2012) Disease progression in keratoconus can be stabilised with CXL, and although corneal shape can improve, I have shown in chapter 4 that significant irregular astigmatism may remain. For this reason, most patients already dependent on RGP lenses will continue to be so following CXL treatment.

Excimer laser treatment designed to regularise the corneal shape may offer these patients improvements in vision without the need for rigid contact lenses. Transepithelial photorefractive keratectomy (transPRK) has previously been used to reduce irregular astigmatism post keratoplasty.(Allan & Hassan 2013) In this study the authors based their treatment on corneal topography, creating a corresponding pattern of tissue removal from the corneal surface designed to produce a smoother, more regular focusing shape.

Simultaneous transPRK with CXL in progressive keratoconus is an exciting new development. Performing both treatments simultaneously may offer advantages over sequential treatments: faster visual improvement, only one painful procedure and reduced risk of delayed disease progression. Promising results report improvements in spherical equivalent, uncorrected distance visual acuity (UDVA) and corrected distance visual acuity (CDVA), with stabilisation of corneal shape up to 12 months. (Kymionis et al. 2009; Kanellopoulos 2009)

In this chapter, I present 6-month interim outcomes from a prospective study of simultaneous ocular wavefront-guided transPRK and CXL.

7.2 Methodology

The primary objective of the study was to investigate the visual benefits in patients with progressive keratoconus treated with combined CXL and ocular wavefront-guided transPRK.

7.2.1.1 Design

Prospective interventional series.

7.2.1.2 Primary outcome

LogMAR CDVA at 12 months

7.2.1.3 Secondary outcomes

LogMAR UCVA

Manifest refraction

Pentacam indices

Rate of infective keratitis

7.2.1.4 Subject selection

Inclusion criteria

- Patients with progressive stage I - III keratoconus
- CDVA < 0.00 logMAR

Exclusion criteria

- Patients under the age of 18 years
- Active ocular surface disease
- Minimum corneal thickness <390 µm (leaving 325 µm residual stromal thickness after transPTK)

7.2.1.5 Study interventions

TransPRK programming

Three consistent scotopic ocular wavefront scans (Ocular Wavefront Analyzer, SCHWIND eye-tech-solutions GmbH, Germany) were acquired within 0.5 D spherical equivalent refraction of each other. Corneal topography (*Schwind Sirius*) was also recorded to allow a comparison of planned wavefront and topography-guided treatments. Patients were required to remove gas permeable contact lenses for 2 weeks and soft contact lenses for 1 week prior to scanning. Pharmacological pupil dilation with tropicamide 1% was used where pupil diameter was less than 5.5 mm. The scan with the lowest sphere and highest coma was exported for treatment programming. Iris scans were taken for static cyclotorsion control during the treatment. Ablation depth was minimised during treatment programming by removing all sphero-cylindrical constraints. I aimed to preserve a minimum corneal stromal thickness prior to CXL of 325 µm. To ensure effective CXL was not compromised by a smaller diameter zone of epithelial removal, epithelial transPTK and stromal PRK was delivered separately where the programmed laser ablation zone for transPRK was predicted to be less than 8mm in diameter.

TransPRK/CXL surgery

Treatments were performed by either by myself or Bruce Allan. Following topical instillation of proxymetacaine 0.5%, tetracaine 1% and povidone-iodine 5%, a lid speculum inserted. After the laser treatment was complete, dextran-free 0.1 % w/v riboflavin 5'-monophosphate solution in saline and

hydroxypropyl methylcellulose (VibeX Rapid, Avedro, MA, USA) was applied every 2 minutes for a total of 10 minutes before UVA exposure (KXL®, Avedro, MA, USA) at 30 mW/cm^2 for 4 minutes (pulsed every 1.5 seconds) was then applied (total energy 7.2 mJ/cm^2). Mitomycin C was not used.

At the end of the procedure, preservative-free dexamethasone 0.1% and chloramphenicol 0.5% were instilled and a bandage contact lens applied. Post-operatively, patients were prescribed a tapered course of preservative-free topical dexamethasone 0.1%, moxifloxacin and hyaluronic acid 0.1% for 1 week, along with topical diclofenac 0.1%, cyclopentolate 1% twice a day and 50 mg oral diclofenac 3 times a day for 3 days. Patients were additionally provided with 3 minims of proxymetacaine 0.5% for use in the early post-operative period. The bandage contact lens was removed at 1 week after which all therapy was discontinued except topical hyaluronic acid 0.1% and fluorometholone 0.1% 4 times a day for 1 month.

7.4 Results

At the time of writing, 52 eyes of 55 recruited patients have been treated. Twenty-nine (53%) eyes have at least 3-month follow-up data; 13 (24%) eyes have 6-month follow-up data. Data on those patients who have reached at least 3-month follow-up is presented here.

7.4.1 Surgical parameters

All surgery was uncomplicated. Mean ± SD transPRK ablation diameter was 8.25 ± 0.56 mm, with a mean optical zone of 7.02 ± 0.56 mm. Mean stromal ablation depths based on ocular wavefront-guided treatments were significantly shallower than projected treatments based on surface topography alone ($p < 0.001$, Table 7.1). At the thinnest part of the cornea (cone apex), the mean saving for ocular-wavefront guided treatments was 15 ± 10 µm.

Table 7.1 Stromal ablation depths

Parameter	OWF (µm)	Topography (µm)	P value
Cone Apex	33 ± 12	48 ± 11	< 0.001
Corneal center	19 ± 11	33 ± 7	< 0.001
Maximum ablation	34 ± 12	52 ± 10	< 0.001

Mean ± SD; OWF, ocular wavefront; µm, micrometer

7.4.2 Functional and Keratometric outcomes

At 3-months, neither UDVA nor CDVA had significantly improved, despite clear topographical shape regularisation. This was attributed to stromal haze underling the 7 (24%) of 29 eyes that lost more than 1 line of LogMAR acuity at 3-months. For the 13 eyes with 6-month follow-up, no eye has lost vision,

with a mean improvement of 1.5 lines of LogMAR acuity. Refractive, visual and keratometric outcomes are summarised in Table 7.2 and Figure 7.3

Table 7.2 Visual and keratometric outcomes

Parameter	Baseline (n = 29)	3 months (n = 29)	6 months (n = 13)	P value†
CDVA	0.30 ± 0.23	0.24 ± 0.23	0.15 ± 0.18	0.019
UDVA	0.75 ± 0.41	0.62 ± 0.37	0.45 ± 0.34	0.003
Sphere	0.95 ± 2.90	-1.42 ± 2.04	-1.06 ± 2.66	0.095
Cylinder	-5.59 ± 3.34	-3.81 ± 2.96	-3.02 ± 3.00	< 0.001
Kmax	58.94 ± 4.65	53.97 ± 4.51	52.68 ± 4.60	< 0.001
K2 front	50.91 ± 3.31	49.84 ± 3.43	49.11 ± 3.23	0.739
K1 front	47.13 ± 2.84	46.07 ± 2.76	45.45 ± 2.07	0.010
Pachymetry*	447 ± 71	415 ± 42	420 ± 50	0.739

Mean ± SD; † Baseline vs. 6-months; *minimum pachymetry; UDVA uncorrected distance visual acuity; CDVA corrected distance visual acuity; ECC endothelial cell count

7.4.3 Functional and keratometric outcomes

One patient was temporarily lost to follow-up following surgery, presenting to his local eye unit some weeks later with the bandage contact lens still in situ and microbial keratitis. A central corneal scar was present at 3-months with a 4-line loss of CDVA. One other eye developed a small peripheral sterile infiltrate which readily responded to further topical steroids. No post-operative ectasia has occurred to date.

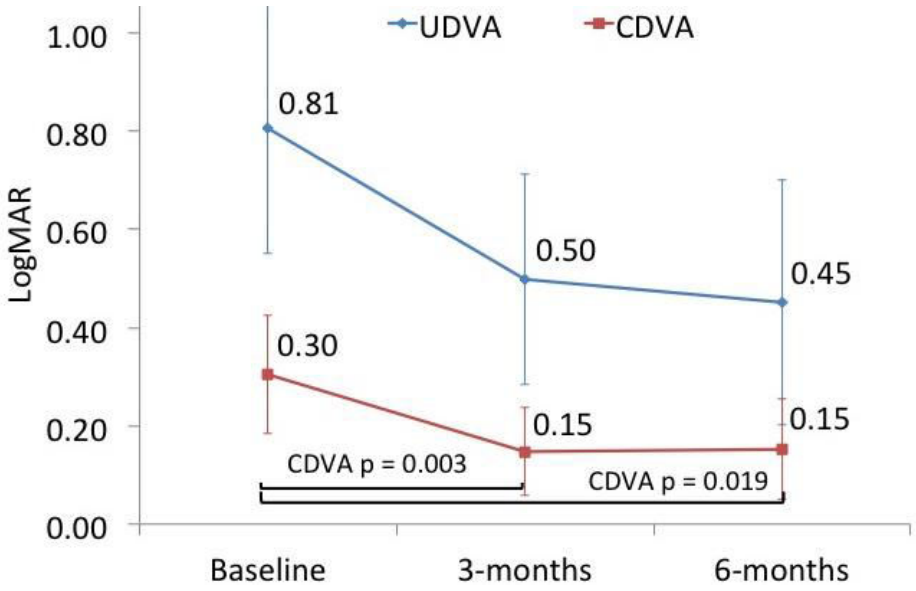

Figure 7.1 Mean visual acuities post-transPRK/CXL

Data plotted only for eyes with 6 month follow-up (n = 13)

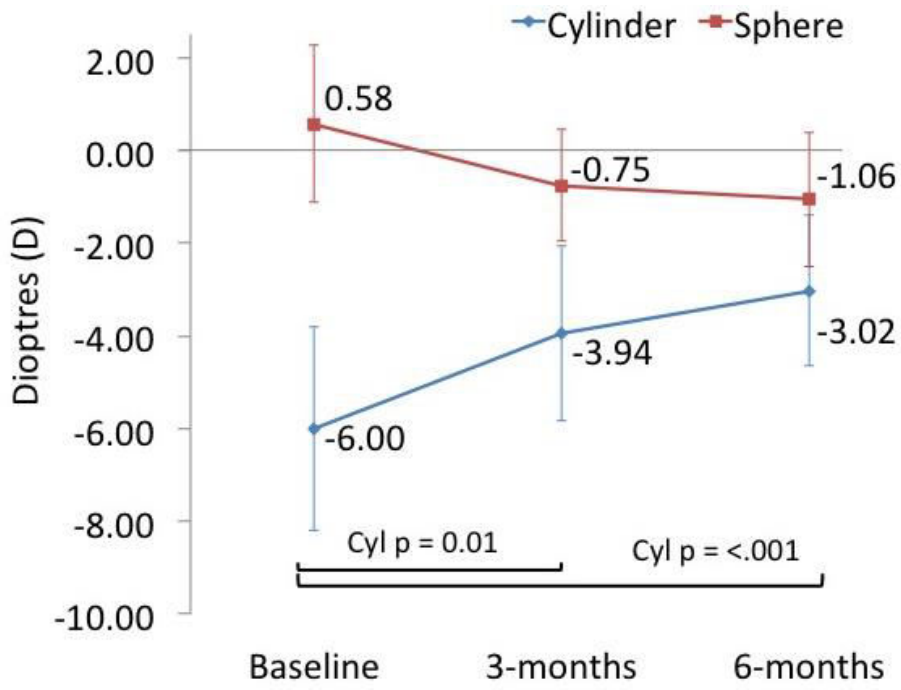

Figure 7.2 Mean refractive changes post-transPRK/CXL

Data plotted only for eyes with 6 month follow-up (n = 13)

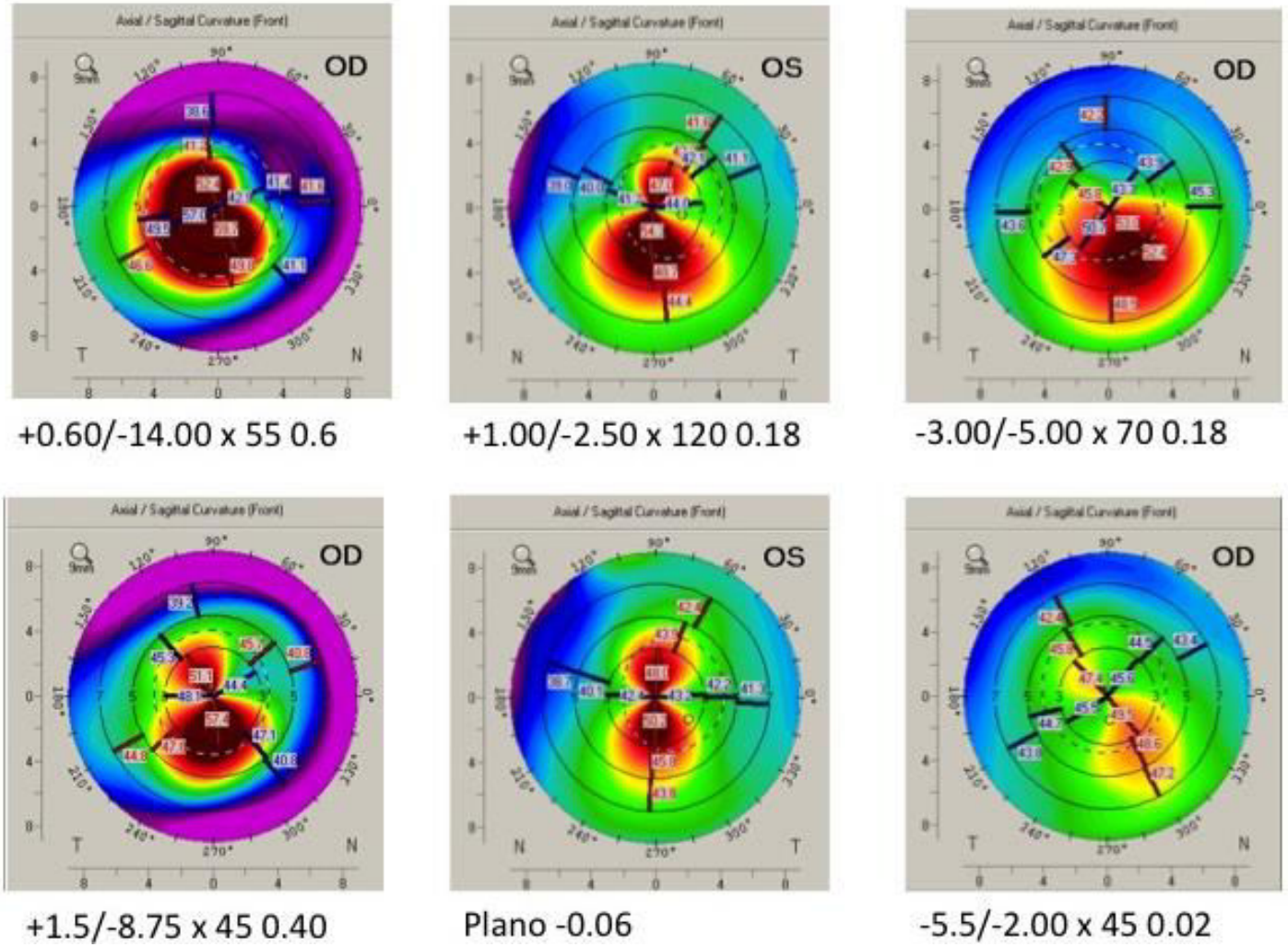

Figure 7.3 Example topography pre- and post-transPRK/CXL

Upper row: Pre-op; lower row: 3-months post-op

7.5 Discussion

While clearly too early to pass judgement on longer-term viability, these interim data demonstrate promising early results for a combined transPRK and CXL approach to both improving visual acuity and achieving stabilisation in progressive keratoconus.

The principle criticism of photoablative corneal surgery in keratoconus is the risk of further destabilising an inherently 'weak' cornea. While the underlying mechanisms of keratectasia post-excimer laser refractive surgery are poorly understood, keratoconus has traditionally been considered an absolute contraindication for any photoablative procedure. CXL is considered to 'strengthen' the cornea, but tissue changes following treatment are not well defined, principally due to the lack of validated in vivo measures of relevant corneal biomechanic properties.(Meek & Hayes 2013) In ex vivo studies, CXL has been shown to significantly increases corneal rigidity with a 450% increase of Young's modulus in human corneas at 6% strain.(Wollensak, Spoerl, et al. 2003b)

This potential protective effect of CXL has driven the argument against excimer laser surgery in keratoconus full circle, with a number of investigators specifically advocating its use in keratoconics. (Kymionis et al. 2009; Kanellopoulos 2009; Labiris et al. 2012; Kymionis et al. 2012; Mukherjee et al. 2013)(Table 2.13) The most basic embodiment of transPRK involves removal of the corneal epithelium (transphototherapeutic keratectomy, transPTK). Using a standard 7.0 mm wide, 50 µm deep ablation, Kymionis et al yielded

significant visual gains as compared to mechanical debridement. (Kymionis et al. 2012) This ablation takes advantage of the varying epithelial thickness that, to an extent, masks underlying stromal surface irregularity (i.e. irons out the peaks and troughs) as well as being thinnest over the cone.

TransPRK is a step up from transPTK. Where transPRK is applied immediately before CXL (i.e. simultaneous combined treatment), the aim is to improve CDVA by reducing irregular astigmatism rather than to fully correct spherocylindrical errors. This is in order to maintain a sufficient residual stromal bed after ablation to allow safe CXL, as well as reduce the risk of hypermetropic overcorrection if spherical equivalent reductions induced by CXL are not anticipated. TransPRK treatments can be based on manifest refraction (Mukherjee et al. 2013) or be guided by topography or whole eye wavefront data. With advanced disease, all of these approaches are likely to become less accurate, with indeterminate subjective spherocylindrical endpoints on refraction, reduced topographic reliability and poor quality aberrometry scan acquisition all occurring as corneal shape becomes more irregular. Mukherjee et al reported TransPRK/CXL outcomes in 22 eyes of 14 patients based on spherocylindrical parameters only, aiming to fully correct the subjective refractive cylinder up to a maximum ablation depth of 50 µm. Where the topographic and subjective cylinder did not correlate, a lower proportion of cylinder was corrected. If the cylindrical correction did not require the maximal permitted 50 µm ablation, then the remaining available ablation depth was used to correct as much spherical error as possible. Mitomycin-C was not used. At 12-months, mean LogMAR CDVA improved

from 0.31 ± 0.2 to 0.11 ± 0.13 ($p < .05$) and spherical equivalent improved from -2.74 ± 4.1 D to -0.3 ± 3.2 D ($p = 0.002$). However, these results belie large and unfortunate hypermetropic shifts, with a mean spherical equivalent prediction error (achieved – expected spherical equivalent) of 1.3 D (range -4.75 to +10 D). 4 eyes (18 %) developed some haze, although all gained vision compared with pre-operative values. We chose not to use mitomycin C in this present study on the expectation that keratocyte apoptosis may be achieved by CXL itself. However, the 24% of eyes developing haze within the first 3 months suggests this CXL-mediated stromal keratocyte depopulation is insufficient to prevent clinical significant haze.

The largest study based on topography-guided ablations is a series with minimum 2 year postoperative follow-up (Kanellopoulos 2009) comparing prospective outcomes of 198 eyes treated with topography guided PRK followed immediately by CXL (simultaneous combined treatment) with an earlier retrospective series of 127 eyes treated with topography guided PRK a minimum of 6 months after CXL (sequential combined treatment). Simultaneous combined treatment produced greater improvement across a range of measures: LogMAR CDVA improved from 0.39 ± 0.3 D to 0.11 ± 0.2 D, with a reduction in spherical equivalent of -3.2 ± 1.4 D and mean keratometry of -3.5 ± 1.3 D. This compares with the sequential group's CDVA improvement from 0.41 ± 0.3 D to 0.16 ± 0.2 D, spherical equivalent reduction of -2.5 ± 1.2 D and mean keratometry reduction of -2.75 ± 1.3 D. Haze scores were also significantly better for simultaneous combined treatment. 20 second intraoperative applications of mitomycin C were used throughout, and the

maximum ablation depth was limited to 50µm. The essential problem for this comparison is that the time interval between CXL and PRK for sequential treatment was not specified, and may have been considerably shorter than the 2 year period in which refractive results typically continue to improve after CXL alone.(Caporossi et al. 2010)

No reports of ocular wavefront-guided transPRK and CXL in keratoconus exist in the literature. In this study I have demonstrated that ocular wavefront-guided treatments targeting irregular astigmatism ablate significantly less tissue compared with treatments based on anterior corneal surface aberrotmetry alone. The implication is that the posterior corneal surface partially offsets anterior corneal surface irregularities. This is analogous to the negatively powered posterior corneal surface reducing whole corneal power by partially correcting the positively powered anterior corneal surface. Less tissue ablation has theoretical advantages in terms of maintained corneal biomechanics and reduced haze formation post-ablation.

In conclusion, these interim results show great promise for combined simultaneous transPRK and CXL to provide rapid visual rehabilitation in patients with progressive keratoconus. Simultaneous combined treatments have clear advantages for patient comfort (the epithelium is only removed once) as well as promising faster visual recovery without the need to wait for corneal shape improvement. As compared with sequential transPRK and CXL, simultaneous treatment also avoids the risk of destabilizing the cornea by ablating previously cross-linked tissue which is concentrated in the anterior stroma. (Lombardo, Serrao, et al. 2014) Further study is required to determine

whether increased haze scores for sequential combined treatment observed by Kanellopoulos are still evident where PRK is performed later in the post CXL wound healing cycle, a minimum of 2 years after treatment.

8 Conclusions – Past, present and future

The last few years have seen new and exciting developments in the management of keratoconus, both stabilizing and reversing corneal shape changes, with interventions for visual rehabilitation originally developed in the field of refractive surgery finding new applications in ectatic corneas. The evidence favouring the safe and efficacious use of (standard) epithelium-off CXL is robust, backed by over a decade of clinical data, crucially underpinning existing and emerging combined-treatment algorithms. The substantial interest in CXL (Figure 8.1) is likely to continue, with a drive (both clinical and pragmatic) for safer and quicker office-based treatments.

Figure 8.1 PubMed listings for collagen cross-linking

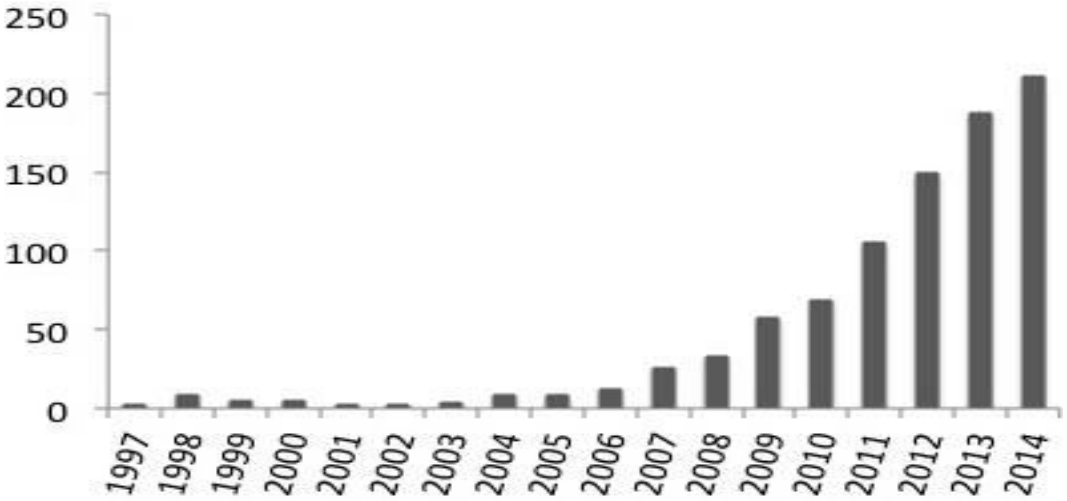

Supporting on-going development will be improvements in our understanding of corneal biomechanics, the mechanisms of CXL and the tissue changes it induces. X-ray scattering, dynamic deformational Scheimpflug imaging and

Brillouin microscopy are three examples from where this new knowledge will likely arise. Someone, one-day, may be even rebut the misnomer claims for CXL and prove once and for all that collagen cross-linking does, in fact, generate collagen cross-links.

More pragmatically perhaps, significant improvements in CXL are also likely to be industry driven. Even if Avedro Inc.'s ultimate goal is to develop CXL into a bespoke "no laser" refractive procedure for the correction of low myopic astigmatism, their involvement should be no less welcomed within the world of keratoconus. Keratoconus is not comparable to age-related macular degeneration in terms of societal burden of disease and cannot, of itself, attract the same level of industry-funded research. Outcomes describing 'Photorefractive CXL' have already been published, applying topography-guided high-irradiance CXL in a bow-tie pattern in order to achieve corneal astigmatic changes.(Kanellopoulos et al. 2014) The aim here is to achieve guided corneal flattening which could be along the steep axis in physiological astigmatism (Seven et al. 2014) or over the cone in ectasia. A further ingredient in such a photorefractive CXL algorithm for keratoconus would be combining spatially-derived Brillouin maps with corneal topography and refraction to definitively lock-in a new emmetropic shape.

In the shorter term, it is anticipated that results from clinical studies reporting outcomes compared to the gold-standard 'Dresden' protocol will continue to

guide clinicians as to best practice. A number of randomised controlled trials (RCT) are on-going which will significantly add to the evidence base, but RCTs are not the only answer. Despite a recent statement by the Cornea Clinical Committee of the American Society of Cataract and Refractive Surgery that, '*robust evidence will only be forthcoming from well designed, multicenter, prospective, sham-controlled RCTs*,' (Ziaei et al. 2015) there are very good reasons to oppose this path in favour of patient registries. With so many different protocol permutations in current use (riboflavin formulation /instillation, epithelium status, UV device/irradiance/power/exposure, oxygen supplementation etc.) RCTs cannot be expected to appropriately reflect, let alone keep up-to-date with real-world practice. Nor can their results be assumed to apply to keratoconus subpopulations who, for example, may have different risk profiles for disease progression both before and after treatment. Registry data, on the other hand, would perfectly complement the use of different treatment parameters and patient groups. An electronic registry, with in-built temporal trend analysis, also has the potential to improve patient care by making the process of disease monitoring easier and more robust (visual acuity, astigmatism, keratometry, pachymetry and specular microscopy are all continuous variables). Furthermore, on a national level, by virtue of numbers, a web-based CXL registry represents a much less expensive way to answer the same question driving RCTs: which protocol is best for my patient?

To date, the conventional approach remains to intervene with CXL only for patients with documented disease progression. Factors predictive at diagnosis of an increased risk of disease progression in keratoconus include

young age, steep keratometry, high astigmatism, reduced CDVA and non-Caucasian ethnicity.(Tuft et al. 1994; Gordon et al. 2006) As experience is accrued on the safety and efficacy of this treatment, the era of prophylactic treatment in all newly diagnosed young keratoconics is likely to emerge. No patient is born with keratoconus; a diagnosis during the adolescence or early adulthood could be considered progression *de facto*. Assuming the treatment works, the inevitable question is why wait?

And the future? As CXL becomes more widespread (FDA approval is not granted yet), and focus shifts from treating the prevalence to the incidence, it is a given that the need for interventions for advanced disease will become less common. One university-based corneal department in Norway has reported the frequency of keratoplasty halving over the past decade since their introduction of CXL. (Sandvik et al. 2015) The provision of CXL within the UK's National Health Service remains wholly inadequate (Papamichael & Harman 2013) but I predict that our own keratoplasty trends (both numbers and indications) will markedly change over the next decade. The same trend is likely to be seen in ICRS implantation: Already a niche service, the pool of keratoconic corneas in need of such gross shape correction can be expected to decline.

146 years ago, the Swiss ophthalmologist Johann Horner presented a thesis entitled '*On the treatment of keratoconus'*, to the University of Zurich. Besides the first reference in the literature giving the condition its current name, Horner also described the accepted interventions of the day: Pharmacological miosis

and silver nitrate cautery to flatten the cornea by scarring. (Horner 1869) Fittingly, another Swiss ophthalmologist, Theo Seiler, through his original work on corneal cross-linking has since revolutionised the management of this disease - paradigm shifts in medicine are uncommon, but it is no exaggeration in the case of keratoconus over the past few years. Thick case note files documenting the progression of keratoconus towards corneal transplantation and blindness will be a welcome historical anecdote among ophthalmologists by the time I retire.

Bibliography

Agrawal, V.B., 2009. Corneal collagen cross-linking with riboflavin and ultraviolet - a light for keratoconus: results in Indian eyes. *Indian Journal of Ophthalmology*, 57(2), pp.111–114.

Alessio, G. et al., 2014. Confocal Microscopy Analysis of Corneal Changes After Photorefractive Keratectomy Plus Cross-Linking for Keratoconus: 4-Year Follow-up. *American Journal of Ophthalmology*, 158(3), pp.476–484.e1.

Alfonso, J.F. et al., 2010. Collagen copolymer toric posterior chamber phakic intraocular lens in eyes with keratoconus. *Journal of Cataract & Refractive Surgery*, 36(6), pp.906–916.

Alfonso, J.F. et al., 2013. Inferior intrastromal corneal ring segments in paracentral keratoconus with no coincident topographic and coma axis. *Journal of refractive surgery (Thorofare, NJ : 1995)*, 29(4), pp.266–272.

Alfonso, J.F. et al., 2011. Intrastromal corneal ring segment implantation in 219 keratoconic eyes at different stages. *Graefe's archive for clinical and experimental ophthalmology = Albrecht von Graefes Archiv für klinische und experimentelle Ophthalmologie*, 249(11), pp.1705–1712.

Alfonso, J.F. et al., 2012. Intrastromal corneal ring segment implantation in paracentral keratoconus with coincident topographic and coma axis. *Journal of Cataract & Refractive Surgery*, 38(9), pp.1576–1582.

Alfonso, J.F. et al., 2009. Posterior chamber phakic intraocular lenses after penetrating keratoplasty. *Journal of Cataract & Refractive Surgery*, 35(7), pp.1166–1173.

Alfonso, J.F., Palacios, A. & Montés-Micó, R., 2008. Myopic phakic STAAR collamer posterior chamber intraocular lenses for keratoconus. *Journal of refractive surgery (Thorofare, NJ : 1995)*, 24(9), pp.867–874.

Alhamad, T.A. et al., 2012. Evaluation of transepithelial stromal riboflavin absorption with enhanced riboflavin solution using spectrophotometry. *Journal of Cataract & Refractive Surgery*, 38(5), pp.884–889.

Alió, J.L. et al., 2005. One or 2 Intacs segments for the correction of keratoconus. *Journal of Cataract & Refractive Surgery*, 31(5), pp.943–953.

Alio, J.L., Shabayek, M.H. & Artola, A., 2006. Intracorneal ring segments for keratoconus correction: long-term follow-up. *Journal of Cataract & Refractive Surgery*, 32(6), pp.978–985.

Allan, B.D. & Hassan, H., 2013. Topography-guided transepithelial photorefractive keratectomy for irregular astigmatism using a 213 nm solid-state laser. *Journal of Cataract & Refractive Surgery*, 39(1), pp.97–104.

Ameerh, M.A.A. et al., 2012. Ferrara ring segments implantation for treating keratoconus. *International journal of ophthalmology*, 5(5), pp.586–590.

Arora, R. et al., 2013. Comparative Analysis of Refractive and Topographic Changes in Early and Advanced Keratoconic Eyes Undergoing Corneal Collagen Crosslinking. *Cornea*, 32(10), pp.1359–1364.

asri, D. et al., 2011. Corneal collagen crosslinking in progressive keratoconus: Multicenter results from the French National Reference Center for

Keratoconus. *Journal of Cataract & Refractive Surgery*, 37(12), pp.2137–2143.
Baiocchi, S. et al., 2009. Corneal crosslinking: Riboflavin concentration in corneal stroma exposed with and without epithelium. *Journal of Cataract & Refractive Surgery*, 35(5), pp.893–899.
Beems, E.M. & Van Best, J.A., 1990. Light transmission of the cornea in whole human eyes. *Experimental eye research*, 50(4), pp.393–395.
Beshtawi, I.M. et al., 2013. Biomechanical Properties of Human Corneas Following Low- and High-Intensity Collagen Cross-Linking Determined With Scanning Acoustic Microscopy. *Investigative Ophthalmology & Visual Science*, 54(8), pp.5273–5280.
Bikbova, G. & Bikbov, M., 2013. Transepithelial corneal collagen cross-linking by iontophoresis of riboflavin. *Acta Ophthalmologica*, 92(1), pp.e30–e34.
Bonnel, S. et al., 2015. Demarcation Line Evaluation of Iontophoresis-Assisted Transepithelial Corneal Collagen Cross-linking for Keratoconus. *Journal of Refractive Surgery*, 31(1), pp.36–40.
Borderie, V.M. et al., 2012. Long-term results of deep anterior lamellar versus penetrating keratoplasty. *Ophthalmology*, 119(2), pp.249–255.
Bouheraoua, N. et al., 2014. Optical coherence tomography and confocal microscopy following three different protocols of corneal collagen-crosslinking in keratoconus. *Investigative Ophthalmology & Visual Science*, 55(11), pp.7601–7609.
Boxer Wachler, B.S. et al., 2003. Intacs for keratoconus. *Ophthalmology*, 110(5), pp.1031–1040.
Buzzonetti, L. et al., 2015. Iontophoretic Transepithelial Corneal Cross-linking to Halt Keratoconus in Pediatric Cases: 15-Month Follow-up. *Cornea*, 34(5), pp.512 – 515.
Cakir, H. & Utine, C.A., 2010. Combined Kerarings and Artisan/Artiflex IOLs in Keratectasia. *Journal of refractive surgery (Thorofare, NJ : 1995)*, 27(2), pp.119–126.
Caporossi, A. et al., 2010. Long-term results of riboflavin ultraviolet a corneal collagen cross-linking for keratoconus in Italy: the Siena eye cross study. *American journal of ophthalmology*, 149(4), pp.585–593.
Caporossi, A. et al., 2012. Riboflavin-UVA-induced corneal collagen cross-linking in pediatric patients. *Cornea*, 31(3), pp.227–231.
Caporossi, A. et al., 2013. Transepithelial corneal collagen crosslinking for progressive keratoconus: 24-month clinical results. *Journal of Cataract & Refractive Surgery*, 39(8), pp.1157–1163.
Cassagne, M. et al., 2014. Iontophoresis transcorneal delivery technique for transepithelial corneal collagen crosslinking with riboflavin in a rabbit model. *Investigative Ophthalmology & Visual Science*. Available at: http://eutils.ncbi.nlm.nih.gov/entrez/eutils/elink.fcgi?dbfrom=pubmed&id=24644053&retmode=ref&cmd=prlinks.
Celik, H.U. et al., 2012. Accelerated corneal crosslinking concurrent with laser in situ keratomileusis. *Journal of Cataract & Refractive Surgery*, 38(8), pp.1424–1431.
Celik, U. et al., 2015. New microwave thermokeratoplasty and accelerated crosslinking method for keratoconus: Results in 24 eyes during a 1-

year follow-up. *Journal of Cataract & Refractive Surgery*, 41(2), pp.422–427.
Chan, C.C.K., Sharma, M. & Wachler, B.S.B., 2007. Effect of inferior-segment Intacs with and without C3-R on keratoconus. *Journal of Cataract & Refractive Surgery*, 33(1), pp.75–80.
Cinar, Y. et al., 2013. Comparison of accelerated and conventional corneal collagen cross-linking for progressive keratoconus. *Cutaneous and ocular toxicology*, pp.1–5.
Cingü, A.K. et al., 2013. Transient corneal endothelial changes following accelerated collagen cross-linking for the treatment of progressive keratoconus. *Cutaneous and ocular toxicology*, 33(2), pp.127–131.
Cınar, Y. et al., 2013. Accelerated corneal collagen cross-linking for progressive keratoconus. *Cutaneous and ocular toxicology*, 33(2), pp.168–171.
Coimbra, C.C. et al., 2012. Femtosecond assisted intrastromal corneal ring (ISCR) implantation for the treatment of corneal ectasia. *Arquivos brasileiros de oftalmologia*, 75(2), pp.126–130.
Colin, J., 2006. European clinical evaluation: use of Intacs for the treatment of keratoconus. *Journal of Cataract & Refractive Surgery*, 32(5), pp.747–755.
Colin, J. et al., 2001. INTACS inserts for treating keratoconus: one-year results. *Ophthalmology*, 108(8), pp.1409–1414.
Colin, J., Cochener, B. & Savary, G., 2000. Correcting keratoconus with intracorneal rings. *Journal of Cataract & Refractive Surgery*. Available at: http://www.sciencedirect.com/science/article/pii/S088633500000451X.
Colin, J. & Malet, F.J., 2007. Intacs for the correction of keratoconus: two-year follow-up. *Journal of Cataract & Refractive Surgery*, 33(1), pp.69–74.
Colin, J. & Velou, S., 2003. Current surgical options for keratoconus. *Journal of Cataract & Refractive Surgery*, 29(2), pp.379–386.
Coskunseven, E. et al., 2011. Complications of intrastromal corneal ring segment implantation using a femtosecond laser for channel creation: a survey of 850 eyes with keratoconus. *Acta Ophthalmologica*, 89(1), pp.54–57.
Coskunseven, E. et al., 2009. Effect of treatment sequence in combined intrastromal corneal rings and corneal collagen crosslinking for keratoconus. *Journal of Cataract & Refractive Surgery*, 35(12), pp.2084–2091.
Coskunseven, E. et al., 2008. One-year results of intrastromal corneal ring segment implantation (KeraRing) using femtosecond laser in patients with keratoconus. *American journal of ophthalmology*, 145(5), pp.775–779.
Cui, L. et al., 2011. High-resolution, noninvasive, two-photon fluorescence measurement of molecular concentrations in corneal tissue. *Investigative Ophthalmology & Visual Science*, 52(5), pp.2556–2564.
Daxer, A. & Fratzl, P., 1997. Collagen fibril orientation in the human corneal stroma and its implication in keratoconus. *Investigative Ophthalmology and Visual Science*, 38(1), pp.121–129.

Doors, M. et al., 2009. Use of anterior segment optical coherence tomography to study corneal changes after collagen cross-linking. *American journal of ophthalmology*, 148(6), pp.844–851.
Edelhauser, H.F. et al., 2004. Corneal endothelial assessment after ICL implantation. *Journal of Cataract & Refractive Surgery*, 30(3), pp.576–583.
El-Raggal, T.M., 2011. Sequential versus concurrent KERARINGS insertion and corneal collagen cross-linking for keratoconus. *The British journal of ophthalmology*, 95(1), pp.37–41.
El-Raggal, T.M. & Abdel Fattah, A.A., 2007. Sequential Intacs and Verisyse phakic intraocular lens for refractive improvement in keratoconic eyes. *Journal of Cataract & Refractive Surgery*, 33(6), pp.966–970.
Ertan, A. & Colin, J., 2007. Intracorneal rings for keratoconus and keratectasia. *Journal of Cataract & Refractive Surgery*, 33(7), pp.1303–1314.
Ertan, A. & Kamburoğlu, G., 2008. Intacs implantation using a femtosecond laser for management of keratoconus: Comparison of 306 cases in different stages. *Journal of Cataract & Refractive Surgery*, 34(9), pp.1521–1526.
Ertan, A., Karacal, H. & Kamburoğlu, G., 2009. Refractive and topographic results of transepithelial cross-linking treatment in eyes with intacs. *Cornea*, 28(7), pp.719–723.
Fadlallah, A. et al., 2014. Non-topography–guided PRK Combined With CXL for the Correction of Refractive Errors in Patients With Early Stage Keratoconus. *Journal of Refractive Surgery*, 30(10), pp.688–693.
Fahd, D.C., Jabbur, N.S. & Awwad, S.T., 2012. Intrastromal corneal ring segment SK for moderate to severe keratoconus: a case series. *Journal of refractive surgery (Thorofare, NJ : 1995)*, 28(10), pp.701–705.
Ferrara, G. et al., 2011. Intrastromal corneal ring segments: visual outcomes from a large case series. *Clinical & Experimental Ophthalmology*, p.no–no.
Filippello, M., Stagni, E. & O'Brart, D., 2012. Transepithelial corneal collagen crosslinking: Bilateral study. *Journal of Cataract & Refractive Surgery*, 38(2), pp.283–291.
Fontana, L. et al., 2009. Deep anterior lamellar keratoplasty after Intacs implantation in patients with keratoconus. *Cornea*, 28(1), pp.32–35.
Fraser, C.G. & Fogarty, Y., 1989. Interpreting laboratory results. *BMJ*, 298(6689), pp.1659–1660.
Gatzioufas, Z. et al., 2013. Safety profile of high-fluence corneal collagen cross-linking for progressive keratoconus: preliminary results from a prospective cohort study. *Journal of refractive surgery (Thorofare, NJ : 1995)*, 29(12), pp.846–848.
Ghanem, R.C. et al., 2014. Topographic, corneal wavefront, and refractive outcomes 2 years after collagen crosslinking for progressive keratoconus. *Cornea*, 33(1), pp.43–48.
Gharaibeh, A.M. et al., 2012. KeraRing intrastromal corneal ring segments for correction of keratoconus. *Cornea*, 31(2), pp.115–120.

Girard, M.J.A. et al., 2015. Translating Ocular Biomechanics into Clinical Practice: Current State and Future Prospects. *Current Eye Research*, 40(1), pp.1–18.
Gokhale, N.S., 2011. Corneal endothelial damage after collagen cross-linking treatment. *Cornea*, 30(12), pp.1495–1498.
Gordon, M.O. et al., 2006. Baseline factors predictive of incident penetrating keratoplasty in keratoconus. *American journal of ophthalmology*, 142(6), pp.923–930.
Gore et al., 2015. Transepithelial Riboflavin Absorption in an Ex Vivo Rabbit Corneal Model. *Investigative Opthalmology & Visual Science*, 56(8), p.5006.
Gore, D. et al., 2015. Two-photon fluorescence microscopy of corneal riboflavin absorption through an intact epithelium. *Investigative Ophthalmology & Visual Science*, in press.
Gore, D.M. et al., 2014. Two-photon fluorescence microscopy of corneal riboflavin absorption. *Investigative Ophthalmology & Visual Science*, 55(4), pp.2476–2481.
Gore, D.M., Shortt, A.J. & Allan, B.D., 2012. New clinical pathways for keratoconus. *Eye*, 27(3), pp.329–339.
Greenstein, S.A., Shah, V.P., et al., 2011. Corneal thickness changes after corneal collagen crosslinking for keratoconus and corneal ectasia: one-year results. *Journal of Cataract & Refractive Surgery*, 37(4), pp.691–700.
Greenstein, S.A., Fry, K.L., Hersh, M.J., et al., 2012. Higher-order aberrations after corneal collagen crosslinking for keratoconus and corneal ectasia. *Journal of Cataract & Refractive Surgery*, 38(2), pp.292–302.
Greenstein, S.A. et al., 2010. Natural history of corneal haze after collagen crosslinking for keratoconus and corneal ectasia: Scheimpflug and biomicroscopic analysis. *Journal of Cataract & Refractive Surgery*, 36(12), pp.2105–2114.
Greenstein, S.A., Fry, K.L. & Hersh, P.S., 2012. Effect of topographic cone location on outcomes of corneal collagen cross-linking for keratoconus and corneal ectasia. *Journal of refractive surgery (Thorofare, NJ : 1995)*, 28(6), pp.397–405.
Greenstein, S.A., Fry, K.L. & Hersh, P.S., 2011. In Vivo Biomechanical Changes After Corneal Collagen Cross-linking for Keratoconus and Corneal Ectasia: 1-Year Analysis of a Randomized, Controlled, Clinical Trial. *Cornea*.
Grewal, D.S. et al., 2009. Corneal collagen crosslinking using riboflavin and ultraviolet-A light for keratoconus: one-year analysis using Scheimpflug imaging. *Journal of Cataract & Refractive Surgery*, 35(3), pp.425–432.
Guber, I. et al., 2013. Visual recovery after corneal crosslinking for keratoconus: a 1-year follow-up study. *Graefe's archive for clinical and experimental ophthalmology = Albrecht von Graefes Archiv für klinische und experimentelle Ophthalmologie*, 251(3), pp.803–807.
Gupta, S. et al., 2015. Trans-epithelial versus conventional corneal collagen crosslinking: A randomized trial in keratoconus. *Oman Journal of Ophthalmology*, 8(1), p.9.

Haddad, W. et al., 2012. Comparison of 2 types of intrastromal corneal ring segments for keratoconus. *J Cartaract Refract Surg*, 38(7), pp.1214–1221.
Hafezi, F. et al., 2009. Collagen crosslinking with ultraviolet-A and hypoosmolar riboflavin solution in thin corneas. *Journal of Cataract & Refractive Surgery*, 35(4), pp.621–624.
Hamdi, I.M., 2011. Preliminary results of intrastromal corneal ring segment implantation to treat moderate to severe keratoconus. *Journal of Cataract & Refractive Surgery*, 37(6), pp.1125–1132.
Hashemi, H. et al., 2013. Corneal Collagen Cross-linking with Riboflavin and Ultraviolet A Irradiation for Keratoconus. *Ophthalmology*, 120(8), pp.1515–1520.
Hashemi, K. et al., 2015. Reduced Precision of the Pentacam HR in Eyes with Mild to Moderate Keratoconus. *Ophthalmology*, 122, pp.211–212.
Hassan, Z. et al., 2013. Assessment of corneal topography indices after collagen crosslinking for keratoconus. *European journal of ophthalmology*, 23(5), pp.635–640.
Hatami-Marbini, H., Etebu, E. & Rahimi, A., 2013. Swelling pressure and hydration behavior of porcine corneal stroma. *Current eye research*, 38(11), pp.1124–1132.
Hayes, S. et al., 2008. Effect of complete epithelial debridement before riboflavin–ultraviolet-A corneal collagen crosslinking therapy. *Journal of Cataract & Refractive Surgery*, 34(4), pp.657–661.
Hayes, S. et al., 2013. The Effect of Riboflavin/UVA Collagen Cross-linking Therapy on the Structure and Hydrodynamic Behaviour of the Ungulate and Rabbit Corneal Stroma. *PloS one*, 8(1), p.e52860.
Hellstedt, T. et al., 2005. Treating keratoconus with intacs corneal ring segments. *Journal of refractive surgery (Thorofare, NJ : 1995)*, 21(3), pp.236–246.
Hersh, Greenstein, S.A. & Fry, K.L., 2011. Corneal collagen crosslinking for keratoconus and corneal ectasia: One-year results. *Journal of Cataract & Refractive Surgery*, 37(1), pp.149–160.
Horner, J.F., 1869. Zur Behandlung des Keratoconus. *Klinische Monatsblätter für Augenheilkunde*.
Hoyer, A. et al., 2009. [Collagen cross-linking with riboflavin and UVA light in keratoconus. Results from Dresden]. *Der Ophthalmologe*, 106(2), pp.133–140.
Huang, A.J., Tseng, S.C. & Kenyon, K.R., 1989. Paracellular permeability of corneal and conjunctival epithelia. *Investigative ophthalmology & visual science*, 30(4), pp.684–689.
Huang, D. et al., 2009. Phakic Intraocular Lens Implantation for the Correction of Myopia. *Ophthalmology*, 116(11), pp.2244–2258.
Ivarsen, A. & Hjortdal, J., 2013. Collagen Cross-linking for Advanced Progressive Keratoconus. *Cornea*. Available at: http://eutils.ncbi.nlm.nih.gov/entrez/eutils/elink.fcgi?dbfrom=pubmed&id=23449485&retmode=ref&cmd=prlinks.
Izquierdo, L., Henriquez, M.A. & McCarthy, M., 2011. Artiflex phakic intraocular lens implantation after corneal collagen cross-linking in keratoconic eyes. *Journal of refractive surgery (Thorofare, NJ : 1995)*, 27(7), pp.482–487.

Jones, M.N.A. et al., 2009. Penetrating and Deep Anterior Lamellar Keratoplasty for Keratoconus: A Comparison of Graft Outcomes in the United Kingdom. *Investigative Ophthalmology & Visual Science*, 50(12), pp.5625–5629.

Jordan, C. et al., 2014. In Vivo Confocal Microscopy Analyses of Corneal Microstructural Changes in a Prospective Study of Collagen Cross-linking in Keratoconus. *Ophthalmology*, 121(2), pp.469–474.

Kamaev, P. et al., 2012. Photochemical Kinetics of Corneal Cross-Linking with Riboflavin. *Investigative Ophthalmology & Visual Science*, 53(4), pp.2360–2367.

Kamiya, K. et al., 2011. Clinical outcomes of posterior chamber toric phakic intraocular lens implantation for the correction of high myopic astigmatism in eyes with keratoconus: 6-month follow-up. *Graefe's archive for clinical and experimental ophthalmology = Albrecht von Graefes Archiv für klinische und experimentelle Ophthalmologie*, 249(7), pp.1073–1080.

Kampik, D. et al., 2011. [Corneal riboflavin/UV-A collagen cross-linking (CXL) in keratoconus: two-year results]. *Klinische Monatsblätter für Augenheilkunde*, 228(6), pp.525–530.

Kampik, D. et al., 2010. Influence of Corneal Collagen Crosslinking with Riboflavin and Ultraviolet-A Irradiation on Excimer Laser Surgery. *Investigative Ophthalmology & Visual Science*, 51(8), pp.3929–3934.

Kanellopoulos, A.J. et al., 2014. Toric Topographically Customized Transepithelial, Pulsed, Very High-Fluence, Higher Energy and Higher Riboflavin Concentration Collagen Cross-Linking in Keratoconus. *Case Reports in Ophthalmology*, 5(2), pp.172–180.

Kanellopoulos, A.J. & Asimellis, G., 2014. Keratoconus management: long-term stability of topography-guided normalization combined with high-fluence CXL stabilization (the Athens Protocol). *Journal of refractive surgery (Thorofare, NJ : 1995)*, 30(2), pp.88–93.

Kanellopoulos, A.J. & Binder, P.S., 2011. Management of corneal ectasia after LASIK with combined, same-day, topography-guided partial transepithelial PRK and collagen cross-linking: the athens protocol. *Journal of refractive surgery (Thorofare, NJ : 1995)*, 27(5), pp.323–331.

Kanellopoulos, J., 2009. Comparison of sequential vs same-day simultaneous collagen cross-linking and topography-guided PRK for treatment of keratoconus. *Journal of refractive surgery (Thorofare, NJ : 1995)*, 25(9), pp.S812–8.

Kanellopoulos, J., 2012a. Long term results of a prospective randomized bilateral eye comparison trial of higher fluence, shorter duration ultraviolet A radiation, and riboflavin collagen cross linking for progressive keratoconus. *Clinical ophthalmology (Auckland, NZ)*, 6, pp.97–101.

Kanellopoulos, J., 2012b. Long-term safety and efficacy follow-up of prophylactic higher fluence collagen cross-linking in high myopic laser-assisted in situ keratomileusis. *Clinical ophthalmology (Auckland, NZ)*, p.1125.

Kanellopoulos, J. et al., 2006. Modified intracorneal ring segment implantations (INTACS) for the management of moderate to advanced keratoconus: efficacy and complications. *Cornea*, 25(1), pp.29–33.

Kanellopoulos, J. & Binder, P.S., 2007. Collagen cross-linking (CCL) with sequential topography-guided PRK: a temporizing alternative for keratoconus to penetrating keratoplasty. *Cornea*, 26(7), pp.891–895.
Kapasi, M. et al., 2012. Phototherapeutic keratectomy versus mechanical epithelial removal followed by corneal collagen crosslinking for keratoconus. *Canadian journal of ophthalmology Journal canadien d'ophtalmologie*, 47(4), pp.344–347.
Kato, N. et al., 2011. Phakic intraocular lens for keratoconus. *Ophthalmology*, 118(3), pp.605–605.e2.
Kato, N. et al., 2010. Topography-guided conductive keratoplasty: treatment for advanced keratoconus. *American journal of ophthalmology*, 150(4), pp.481–489.e1.
Kelly, T.L., Williams, K.A., et al., 2011. Corneal Transplantation for Keratoconus: A Registry Study. *Archives of Ophthalmology*, 129(6), pp.691–697.
Kelly, T.L., Coster, D.J. & Williams, K.A., 2011. Repeat Penetrating Corneal Transplantation in Patients with Keratoconus. *Ophthalmology*, 118(8), pp.1538–1542.
Khan, M.I., Injarie, A. & Muhtaseb, M., 2011. Intrastromal corneal ring segments for advanced keratoconus and cases with high keratometric asymmetry. *Journal of Cataract & Refractive Surgery*. Available at: http://eutils.ncbi.nlm.nih.gov/entrez/eutils/elink.fcgi?dbfrom=pubmed&id=22055076&retmode=ref&cmd=prlinks.
Kocak, I. et al., 2014. Comparison of transepithelial corneal collagen crosslinking with epithelium-off crosslinking in progressive keratoconus. *Journal Français d'Ophtalmologie*, 37(5), pp.371–6.
Kohlhaas, M. et al., 2006. Biomechanical evidence of the distribution of cross-links in corneas treated with riboflavin and ultraviolet A light. *Journal of Cataract & Refractive Surgery*, 32(2), pp.279–283.
Kohnen, T. et al., 2010. Phakic intraocular lenses: part 2: results and complications. *Journal of Cataract & Refractive Surgery*, 36(12), pp.2168–2194.
Koller, T., Mrochen, M. & Seiler, T., 2009. Complication and failure rates after corneal crosslinking. *Journal of Cataract & Refractive Surgery*, 35(8), pp.1358–1362.
Kontadakis, G.A. et al., 2013. Effect of corneal collagen cross-linking on corneal innervation, corneal sensitivity, and tear function of patients with keratoconus. *Ophthalmology*, 120(5), pp.917–922.
Koo, T.S. et al., 2011. Incremental cost-utility analysis of deep anterior lamellar keratoplasty compared with penetrating keratoplasty for the treatment of keratoconus. *American journal of ophthalmology*, 152(1), pp.40–47.e2.
Koppen, C. et al., 2012a. Refractive and topographic results of benzalkonium chloride-assisted transepithelial crosslinking. *Journal of Cataract & Refractive Surgery*, 38(6), pp.1000–1005.
Koppen, C. et al., 2012b. Refractive and topographic results of benzalkonium chloride-assisted transepithelial crosslinking. *Journal of Cataract & Refractive Surgery*, 38(6), pp.1000–1005.

Kotb, A.M.E.-M. & Hantera, M., 2013. Efficacy and safety of Intacs SK in moderate to severe keratoconus. *Middle East African Journal of Ophthalmology*, 20(1), pp.46–50.
Kránitz, K. et al., 2012. Corneal changes in progressive keratoconus after cross-linking assessed by Scheimpflug camera. *Journal of refractive surgery (Thorofare, NJ : 1995)*, 28(9), pp.645–649.
Krüger, A. et al., 2011. Combined nonlinear and femtosecond confocal laser-scanning microscopy of rabbit corneas after photochemical cross-linking. *Investigative Ophthalmology & Visual Science*, 52(7), pp.4247–4255.
Kubaloglu, A., Sari, E.S., Cinar, Y., Koytak, A., et al., 2010. A single 210-degree arc length intrastromal corneal ring implantation for the management of pellucid marginal corneal degeneration. *American journal of ophthalmology*, 150(2), pp.185–192.e1.
Kubaloglu, A., Cinar, Y., Sari, E.S., Koytak, A., et al., 2010. Comparison of 2 intrastromal corneal ring segment models in the management of keratoconus. *Journal of Cataract & Refractive Surgery*, 36(6), pp.978–985.
Kubaloglu, A., Sari, E.S., Cinar, Y., Cingu, K., et al., 2010. Comparison of mechanical and femtosecond laser tunnel creation for intrastromal corneal ring segment implantation in keratoconus: prospective randomized clinical trial. *Journal of Cataract & Refractive Surgery*, 36(9), pp.1556–1561.
Kubaloglu, A. et al., 2011. Intrastromal corneal ring segment implantation for the treatment of keratoconus. *Cornea*, 30(1), pp.11–17.
Kwitko, S. & Severo, N.S., 2004. Ferrara intracorneal ring segments for keratoconus. *Journal of Cataract & Refractive Surgery*, 30(4), pp.812–820.
Kymes, S.M. et al., 2008. Changes in the Quality-of-Life of People with Keratoconus. *American journal of ophthalmology*, 145(4), pp.611–617.e1.
Kymionis et al., 2012. Corneal collagen cross-linking with riboflavin and ultraviolet-A irradiation in patients with thin corneas. *American journal of ophthalmology*, 153(1), pp.24–28.
Kymionis, G.D. et al., 2012. Combined Transepithelial Phototherapeutic Keratectomy and Corneal Collagen Cross-Linking for Progressive Keratoconus. *Ophthalmology*, 119(9), pp.1777–1784.
Kymionis, G.D. et al., 2014. Evaluation of corneal stromal demarcation line depth following standard and a modified-accelerated collagen cross-linking protocol. *American journal of ophthalmology*. Available at: http://eutils.ncbi.nlm.nih.gov/entrez/eutils/elink.fcgi?dbfrom=pubmed&id=25034113&retmode=ref&cmd=prlinks.
Kymionis, G.D. et al., 2010. Intraocular pressure measurements after corneal collagen crosslinking with riboflavin and ultraviolet A in eyes with keratoconus. *Journal of Cataract & Refractive Surgery*, 36(10), pp.1724–1727.
Kymionis, G.D. et al., 2007. Long-term follow-up of Intacs in keratoconus. *American journal of ophthalmology*, 143(2), pp.236–244.

Kymionis, G.D. et al., 2009. Simultaneous topography-guided PRK followed by corneal collagen cross-linking for keratoconus. *Journal of refractive surgery (Thorofare, NJ : 1995)*, 25(9), pp.S807–11.
Labiris, G. et al., 2012. Impact of keratoconus, cross-linking and cross-linking combined with photorefractive keratectomy on self-reported quality of life. *Cornea*, 31(7), pp.734–739.
Lamy, R. et al., 2013. Effects of corneal cross-linking on contrast sensitivity, visual acuity, and corneal topography in patients with keratoconus. *Cornea*, 32(5), pp.591–596.
Lange, C., Böhringer, D. & Reinhard, T., 2012. Corneal endothelial loss after crosslinking with riboflavin and ultraviolet-A. *Graefe's Archive for Clinical and Experimental Ophthalmology*, 250(11), pp.1689–1691.
Lass, J.H. et al., 1990. Clinical management of keratoconus. A multicenter analysis. *Ophthalmology*, 97(4), pp.433–445.
Leccisotti, A. & Islam, T., 2010. Transepithelial corneal collagen cross-linking in keratoconus. *Journal of Refractive Surgery*, 26(12), pp.942–948.
Legare, M.E. et al., 2013. Corneal collagen cross-linking using riboflavin and ultraviolet A for the treatment of mild to moderate keratoconus: 2-year follow-up. *Canadian journal of ophthalmology Journal canadien d'ophtalmologie*, 48(1), pp.63–68.
Levinger, S. & Pokroy, R., 2005. Keratoconus managed with intacs: one-year results. *Arch Ophthalmol*, 123(10), pp.1308–1314.
Lin, D.T.C. et al., 2012. Clinical results of topography-based customized ablations in highly aberrated eyes and keratoconus/ectasia with cross-linking. *Journal of refractive surgery (Thorofare, NJ : 1995)*, 28(11 Suppl), pp.S841–8.
Lombardo, M., Serrao, S., et al., 2014. Biomechanical changes in the human cornea after transepithelial corneal crosslinking using iontophoresis. *Journal of Cataract & Refractive Surgery*, 40(10), pp.1706–1715.
Lombardo, M., Pucci, G., et al., 2014. Interaction of ultraviolet light with the cornea: Clinical implications for corneal crosslinking. *Journal of Cataract & Refractive Surgery*, pp.1–14.
MacGregor, C., Tsatsos, M. & Hossain, P., 2014. Is accelerated corneal collagen cross-linking for keratoconus the way forward? No. , pp.1–2.
Magli, A. et al., 2013. Epithelium-off corneal collagen cross-linking versus transepithelial cross-linking for pediatric keratoconus. *Cornea*, 32(5), pp.597–601.
Marshall, J., Hersh, P.S. & Muller, D., 2013. *Corneal collagen cross-linking. Past, present, future* e-book., Available at: http://avedro.com/science-innovation/cross-linking-ebook/ [Accessed June 1, 2015].
Martin, J. et al., 2009. NC-1059: A Channel-Forming Peptide That Modulates Drug Delivery across In Vitro Corneal Epithelium. *Investigative Ophthalmology & Visual Science*, 50(7), pp.3337–3345.
Mastropasqua, L. et al., 2014. Corneal Cross-linking: Intrastromal Riboflavin Concentration in Iontophoresis-Assisted Imbibition Versus Traditional and Transepithelial Techniques. *AJOPHT*, 157(3), pp.623–630.e1.
Mastropasqua, L. et al., 2013. Morphological modification of the cornea after standard and transepithelial corneal cross-linking as imaged by anterior segment optical coherence tomography and laser scanning in vivo confocal microscopy. *Cornea*, 32(6), pp.855–861.

Mazzotta, C. et al., 2008. Corneal healing after riboflavin ultraviolet-A collagen cross-linking determined by confocal laser scanning microscopy in vivo: early and late modifications. *American journal of ophthalmology*, 146(4), pp.527–533.
Mazzotta, C. et al., 2012. Morphological and functional correlations in riboflavin UV A corneal collagen cross-linking for keratoconus. *Acta Ophthalmologica*, 90(3), pp.259–265.
McCall, A.S. et al., 2010. Mechanisms of Corneal Tissue Cross-linking in Response to Treatment with Topical Riboflavin and Long-Wavelength Ultraviolet Radiation (UVA). *Investigative Ophthalmology & Visual Science*, 51(1), pp.129–138.
McDonald, M.B. et al., 2002. Conductive keratoplasty for the correction of low to moderate hyperopia: US clinical trial 1-year results on 355 eyes. *Ophthalmology*, 109(11), pp.1978–1989.
Meek, K.M. et al., 2005. Changes in Collagen Orientation and Distribution in Keratoconus Corneas. *Investigative Ophthalmology & Visual Science*, 46(6), pp.1948–1956.
Meek, K.M. & Hayes, S., 2013. Corneal cross-linking - a review. *Ophthalmic & physiological optics : the journal of the British College of Ophthalmic Opticians (Optometrists)*, 33(2), pp.78–93.
Mencucci, R. et al., 2012. Corneal thickness measurements using time-domain anterior segment OCT, ultrasound, and Scheimpflug tomographer pachymetry before and after corneal cross-linking for keratoconus. *Journal of refractive surgery (Thorofare, NJ : 1995)*, 28(8), pp.562–566.
Moshirfar, M. et al., 2011. Simultaneous and sequential implantation of intacs and verisyse phakic intraocular lens for refractive improvement in keratectasia. *Cornea*, 30(2), pp.158–163.
Mukherjee, A.N., Selimis, V. & Aslanides, I., 2013. Transepithelial photorefractive keratectomy with crosslinking for keratoconus. *The open ophthalmology journal*, 7, p.63.
Naderan, M. et al., 2014. Association between diabetes and keratoconus: a case-control study. *Cornea*, 33(12), pp.1271–1273.
Niknam, S. et al., 2012. Treatment of moderate to severe keratoconus with 6-mm Intacs SK. *International journal of ophthalmology*, 5(4), pp.513–516.
O'Brart, D.P.S. et al., 2011. A randomised, prospective study to investigate the efficacy of riboflavin/ultraviolet A (370 nm) corneal collagen cross-linkage to halt the progression of keratoconus. *British Journal of Ophthalmology*, 95(11), pp.1519–1524.
O'Brart, D.P.S. et al., 2013. Long-term follow-up of riboflavin/ultraviolet A (370 nm) corneal collagen cross-linking to halt the progression of keratoconus. *British Journal of Ophthalmology*, 97(4), pp.433–437.
Ostacolo, C. et al., 2013. Enhancement of corneal permeation of riboflavin-5'-phosphate through vitamin E TPGS: a promising approach in corneal trans-epithelial cross linking treatment. *International journal of pharmaceutics*, 440(2), pp.148–153.
Ozbek, Z. & Cohen, E.J., 2006. Use of intralimbal rigid gas-permeable lenses for pellucid marginal degeneration, keratoconus, and after penetrating keratoplasty. *Eye & contact lens*, 32(1), pp.33–36.

Papamichael, E. & Harman, F., 2013. Corneal cross-linking service survey in England. *Eye*, pp.1–2.
Pearson, A., Soneji, B. & Sarvananthan, N., 2000. Does ethnic origin influence the incidence or severity of keratoconus? *Eye*, 14, pp.625–628.
Pecego, M. et al., 2012. Jupiter Scleral Lenses: the UC Davis Eye Center experience. *Eye & contact lens*, 38(3), pp.179–182.
Pesando, P.M. et al., 2007. Posterior chamber phakic intraocular lens (ICL) for hyperopia: Ten-year follow-up. *Journal of Cataract & Refractive Surgery*, 33(9), pp.1579–1584.
Pesando, P.M. et al., 2010. Treatment of keratoconus with Ferrara ICRS and consideration of the efficacy of the Ferrara nomogram in a 5-year follow-up. *European journal of ophthalmology*, 20(5), pp.865–873.
Piñero, D.P. et al., 2009. Refractive and aberrometric outcomes of intracorneal ring segments for keratoconus: mechanical versus femtosecond-assisted procedures. *Ophthalmology*, 116(9), pp.1675–1687.
Poli, M. et al., 2013. Prospective study of corneal collagen cross-linking efficacy and tolerance in the treatment of keratoconus and corneal ectasia: 3-year results. *Cornea*, 32(5), pp.583–590.
Rabinowitz, Y.S. et al., 2006. INTACS inserts using the femtosecond laser compared to the mechanical spreader in the treatment of keratoconus. *Journal of refractive surgery (Thorofare, NJ : 1995)*, 22(8), pp.764–771.
Raiskup, F. et al., 2011. Hornhautvernetzung mit hypoosmolarer Riboflavin-Lösung beim Keratokonus mit dünner Hornhaut (Corneal cross-linking with hypo-osmolar riboflavin solution for keratoconus with thin corneas). *Der Ophthalmologe*, 108(9), pp.846–851.
Raiskup, F., Hoyer, A. & Spoerl, E., 2009. Permanent corneal haze after riboflavin-UVA-induced cross-linking in keratoconus. *Journal of refractive surgery (Thorofare, NJ : 1995)*, 25(9), pp.S824–8.
Raiskup, F. & Spoerl, E., 2011. Corneal cross-linking with hypo-osmolar riboflavin solution in thin keratoconic corneas. *American journal of ophthalmology*, 152(1), pp.28–32.e1.
Raiskup-Wolf, F. et al., 2008. Collagen crosslinking with riboflavin and ultraviolet-A light in keratoconus: Long-term results. *Journal of Cataract & Refractive Surgery*, 34(5), pp.796–801.
Rebenitsch, R.L. et al., 2011. The lifetime economic burden of keratoconus: a decision analysis using a markov model. *American journal of ophthalmology*, 151(5), pp.768–773.e2.
Rechichi, M. et al., 2013. Epithelial-disruption collagen crosslinking for keratoconus: one-year results. *Journal of Cataract & Refractive Surgery*, 39(8), pp.1171–1178.
Reinhart, W.J. et al., 2011. Deep Anterior Lamellar Keratoplasty as an Alternative to Penetrating Keratoplasty. *Ophthalmology*, 118(1), pp.209–218.
Rho, C.R. et al., 2013. Changes in anterior and posterior corneal parameters in patients with keratoconus after intrastromal corneal-ring segment implantation. *Current eye research*, 38(8), pp.843–850.

Riau, A.K. et al., 2012. Reproducibility and age-related changes of ocular parametric measurements in rabbits. *BMC Veterinary Research*, 8(1), pp.1–1.

Roe, R.H. et al., 2008. The value-based medicine comparative effectiveness and cost-effectiveness of penetrating keratoplasty for keratoconus. *Cornea*, 27(9), pp.1001–1007.

Saelens, I.E.Y. et al., 2011. Refractive, topographic, and visual outcomes of same-day corneal cross-linking with ferrara intracorneal ring segments in patients with progressive keratoconus. *Cornea*, 30(12), pp.1406–1408.

Sakla, H. et al., 2014. Simultaneous topography-guided partial photorefractive keratectomy and corneal collagen crosslinking for keratoconus. *Journal of Cataract & Refractive Surgery*, 40(9), pp.1430–1438.

Samaras, K. et al., 2009. Effect of Epithelial Retention and Removal on Riboflavin Absorption in Porcine Corneas. *Journal of Refractive Surgery*, 25(9), pp.771–775.

Sandvik, G., Thorsrud, A. & Raen, M., 2015. Does Corneal Collagen Cross-linking Reduce the Need for Keratoplasties in Patients With Keratoconus? Available at: http://pdfs.journals.lww.com/corneajrnl/9000/00000/Does_Corneal_Collagen_Cross_linking_Reduce_the.97996.pdf [Accessed June 17, 2015].

Sansanayudh, W. et al., 2010. Intrastromal corneal ring segment SK implantation for moderate to severe keratoconus. *Journal of Cataract & Refractive Surgery*, 36(1), pp.110–113.

Scarcelli, G. et al., 2013. Brillouin Microscopy of Collagen Crosslinking: Noncontact Depth-Dependent Analysis of Corneal Elastic Modulus. *Investigative Ophthalmology & Visual Science*, 54(2), pp.1418–1425.

Scarcelli, G., Pineda, R. & Yun, S.H., 2012. Brillouin Optical Microscopy for Corneal Biomechanics. *Investigative Ophthalmology & Visual Science*, 53(1), pp.185–190.

Scarcelli, G. & Yun, S.H., 2008. Confocal Brillouin microscopy for three-dimensional mechanical imaging. *Nature Photonics*, 2(1), pp.39–43.

Schafer, D. et al., 2007. Three-dimensional chemical concentration maps in a microfluidic device using two-photon absorption fluorescence imaging. *Optics letters*, 32(17), pp.2568–2570.

Schumacher, S., Oeftiger, L. & Mrochen, M., 2011. Equivalence of Biomechanical Changes Induced by Rapid and Standard Corneal Cross-linking, Using Riboflavin and Ultraviolet Radiation. *Investigative Ophthalmology & Visual Science*, 52(12), pp.9048–9052.

Sedaghat, M. et al., 2011. Artisan iris-supported phakic IOL implantation in patients with keratoconus: a review of 16 eyes. *Journal of refractive surgery (Thorofare, NJ : 1995)*, 27(7), pp.489–493.

Seiler, T. & Hafezi, F., 2006. Corneal cross-linking-induced stromal demarcation line. *Cornea*, 25(9), pp.1057–1059.

Seven, I., Roy, A.S. & Dupps, W.J., 2014. Patterned corneal collagen crosslinking for astigmatism: Computational modeling study. *Journal of Cataract & Refractive Surgery*, 40(6), pp.943–953.

Shabayek, M.H. & Alio, J.L., 2007. Intrastromal corneal ring segment implantation by femtosecond laser for keratoconus correction. *Ophthalmology*, 114(9), pp.1643–1652.

Sharma, A. et al., 2012. Persistent Corneal Edema after Collagen Cross-Linking for Keratoconus. *American Journal of Ophthalmology*, 154(6), pp.922–926.e1.
Sherif, A., 2014. Accelerated versus conventional corneal collagen cross-linking in the treatment of mild keratoconus: a comparative study. *Clinical ophthalmology (Auckland, NZ)*, p.1435.
Sherif, A.M. et al., 2015. One-Year Results of Simultaneous Topography-Guided Photorefractive Keratectomy and Corneal Collagen Cross-Linking in Keratoconus Utilizing a Modern Ablation Software. *Journal of Ophthalmology*, 2015, pp.1–7.
Shetty, R. et al., 2015. Cone Location–Dependent Outcomes After Combined Topography-Guided Photorefractive Keratectomy and Collagen Cross-linking. *American Journal of Ophthalmology*, 159(3), pp.419–425.e2.
Shetty, R. et al., 2008. Intacs in advanced keratoconus. *Cornea*, 27(9), pp.1022–1029.
Shetty, R. et al., 2009. Safety and efficacy of Intacs in Indian eyes with keratoconus: an initial report. *Indian Journal of Ophthalmology*, 57(2), pp.115–119.
Siganos, C.S. et al., 2003. Management of keratoconus with Intacs. *American journal of ophthalmology*, 135(1), pp.64–70.
Sloot, F. et al., 2013. Effective corneal collagen crosslinking in advanced cases of progressive keratoconus. *Journal of Cataract & Refractive Surgery*, 39(8), pp.1141–1145.
Snibson, G.R., 2010. Collagen cross-linking: a new treatment paradigm in corneal disease - a review. *Clinical & Experimental Ophthalmology*, 38(2), pp.141–153.
Soeters, N. et al., 2015. Transepithelial Versus Epithelium-off Corneal Cross-linking for the Treatment of Progressive Keratoconus: A Randomized Controlled Trial. *American Journal of Ophthalmology*, 159(5), pp.821–828.e3.
Søndergaard, A.P. et al., 2010. Corneal distribution of riboflavin prior to collagen cross-linking. *Current eye research*, 35(2), pp.116–121.
Spoerl, E. et al., 2011. Detection of biomechanical changes after corneal cross-linking using Ocular Response Analyzer software. *Journal of refractive surgery (Thorofare, NJ : 1995)*, 27(6), pp.452–457.
Spoerl, E. et al., 2007. Safety of UVA-riboflavin cross-linking of the cornea. *Cornea*, 26(4), pp.385–389.
Spoerl, E., Wollensak, G., Dittert, D.-D., et al., 2004. Thermomechanical Behavior of Collagen-Cross-Linked Porcine Cornea. *Ophthalmologica*, 218(2), pp.136–140.
Spoerl, E., Huhle, M. & Seiler, T., 1998. Induction of cross-links in corneal tissue. *Experimental eye research*, 66(1), pp.97–103.
Spoerl, E., Wollensak, G. & Seiler, T., 2004. Increased resistance of crosslinked cornea against enzymatic digestion. *Current eye research*, 29(1), pp.35–40.
Stojanovic, A. et al., 2012. Safety and Efficacy of Epithelium-On Corneal Collagen Cross-Linking Using a Multifactorial Approach to Achieve Proper Stromal Riboflavin Saturation. *Journal of Ophthalmology*, 2012, pp.1–8.

Szalai, E. et al., 2012. Reliability and repeatability of swept-source Fourier-domain optical coherence tomography and Scheimpflug imaging in keratoconus. *Journal of Cataract & Refractive Surgery*, 38(3), pp.485–494.

Taneri, S. et al., 2014. Evaluation of Epithelial Integrity with Various Transepithelial Corneal Cross-Linking Protocols for Treatment of Keratoconus. *Journal of Ophthalmology*, 2014, pp.1–5.

Tomita, M., Mita, M. & Huseynova, T., 2014. Accelerated versus conventional corneal collagen crosslinking. *Journal of Cataract & Refractive Surgery*, 40(6), pp.1013–1020.

Toprak, I. & Yildirim, C., 2013. Effects of corneal collagen crosslinking on corneal topographic indices in patients with keratoconus. *Eye & contact lens*, 39(6), pp.385–387.

Torquetti, L. et al., 2014. Intrastromal corneal ring segments implantation in patients with keratoconus: 10-year follow-up. *Journal of refractive surgery (Thorofare, NJ : 1995)*, 30(1), pp.22–26.

Torquetti, L. & Berbel, R., 2009. Long-term follow-up of intrastromal corneal ring segments in keratoconus. *Journal of Cataract & Refractive \ldots*. Available at: http://www.sciencedirect.com/science/article/pii/S0886335009006683.

Torquetti, L., Berbel, R.F. & Ferrara, P., 2009. Long-term follow-up of intrastromal corneal ring segments in keratoconus. *Journal of Cataract & Refractive Surgery*, 35(10), pp.1768–1773.

Touboul, D. et al., 2012. Corneal confocal microscopy following conventional, transepithelial, and accelerated corneal collagen cross-linking procedures for keratoconus. *Journal of refractive surgery (Thorofare, NJ : 1995)*, 28(11), pp.769–776.

Touboul, D. et al., 2014. Supersonic Shear Wave Elastography for the In Vivo Evaluation of Transepithelial Corneal Collagen Cross-Linking. *Investigative Ophthalmology & Visual Science*, 55(3), pp.1976–1984.

Tsatsos, M. et al., 2014. Is accelerated corneal collagen cross-linking for keratoconus the way forward? Yes. , pp.1–2.

Tuft, S.J. et al., 1994. Prognostic factors for the progression of keratoconus. *Ophthalmology*, 101(3), pp.439–447.

Tunc, Z., Helvacioglu, F. & Sencan, S., 2013. Evaluation of intrastromal corneal ring segments for treatment of keratoconus with a mechanical implantation technique. *Indian Journal of Ophthalmology*, 61(5), pp.218–225.

Tuwairqi, W.S. & Sinjab, M.M., 2012. Safety and efficacy of simultaneous corneal collagen cross-linking with topography-guided PRK in managing low-grade keratoconus: 1-year follow-up. *Journal of refractive surgery (Thorofare, NJ : 1995)*, 28(5), pp.341–345.

Vega-Estrada, A. et al., 2013. Outcome Analysis of Intracorneal Ring Segments for the Treatment of Keratoconus Based on Visual, Refractive, and Aberrometric Impairment. *American Journal of Ophthalmology*, 155(3), pp.575–584.e1.

Vinciguerra, P. et al., 2010. Intra- and postoperative variation in ocular response analyzer parameters in keratoconic eyes after corneal cross-linking. *Journal of refractive surgery (Thorofare, NJ : 1995)*, 26(9), pp.669–676.

Vinciguerra, P., Albè, E., Trazza, S., Seiler, T., et al., 2009. Intraoperative and postoperative effects of corneal collagen cross-linking on progressive keratoconus. *Arch Ophthalmol*, 127(10), pp.1258–1265.
Vinciguerra, P., Albè, E., Trazza, S., Rosetta, P., et al., 2009. Refractive, topographic, tomographic, and aberrometric analysis of keratoconic eyes undergoing corneal cross-linking. *Ophthalmology*, 116(3), pp.369–378.
Vinciguerra, P. et al., 2014. Transepithelial Iontophoresis Corneal Collagen Cross-linking for Progressive Keratoconus: Initial Clinical Outcomes. *Journal of Refractive Surgery*, 30(11), pp.746–753.
Vinciguerra, P. et al., 2012. Two-Year Corneal Cross-Linking Results in Patients Younger than 18 Years with Documented Progressive Keratoconus. *AJOPHT*, pp.1–7.
Wernli, J. et al., 2013. The efficacy of corneal cross-linking shows a sudden decrease with very high intensity UV-light and short treatment time. *Investigative Ophthalmology & Visual Science*. Available at: http://eutils.ncbi.nlm.nih.gov/entrez/eutils/elink.fcgi?dbfrom=pubmed&id=23299484&retmode=ref&cmd=prlinks.
Wittig-Silva, C. et al., 2014. A Randomized, Controlled Trial of Corneal Collagen Cross-Linking in Progressive Keratoconus. *Ophthalmology*, pp.1–10.
Wollensak, G. et al., 2004. Collagen fiber diameter in the rabbit cornea after collagen crosslinking by riboflavin/UVA. *Cornea*, 23(5), pp.503–507.
Wollensak, G., Spörl, E., et al., 2003. Corneal endothelial cytotoxicity of riboflavin/UVA treatment in vitro. *Ophthalmic research*, 35(6), pp.324–328.
Wollensak, G., 2006. Crosslinking treatment of progressive keratoconus: new hope. *Current opinion in ophthalmology*, 17(4), pp.356–360.
Wollensak, G. et al., 2011. Interlamellar cohesion after corneal crosslinking using riboflavin and ultraviolet A light. *British Journal of Ophthalmology*, 95(6), pp.876–880.
Wollensak, G. et al., 2010. Significance of the riboflavin film in corneal collagen crosslinking. *Journal of Cataract & Refractive Surgery*, 36(1), pp.114–120.
Wollensak, G. & Iomdina, E., 2009. Long-term biomechanical properties of rabbit cornea after photodynamic collagen crosslinking. *Acta Ophthalmologica*, 87(1), pp.48–51.
Wollensak, G., Spoerl, E. & Seiler, T., 2003a. Riboflavin/ultraviolet-a-induced collagen crosslinking for the treatment of keratoconus. *American journal of ophthalmology*, 135(5), pp.620–627.
Wollensak, G., Spoerl, E. & Seiler, T., 2003b. Stress-strain measurements of human and porcine corneas after riboflavin-ultraviolet-A-induced cross-linking. *Journal of Cataract & Refractive Surgery*, 29(9), pp.1780–1785.
Xu, X. et al., 2003. Effect of dextran-induced changes in refractive index and aggregation on optical properties of whole blood. *Physics in medicine and biology*, 48(9), pp.1205–1221.
Yildiz, E.H. et al., 2010. Quality of life in keratoconus patients after penetrating keratoplasty. *American journal of ophthalmology*, 149(3), pp.416–22.e1–2.

Zare, M.A., Hashemi, H. & Salari, M.R., 2007. Intracorneal ring segment implantation for the management of keratoconus: safety and efficacy. *Journal of Cataract & Refractive Surgery*, 33(11), pp.1886–1891.
Zhang, Y. et al., 2012. Effect of the Synthetic NC-1059 Peptide on Diffusion of Riboflavin across an Intact Corneal Epithelium. *Investigative Ophthalmology & Visual Science*, 53(6), pp.2620–2629.
Ziaei, M. et al., 2015. Reshaping procedures for the surgical management of corneal ectasia. *Journal of Cataract & Refractive Surgery*, 41(4), pp.842–872.

10 Appendix B – study protocols

10.1 Chapter 1 – meta-analysis

MEDLINE (1950-2015) and the Cochrane Central Register of Controlled Trials was searched using the following search terms: keratoconus; corneal cross-linking; cross-linkage; intracorneal ring segment; topographic photorefractive keratectomy; phakic intraocular lens. For the meta-analysis, two investigators (Alex Shortt & I) independently assessed the search results for randomised controlled trials (RCTs) of corneal cross-linking in keratoconus. The authors of 2 RCTs (O'Brart et al. 2011; Wittig-Silva et al. 2014) were contacted for clarification of trial methodology and provision of additional unpublished data. A risk of bias assessment was performed on studies and only studies with a low risk of selection, performance, detection and attrition bias were included. Data extraction was done independently by DG and AS. Data synthesis was performed using a meta-analysis software package, Review Manager (RevMan, The Nordic Cochrane Centre, The Cochrane Collaboration, Copenhagen, 2008). The effect of the intervention was expressed as odds ratios and confidence intervals were calculated. The Mantel-Haenszel fixed-effect method of meta-analysis was used.

10.2 Chapter 2 – Epithelium-off two-photon microscopy imaging

10.2.1 Two-photon microscope set-up

A Ti:Sapphire laser (Chameleon Vision II, Coherent, CA, USA) equipped with a prism based Group Velocity Dispersion (GVD) compensation unit was used as the excitation laser source. The laser has a tuning range from ~680 nm up to 1080 nm, operating with a 140 femtosecond pulse duration and 80 MHz pulse repetition rate. The excitation laser beam was guided to a Leica DM6000CS upright microscope via an Electro-Optical-Modulator (EOM) to control laser output and coupled into the Leica SP8 Spectral Scan-head (Leica Microsystems, GmBH) where it passes through two galvoscanners, allowing scanning in the x-y plane, before being focused into the sample by a Leica 25X /0.95 NA water immersion objective (coverslip corrected) that facilitated a working depth of up to 2 mm. Theoretical (full-width half-maximum) resolutions were calculated at 0.34 µm laterally and 1.4 µm axially. Employing the two-photon fluorescence principle, I used excitation light of wavelength 890 nm to correspond with the highest absorption wavelength of riboflavin (i.e. 445 x 2 = 890 nm, Figure 3.3). The emitted fluorescence passed through an 800 nm short pass dichroic filter (Chroma Technology Corp., Vermont, USA), which was then spectrally separated by a Leica Acousto-Optic-Beam Splitter (AOBS®) before passing to the Leica HyD® detectors.

10.2.2 Sample preparation

Freshly enucleated porcine eyes (First Link Ltd., Wolverhampton, UK), stored within a sealed bottle of phosphate buffered saline (0.85% NaCl, 0.01M NaPhos, pH 7.2-7.4), were transported on ice to arrive within 24 hours of death. Rabbit globes, more closely matching human corneal epithelial thickness were additionally used to confirm findings in epithelium-on experiments. Each globe was secured within a custom-made perspex cylinder to ensure stability on the microscope stage (Figure 3.4A). A custom reservoir chamber for riboflavin (a coverslip glued onto two rubber O-rings) was placed coverslip down and filled with ~400 µl of riboflavin solution. The epithelium was either left intact or debrided using a hockey stick scraper (e.janach srl, Como, Italy), the cornea of the intact globe was apposed to the O-ring and immersed in riboflavin and a timer was started (time = 0 minutes). Relying on surface tension to keep the O-ring/coverslip and cornea apposed, the assembly was then inverted, creating a bubble-free, sealed lake of riboflavin over the cornea and beneath the coverslip ready for imaging (Figure 3.4B). The assembly was then positioned within a custom-built recessed stage to house the cylinder-supported globes beneath the objective. The first TPF z-stack was started at time = 2.5 minutes.

10.2.3 Imaging protocol and concentration calibration

All TPF experiments were performed with the room lights at a minimum. The microscope stage and objective were enclosed in opaque Perspex casing to reduce incident light being detected. TPF excitation light of 890 nm

wavelength was chosen to correspond with the highest riboflavin absorption peak (445 nm) as determined by spectrophotometry. The average laser output power at 890 nm was 33 mW at the objective with minimal fluctuation in average power being observed during the course of any given day's experiment. Emitted riboflavin fluorescence was collected between 525 nm and 650 nm, to avoid overlap with the absorption spectrum of riboflavin. I confirmed the absence of any reabsorption of this emitted light by demonstrating no change in measured TPF signals with excitation depth in homogeneous riboflavin solutions within a well slide (Figure 3.5).

Serial z-stacks at 10 µm intervals were started within the pre-corneal riboflavin reservoir at approximately 30 µm above the corneal surface to provide a reference TPF signal level for this 0.1% w/v solution. This level provided a signal-to-concentration calibration for each eye. Z-stacks were acquired through the depth of the cornea (scan rate: 600 Hz, 512 x 512 pixels, image size: 445 µm x 445 µm, line average: 2, pinhole wide open). An iterative approach to developing this protocol was used, balancing the need for sufficient axial resolution with 10 µm stacks and a fast total acquisition time (approximately 130 seconds) to limit the possibility to riboflavin migration during each whole corneal scan. Each run was repeated every 2.5 minutes, up to 20 minutes, and then every 5 minutes, up to 60 minutes.

10.3 Chapter 3 – Epithelium-on two-photon microscopy imaging

10.3.1 Sample preparation

Adult pigmented rabbit heads transported on ice in a phosphate buffered saline (PBS) bath were received within 5 hours post-mortem (First Link Ltd., Wolverhampton, UK). Intact globes were enucleated and examined under a low-magnification light microscope to rule out obvious epithelial trauma or scars. The globes were warmed to room temperature in balanced salt solution before different commercially-available riboflavin solutions (Table 4.1) were applied to the corneas of intact globes according to the manufacturers' protocols (Protocols tested, section 4.2.3).

10.3.2 NC-1059 solution preparation

NC-1059 is a synthetic non-selective ion channel-forming peptide. A 200 µM NC-1059 peptide solution (amino acid sequence KKKK-AARVGLGITTVLVTTIGLGVRAA; *LifeTein LLC, New Jersey, USA*) was prepared by dissolving it in either 0.25 % or 0.1 % w/v riboflavin 5'-monophosphate solution (Ricrolin +, Table 4.1)

Table 10.1 Commercially prepared riboflavin solutions

Formulation	Manufacturer	Composition
Vibex Rapid	Avedro, Inc., MA, USA	0.1% wt/vol riboflavin 5'-monophosphate, saline, HPMC
Ribocross TE	IROS Srl, Napoli, Italy	0.125% wt/vol riboflavin 5'-monophosphate, D-alpha-tocopheryl poly(ethylene glycol) 1000 succinate
Medio-Cross TE	Peschke Meditrade GmbH, Germany	0.25% wt/vol riboflavin 5'-monophosphate, HPMC, benzalkonium chloride 0.01%
Ricrolin + 0.1%	Sooft Italia S.p.A. Montegiorgio, Italy	0.1% wt/vol riboflavin 5'-monophosphate, sodium edetate, trometamol, sodium dihydrogen phosphate dihydrate, sodium phosphate dibasic dehydrate
Ricrolin + 0.25%	Sooft Italia S.p.A. Montegiorgio, Italy	0.25% wt/vol riboflavin 5'-monophosphate, sodium edetate, trometamol, sodium dihydrogen phosphate dihydrate, sodium phosphate dibasic dehydrate
ParaCel	Avedro, Inc., MA, USA	0.25% wt/vol riboflavin 5'-monophosphate, HPMC, sodium edetate, trometamol, benzalkonium chloride, saline
VibeX Xtra	Avedro, Inc., MA, USA	0.25% wt/vol riboflavin 5'-monophosphate, saline

All the above solutions (except Vibex Rapid) are designed for transepithelial use. HPMC, hydroxypropyl methylcellulose

10.3.3 Protocols tested

Positive controls were prepared using a 9 mm vacuum well secured to epithelial-debrided corneas of whole globes filled with 0.1 % w/v riboflavin in HPMC and saline (Vibex Rapid) for 30 minutes (n = 5). Unsoaked globes (i.e. no riboflavin) served as negative controls (n = 5).

10.3.3.1 Non-iontophoresis protocols

1. Medio-Cross TE

A 9 mm vacuum well secured on the cornea was filled with approximately 0.5 ml of Medio-Cross TE solution for 30 minutes. Riboflavin was not rinsed from the cornea (n = 5).

2. Ribocross TE

A 9 mm vacuum well secured on the cornea was filled with approximately 0.5 ml of Ribocross TE solution for 30 minutes. Riboflavin was not rinsed from the cornea (n = 5).

3. ParaCel and VibeX Xtra

ParaCel drops were applied at a rate of 1 drop every 90 seconds for 4 minutes. The cornea was then rinsed with VibeX Xtra completely coating the cornea. Additional VibeX Xtra was applied at a rate of 1 drop every 90 seconds for 6 minutes (total riboflavin soak time 10 minutes). Riboflavin was not rinsed from the cornea (n = 5).

4. 200 µM NC-1059 peptide in 0.1 % w/v Ricrolin +

A 9 mm vacuum well secured on the cornea was filled with approximately 0.5 ml of 200 µM NC-1059 peptide in 0.1 % w/v Ricrolin + solution for 30 minutes. Riboflavin was rinsed from the cornea with PBS for 1 minute (n = 3).

5. 200 µM NC-1059 peptide in 0.25 % w/v Ricrolin +

A 9 mm vacuum well secured on the cornea was filled with approximately 0.5 ml of 200 µM NC-1059 peptide in 0.1 % w/v Ricrolin + solution for 30 minutes. Riboflavin was rinsed from the cornea with PBS for 1 minute (n = 3).

10.3.3.2 Iontophoresis protocol

The iontophoresis system comprised 2 electrodes: a negatively-charged metal grid housed within the corneal applicator and a positively-charged 20G needle inserted through the sclera into the vitreous (Figure 4.3A). The corneal applicator was vacuum-attached to the cornea. The reservoir was filled with differing riboflavin formulations to above the level of the metal grid before beginning the iontophoresis treatment. Protocols varied either by iontophoresis dosage, soak time or riboflavin formulation (n = 4, Table 4.2). After the iontophoretic procedure, the applicator was removed and the corneas were rinsed with PBS to both remove any riboflavin on the corneal surface and to try to reduce riboflavin concentration within the epithelium.

Table 10.2 iontophoresis protocols

Protocol	Solution	Current	Soak I	Current	Soak	Rinse

Negative control	None	None	-	-	-	-
Positive Control	Vibex Rapid	None	30 min	-	-	-
A	MedioCross	1mA 5 min	5 min	0.5 mA 5	5 min	5 min *
B	MedioCross	1mA 5 min	15 min	-	-	1 min
C	Ricrolin+	1mA 5 min	5 min	0.5 mA 5	5 min	5 min *
D	Ricrolin+	1mA 10	-	-	-	5 min
E	MedioCross	1mA 5 min	-	-	-	1 min
F	Ricrolin +	1mA 5 min	-	-	-	1 min
G	Vibex Rapid	1mA 5 min	-	-	-	1 min
H	Vibex Rapid	1mA 5 min	5 min	0.5 mA 5	5 min	5 min

Min, minute; * St. Thomas'/Cardiff Iontophoresis protocol (unpublished)

10.3.4 Section preparation

At the end of the riboflavin soak, the globes were immediately immersed in liquid nitrogen for 5 minutes and stored overnight at -25 degrees Celsius. A broad incision across the posterior globe was made just before immersion to prevent the cornea from splitting open on freezing. For each globe, three 35 µm corneal cross-sections were cut on a cryostat 1 mm apart (Figure 4.5). With the frozen section on the blade platform (maintained at -21°C), a knife was used to cut the cornea free and the remaining tissue was brushed away. The cornea itself was meticulously brushed to ensure no ice remained attached that might allow riboflavin to leak out once thawed (transparent images of processed sections during the development of the methodology confirmed the epithelium itself was not removed by this brushing; see Figure 4.4 below). Colour photographs were taken of the sagittally-exposed globe and free corneal section.

The corneal section was then mounted on a slide and covered with

fluorescence-free immersion oil (Immersol 518 F, Carl Zeiss Ltd.) to prevent any leakage of riboflavin out of the tissue. No dye leakage was observed over several minutes during protocol development using immersion oil. This compared with prompt dye leakage when either water-based optimal cutting temperature (OCT) compound or water itself was used as an immersion medium. A coverslip was placed on top prior to imaging under the microscope objective (Figure 4.3B). The time taken from the tissue thawing onto the slide to image acquisition on the microscope was approximately 1 minute, and I refer to this earliest imaging time point as t = 0 minutes. To investigate riboflavin migration within the thawed slide-mounted tissue, serial images were captured every minute for selected samples. For all other measurements, data was acquired as soon as possible following tissue thawing, i.e. after approximately 1 minute.

10.3.5 Two-photon microscope set-up and imaging protocol

The two-photon microscope set-up is based on that described in chapter 2. A Ti:Sapphire laser, operating at a wavelength of 890 nm with a 140 femtosecond pulse duration and 80 MHz pulse repetition rate, was used as the excitation laser source. The excitation laser beam was guided to a Leica DM6000CS upright microscope where it passes through two galvoscanners, allowing scanning in the x-y plane, before being focused into the sample by a Leica 10 X /0.3 NA water immersion objective. Theoretical (full-width half-maximum) axial and lateral resolutions were calculated at 16 µm and 1.1 µm respectively. TPF excitation light of 890 nm wavelength was chosen to correspond with the highest riboflavin absorption peak (445 nm) as

determined by spectrophotometry. Emitted riboflavin fluorescence was collected between 525 nm and 650 nm to avoid overlap with the absorption spectrum of riboflavin. 553 µm x 553 µm (512 x 512 pixel) images were captured at a scan rate of 600Hz (line average 16) with the pinhole wide open.

10.3.6 Image analysis

Grey scale images (Figure 4.6A) were exported and analysed using Java-based imaging software (ImageJ, 1.48v, http:// imagej.nih.gov.ij; provided in the public domain by the National Institutes of Health, Bethesda, MD, USA). For each image, three separate rectangular regions of interest each 40 pixels wide in the x-direction were manually selected. The intensity profiles along the z-direction for each region of interest were then exported to a .txt file (Excel for Mac, 2011; Microsoft Corp, Redmond, WA, USA) (Figure 4.6B). The epithelial/stromal junction was then identified in each trace by the abrupt change in signal and confirmed with reference to the corresponding image region of interest. This information was then used to align all three plots along the z-axis and a mean intensity plot was then generated representing the average TPF signal for that image as a function of depth (z). TPF signals were converted to riboflavin concentration by normalizing to the TPF signal achieved in a well-slide reservoir of 0.1 % riboflavin solution during the same experimental session. Mean (SD) concentrations were calculated from 5 globes tested for each protocol. Unpaired Student *t*-tests were used to compare riboflavin concentrations achieved at a depth of 300 µm. A p value less than 0.05 was considered significant. Analyses were performed in Excel

for Mac, 2011; Microsoft Corp, Redmond, WA, USA).

10.4 Chapter 4 – Accelerated CXL

10.4.1 Ethics and data handling

This study design was reviewed by the Research Governance Committee and approved as an audit project by the Clinical Audit Working Group at Moorfields Eye Hospital NHS Foundation Trust. Patients were identified from a prospective electronic database of all patients aged above 15 years of age attending the *Early Keratoconus Clinic*. The database contains keratometric and refractive data entered prospectively in clinic and at the time of surgery. I extracted data from a consecutive series beginning with the first accelerated treatment in September 2012 through to April 2013. Eyes with 12-months' keratometric follow-up data were included in this study.

10.4.2 Outcomes measures

The primary outcome measure was the failure rate of CXL treatment, defined by an increase in maximum anterior keratometry (Kmax) on corneal tomography of >1.5 D at 12 months. Secondary outcome measures included anterior keratometry of the steep (K2 front) and flat (K1 front) axes in the central 3mm zone, posterior keratometry of the steep axis (K2 back), uncorrected distance visual acuity (UCVA), spectacle-corrected distance visual acuity (CDVA), subjective refraction, corneal thickness at the thinnest point and endothelial cell density. Visual acuities were initially measured in Snellen, before the using LogMAR charts in the clinic from September 2013.

10.4.3 Monitoring for disease progression

Serial corneal tomography (Pentacam HR, Oculus GmbH, Germany) and subjective refractions were used to confirm pre-operative keratoconus progression. Progression was defined by one or more of the following: >1.5 D increase in Kmax or anterior K2 (K2 front); >0.5 D increase in posterior K2 (K2 back); >1 D increase in refractive astigmatism; >1 line loss of CDVA or >13 µm decrease in pachymetry. These criteria were based on published (Szalai et al. 2012) limits of agreement for repeated measurement using the Pentacam in patients with keratoconus, where changes >1.5 D have a >95% probability of not being simply attributable to measurement error. Exclusion criteria included pregnancy or breastfeeding, active ocular surface disease or a minimum stromal thickness less than 375 µm.

10.4.4 Specular microscopy

Corneal endothelial cell densities were measured using the Topcon SP-2000P noncontact specular microscopy and analyzed with IMAGEnet 2000 computerized analysis system (v2.5x; Topcon, Tokyo, Japan). If a clear image could not be acquired centrally, the patient was asked to look just to side of the fixation light. Only whole cells with a continuous border (manually refined) on a frame with 75 or more cells, were accepted for planimetric analysis.

10.4.5 Surgical procedure

Following topical instillation of proxymetacaine 0.5%, tetracaine 1% and povidone-iodine 5%, the eyelashes were taped and a lid speculum inserted. The corneal epithelium was manually debrided to approximately 9mm. Dextran-free riboflavin 5'-monophosphate in saline and hydroxypropyl methylcellulose (VibeX Rapid*,* Avedro, Mass. USA) was applied every 2 minutes for either 20 minutes (if minimum pachymetry ≥ 400 µm) or 10 minutes (if minimum pachymetry < 400 µm). Continuous UVA exposure (KXL®, Avedro, Mass. USA) at 30 mW/cm^2 for 4 minutes was then applied (total energy 7.2 mJ/cm^2).

At the end of the procedure, preservative-free dexamethasone 0.1% and chloramphenicol 0.5% were instilled and a bandage contact lens applied. Post-operatively, patients were prescribed a tapered course of preservative-free topical dexamethasone 0.1%, moxifloxacin and hyaluronic acid 0.1% for 1 week, along with topical diclofenac 0.1%, cyclopentolate 1% twice a day and 50 mg oral diclofenac three times a day for 3 days. Patients were additionally provided with 3 minims of proxymetacaine 0.5% for use in the early post-operative period. The bandage contact lens was removed at 1 week after which all therapy was discontinued except topical hyaluronic acid 0.1% and fluorometholone 0.1% four times a day for 1 month.

10.4.6 Statistical analysis

For purposes of statistical analysis, I have converted Snellen visual acuities to

logMAR equivalents (−log decimal acuity). I present data as means ± standard deviation. I use Paired Student t-tests to compare baseline and 12-month post-operative data, accepting a p value ≤ 0.05 as significant. Analyses were performed in Excel for Mac (2011, Microsoft Corp.).

10.5 Chapter 5 – Gross shape correction

10.5.1 Study design

Retrospective consecutive case series.

10.5.2 Inclusion criteria

The medical records were reviewed for all keratoconic patients receiving KeraRing implantation by 3 surgeons at Moorfields Eye Hospital between 2010 and 2013 inclusive. All patients met all 4 of the following inclusion criteria before surgery:

5. Contact lens intolerance
6. Corrected distance visual acuity (CDVA) ≤ 6/9
7. Corneal thickness at the 6 mm channel site ≥ 450 µm.
8. Controlled ocular surface inflammation

10.5.3 Surgical procedure

Surgical plans based on Scheimpflug tomography and subjective refraction were obtained from the manufacturer (Mediphacos Ltd, Belo Horizonte, Brazil). Following topical instillation of proxymetacaine 0.5%, tetracaine 1% and povidone-iodine 5%, a 360-degree femtosecond laser channel of internal diameter 5mm and external diameter 5.9mm was created at a depth between 350 – 400 µm as dictated in the surgical plan (see example in Figure 6.1 below). Into this channel, either 1 or 2 ring segments were implanted. No

sutures were used. At the end of the procedure, preservative-free dexamethasone 0.1% and chloramphenicol 0.5% were instilled.

10.5.4 Post-operative care

Post-operatively, patients were prescribed preservative-free topical dexamethasone 0.1% and chloramphenicol 0.5% four times a day for 1 week. Serial tomography and subjective refractions were performed to monitor for post-implantation ectasia progression. The first topography scan after 3 months post-surgery was used as an updated baseline with which to compare for ectasia progression.

10.5.5 Outcome measures

The main outcome measure was CDVA. Secondary outcomes measures included UDVA, manifest refraction, corneal coma, contact lens tolerance and complications. Snellen visual acuity was converted to LogMAR equivalent for statistical analysis. Mean ± standard deviation are presented.

10.6 Chapter 6 – Fine shape correction

10.6.1 Design

Prospective interventional series.

10.6.2 Primary outcome

LogMAR CDVA at 12 months

10.6.3 Secondary outcomes

LogMAR UCVA

Manifest refraction

Pentacam indices

Rate of infective keratitis

10.6.4 Subject selection

Inclusion criteria

- Patients with progressive stage I - III keratoconus
- CDVA < 0.00 logMAR

Exclusion criteria

- Patients under the age of 18 years
- Active ocular surface disease
- Minimum corneal thickness <390 µm (leaving 325 µm residual stromal thickness after transPTK)

10.6.5 Study interventions

TransPRK programming

Three consistent scotopic ocular wavefront scans (Ocular Wavefront Analyzer, SCHWIND eye-tech-solutions GmbH, Germany) were acquired within 0.5 D spherical equivalent refraction of each other. Corneal topography (*Schwind Sirius*) was also recorded to allow a comparison of planned wavefront and topography-guided treatments. Patients were required to remove gas permeable contact lenses for 2 weeks and soft contact lenses for 1 week prior to scanning. Pharmacological pupil dilation with tropicamide 1% was used where pupil diameter was less than 5.5 mm. The scan with the lowest sphere and highest coma was exported for treatment programming. Iris scans were taken for static cyclotorsion control during the treatment. Ablation depth was minimised during treatment programming by removing all sphero-cylindrical constraints. I aimed to preserve a minimum corneal stromal thickness prior to CXL of 325 µm. To ensure effective CXL was not compromised by a smaller diameter zone of epithelial removal, epithelial transPTK and stromal PRK was delivered separately where the programmed laser ablation zone for transPRK was predicted to be less than 8mm in diameter.

TransPRK/CXL surgery

Treatments were performed by either by myself or Bruce Allan. Following topical instillation of proxymetacaine 0.5%, tetracaine 1% and povidone-iodine 5%, a lid speculum inserted. After the laser treatment was complete, dextran-free 0.1 % w/v riboflavin 5'-monophosphate solution in saline and hydroxypropyl methylcellulose (VibeX Rapid*,* Avedro, MA, USA) was applied every 2 minutes for a total of 10 minutes before UVA exposure (KXL®, Avedro, MA, USA) at 30 mW/cm^2 for 4 minutes (pulsed every 1.5 seconds) was then applied (total energy 7.2 mJ/cm^2). Mitomycin C was not used.

At the end of the procedure, preservative-free dexamethasone 0.1% and chloramphenicol 0.5% were instilled and a bandage contact lens applied. Post-operatively, patients were prescribed a tapered course of preservative-free topical dexamethasone 0.1%, moxifloxacin and hyaluronic acid 0.1% for 1 week, along with topical diclofenac 0.1%, cyclopentolate 1% twice a day and 50 mg oral diclofenac 3 times a day for 3 days. Patients were additionally provided with 3 minims of proxymetacaine 0.5% for use in the early post-operative period. The bandage contact lens was removed at 1 week after which all therapy was discontinued except topical hyaluronic acid 0.1% and fluorometholone 0.1% 4 times a day for 1 month.